Non-radiative loss mechanisms in InGaN/GaN multiple quantum well light-emitting diodes

vorgelegt von
Diplom-Physiker
Felix Nippert
aus Berlin

von der Fakultät II – Mathematik und Naturwissenschaften
der Technischen Universität Berlin

zur Erlangung des akademischen Grades
Doktor der Naturwissenschaften
– Dr. rer. nat. –

genehmigte Dissertation

Promotionsausschuss:
Vorsitzender: Prof. Dr. Michael Lehmann
Gutachter: Prof. Dr. Axel Hoffmann
Gutachterin: Prof. Dr. Janina Maultzsch
Gutachter: Prof. Dr. Andreas Waag

Tag der wissenschaftlichen Aussprache: 24. 01. 2017

Berlin 2017

Zusammenfassung

InGaN/GaN Quantentöpfe (QW) werden heute standardmäßig für blau- und grün-emittierende Leuchtdioden (LEDs) eingesetzt, zum Beispiel in der Raumbeleuchtung. Obwohl derartige Strukturen im großindustriellen Maßstab hergestellt werden, gibt es noch einige offene Fragen. Zum einen zeigen sie eine drastische Verringerung der internen Quanteneffizienz (IQE) zu längeren Wellenlängen („Green Gap"), zum anderen nimmt die Effizienz auch zu hohen Betriebsströmen deutlich ab („Droop"). Ferner sind Hochleistungsanwendungen, wie zum Beispiel grüne Laserdioden, noch weit von der industriellen Massennutzung entfernt. In dieser Arbeit werden daher die grundlegenden physikalischen Limitierungen der InGaN/GaN-Technologie beleuchtet. Zu diesem Zweck werden dem Stand der Technik entsprechende InGaN/GaN Mehrfach-Quantentöpfe (MQW) in zwei verschiedenen Leistungsregimen untersucht.

In grün-emittierenden QWs wird in quasi-resonanter, optischer Hochanregung eine neuartige Lumineszenz im blauen Spektralbereich beobachtet. Diese ist spektral sehr breit (mehrere Hundert meV), kontinuierlich und weist eine schnelle Zerfallszeit (bis hinab zu 30 ps) auf. Diese Lumineszenzbande kann nicht angeregten elektronischen Zuständen zugeordnet werden. Stattdessen wird sie als Rekombination von Elektronen mit hoch-angeregten Löchern im Confinement (CHC) beschrieben. Das Confinement ergibt sich aus der verkippten Bandstruktur in der Heterostruktur, wobei ein QW und eine Barriere ein dreiecksförmiges Potential bilden. In diesem befinden sich quasi-kontinuierliche Lochzustände. Da diese Zustände energetisch nahe an der GaN Valenzbandkante liegen, stellen sie einen potentiellen Verlustkanal dar, insbesondere für Hochanregungsanwendungen wie Laserdioden.

Für LED-Strukturen, welche in gemäßigteren Leistungsbereichen betrieben werden, und die von „Green Gap" und „Droop" betroffen sind, wird in dieser Arbeit eine neue spektroskopische Technik etabliert. Hierfür wird die differentielle Lebenszeit der Ladungsträger (DLT) mit einem elektrooptischen Pump-Probe-Verfahren, der Klein-Signal zeitaufgelöste Photolumineszenz (SSTRPL), bestimmt. Diese Methode

verbessert konventionelle Verfahren, indem sie elektrische Anregung (Pump) analog zum normalen LED-Betrieb mit zeitabhängiger, quasi-resonanter optischer Anregung (Probe) kombiniert. Im Gegensatz zu Methoden, in denen der Strom moduliert wird, kann bei dieser garantiert werden, dass die zusätzlichen Ladungsträger ausschließlich in den QWs generiert werden. Mit Hilfe der SSTRPL kann ein detaillierter Einblick in die üblicherweise mit dem ABC-Modell modellierten Rekombinationskanäle gewonnen werden. In einer zeitabhängigen Studie von blau- und grün-emittierenden LEDs wird schließlich auch der Ursprung des „Green Gap“ klarer.

Einerseits ist der nicht-strahlende Shockley-Read-Hall-Rekombinationskoeffizient in blauen und grünen LEDs sowohl ungefähr gleich groß und weist auch eine vergleichbare Aktivierungsenergie auf. Dies impliziert sehr vergleichbare Defektdichten in den jeweiligen InGaN-Schichten, sodass Wachstumsprobleme durch die höhere Indiumkonzentration als potentielle Ursache des „Green Gap“ ausgeschlossen werden können. Andererseits zeigt sich im grünen Spektralbereich eine drastische Verringerung der strahlenden und Auger-Rekombination. Nur zum Teil kann diese Verringerung mit dem stärker werdenden Quantum-Confined Stark-Effekt erklärt werden. Zusätzlich ist auch eine stärkere werdende Lochlokalisierung für dieses Phänomen verantwortlich. Diese kann mit Hilfe der abnormalen Temperaturabhängigkeit des strahlenden Rekombinationskoeffizienen bestätigt werden, welcher mit zunehmender Temperatur ansteigt, anstatt zu sinken. Letztendlich kann der „Green Gap“ vor allem auf eine Verschiebung im Rekombinationsgleichgewicht zwischen strahlender und Auger-Rekombination zurückgeführt werden, welche mit einer steigenden Lochlokalisierung verknüpft ist, die selbst bei komplett zufälliger Legierung von InN und GaN unvermeidlich ist.

Schließlich folgt, dass weitere Effizienzsteigerungen in der konventionellen, c-planaren Technologie nur erreicht werden können, wenn die Uniformität der Legierung verbessert wird. Allerdings ist dieser Parameter nur sehr schwer mit strukturellen Methoden bewertbar, da sich die Abweichungen von der idealen Legierung nur auf atomarer Ebene abzeichnen. Daher ist die entwickelte Methode (SSTRPL) insbesondere in Abhängigkeit der Temperatur ideal geeignet, um etwaige Fortschritte auf diesem Gebiet zu bewerten, da sie in einem zerstörungsfreien Messverfahren direkten Zugriff auf die Lokalisierungseigenschaften erlaubt.

Abstract

InGaN/GaN quantum wells (QWs) are commonly used for blue and green light-emitting diodes (LEDs), for example in solid-state lighting (SSL). While such structures are already in mass-production, there are still several open questions. They show drastic reductions in internal quantum efficiency (IQE) towards longer wavelengths ("green gap"), as well as with increased drive current ("droop"). In addition, advanced high-power applications, such as green laser diodes (LDs), are still far from commercial use. In this work, the principal physical limitations of the InGaN/GaN technology are investigated. To this end, state-of-the-art InGaN/GaN multiple quantum wells (MQWs) structures are investigated in two power regimes.

Under intense quasi-resonant, optical excitation a novel high excitation luminescence in the blue spectral region is observed for green-emitting QWs. This, broad (several hundred meV), featureless, fast-decaying (down to 30 ps lifetime) luminescence cannot be attributed to excited electron states, but rather is attributed to the confined hole continuum (CHC). The CHC is formed by excited quasi-continuous hole states confined by the triangular potential created by a QW–barrier pair due to the quantum-confined Stark effect (QCSE). Such states are energetically close to the GaN bulk states, implying that they could contribute to carrier leakage in high-power applications such as laser structures.

State-of-the-art LED structures, operating in conventional power regimes and suffering from the green gap and droop phenomena, are investigated by a novel technique, which is established in this work. It relies on differential lifetime (DLT) measurements, performed in an electro-optical pump-probe setup: small-signal time-resolved photoluminescence (SSTRPL). The technique improves on previous approaches by combining steady-state electrical pumping identical to operating conditions, with time-dependent quasi-resonant optical probe excitation. In contrast to current modulation methods, this guarantees carrier insertion into the active layer only. SSTRPL therefore allows detailed insight into the recombination pathways, as conventionally modeled with the

ABC model. In a temperature-dependent analysis of blue- and green-emitting MQW LEDs, the origin of the green gap phenomenon is elucidated. First, the Shockley-Read-Hall (SRH) recombination coefficient is shown to have the same magnitude and activation energy in blue and green-emitting InGaN layers, implying very similar defect densities. This allows to withdraw growth issues related to the higher incorporation of In from the list of potential causes of the green gap. Second, radiative and Auger recombination are drastically reduced in green-emitting structures. This effect can partly be blamed on the increasing QCSE, but is also caused by increasing hole localization. The latter is confirmed by considering the abnormal temperature dependence of the radiative recombination coefficient, which is increasing, rather than decreasing, with temperature. Finally, the green gap efficiency reduction is shown to originate primarily from a shift in the balance between radiative and Auger recombination, intricately connected to the increasing localization of holes, as it occurs even in the random alloy. The results obtained suggest that any further efficiency increase in conventional c-plane technology may only be reached by improving the uniformity of the random alloy. This parameter is very difficult to access directly with structural investigations. Therefore, (temperature-dependent) SSTRPL will be an important tool to track progress in the future, because it allows to access the atomic-scale localization properties in a non-destructive electro-optical measurement.

Contents

Acronyms x

1 Introduction 1

2 Fundamentals of InGaN Light-Emitting Diodes 3

2.1 The III–Nitride Material System . . . 3

2.1.1 The Quantum-Confined Stark Effect . . . 3

2.1.2 Localization in InGaN Alloys . . . 5

2.2 Properties of InGaN Light-Emitting Diodes . . . 8

2.2.1 Design of Commercial InGaN Light-Emitting Diodes . . . 8

2.2.2 Efficiency of InGaN Light-Emitting Diodes . . . 12

2.2.3 Radiative and Non-Radiative Recombination Processes . . . 13

2.2.4 The “Green Gap” . . . 15

2.2.5 The “Droop” . . . 16

2.3 Open Questions . . . 18

3 Experimental Methods 19

3.1 Sample Growth . . . 19

3.2 Optical Spectroscopy . . . 21

3.2.1 Electroluminescence . . . 21

3.2.2 Photoluminescence . . . 21

3.2.3 Photoluminescence Excitation Spectroscopy . . . 23

3.2.4 Time-Resolved Photoluminescence . . . 24

3.2.5 Small-Signal Time-Resolved Photoluminescence . . . 25

3.2.6 Carrier Injection and Resonance Conditions . . . 25

4 Excited States in InGaN Quantum Wells 29

4.1 High-Excitation Effects in Semiconductors 29

4.1.1 Heating 29

4.1.2 Large Carrier Density 29

4.1.3 Excited States 30

4.2 Optical Properties of High-Quality InGaN Quantum Wells 31

4.3 The Confined Hole Continuum 34

4.4 Conclusion 42

5 Recombination Coefficients in InGaN MQW LEDs 45

5.1 Determination of the Recombination Coefficients 46

5.2 Differential Lifetimes 49

5.3 Carrier Distribution in Multi Quantum Well Stacks 55

5.4 Temperature-Dependence of the Recombination Coefficients 71

5.4.1 Potential Causes of the “Green Gap” 71

5.4.2 Limitations of the ABC-model 72

5.4.3 Expectation 73

5.5 Conclusion: Origin of the “Green Gap” 81

6 Alternative Approaches: Pitfalls and Perspectives 85

6.1 Growth in semi- and non-polar directions 85

6.2 Cubic InGaN 87

6.3 Quantum Dots 87

6.4 Microrods 88

6.5 Lasing 89

6.6 Outlook 91

7 Conclusion 93

7.1 Outlook 95

Publications I

Authored Articles I

Co-Authored Articles II

Unpublished Articles IV

Conference Contributions V

Bibliography VII

Acknowledgements XXXVII

Acronyms

CCD charge-coupled device

CHC confined hole continuum

DAP donor-acceptor-pair

DLT differential lifetime

DOS density of states

EBL electron blocking layer

EL electroluminescence

EQE external quantum efficiency

HRTEM high-resolution transmission electron microscopy

III–N group III–nitride

IQE internal quantum efficiency

LD laser diode

LED light-emitting diode

MBE molecular beam epitaxy

MOVPE metal-organic vapor phase epitaxy

MQW multiple quantum well

PL photoluminescence

PLE photoluminescence excitation spectroscopy

PMT photo-multiplier tube

QCSE quantum-confined Stark effect

QD quantum dot

QE quantum efficiency

QW quantum well

SQW single quantum well

SRH Shockley-Read-Hall

SSL solid-state lighting

SSTRPL small-signal time-resolved photoluminescence

TCSPC time-correlated single photon counting

TRPL time-tesolved photoluminescence

VCSEL vertical cavity surface emitting laser

1 Introduction

Light generated by current - electroluminescence (EL) - was observed in semiconductors as early as the 1950's, e.g. in SiC[1–3]. Early realizations of p–n-junctions in GaAs[4, 5] and GaP[6, 7] led to the first light-emitting diodes (LEDs). The latter material system is still the basis of red InGaAlP-LEDs today. In contrast, blue and green light emission was, for a long time, very challenging, with devices based on ZnSe[8, 9], ZnS[10] or SiC[11, 12] achieving quantum efficiencies of the order of 0.1 %, i.e. one in thousand injected electrons lead to the emission of a photon. In the early 1990's breakthroughs in heterostructure design and epitaxy suggested that widespread application of ZnSe-based blue and green light sources was imminent[13–18]. As it turned out, however, such diodes quickly degrade, as the emission energy of the photons is sufficient to produce defects, which spread throughout the structures[19, 20]. At the same time, previously impossible p-type doping of GaN[21] was realized[22–24], paving the way for highly efficient GaN-based LEDs[25, 26] and laser diodes (LDs)[27, 28]. Despite much progress in the last 20 years, GaN remains a relatively "dirty" material, usually featuring orders of magnitude higher defect densities[29, 30] than other commonly used compound semiconductors such as GaAs or ZnO. Nevertheless, it remains the material of choice for blue-to-green light emission applications, as, for example, the search for an effective p-type dopant in ZnO has remained unsuccessful.

Decade long research and development of GaN technology has led to highly efficient blue InGaN-based LEDs, used for solid-state lighting (SSL), and LDs, used in data storage. Two issues remain largely unsolved: i) efficiency reduction of such devices at high operating currents ("droop") and ii) efficiency reduction towards the green spectral range ("green gap").

In this thesis, detailed spectroscopic studies of state-of-the-art epitaxial structures and devices provide crucial insight into the physical mechanisms responsible for these two phenomena. In chapter 2 on the facing page, a brief overview over the technological background of InGaN/GaN quantum well (QW) LEDs is given and the most pressing questions that this field faces are presented. Chapter 3 on page 19 presents the measurement techniques used to study these questions.

The main part of the thesis is divided into two parts. In the first part (chapter 4 on page 29), excited states in QWs are investigated. Here, a detailed study of a characteristic high-excitation luminescence gives insight into the confined hole continuum (CHC), constituting a relevant loss mechanism in high-power applications such as LDs. In the second part (chapter 5 on page 45), the carrier recombination dynamics of state-of-the-art InGaN/GaN multiple quantum well (MQW) LEDs are investigated. For this purpose, a novel method to estimate the recombination coefficients corresponding to the principal radiative and non-radiative recombination channels is introduced. This technique is used to gain insight into the carrier transport and distribution in MQW LEDs (section 5.3 on page 55). By comparing the temperature dependencies of the recombination coefficients in blue and green LEDs (section 5.4 on page 71), the origin of the green gap is elucidated. Finally, as these results suggest that the quantum efficiency of conventional green devices may be fundamentally limited by properties inherent to the InGaN alloy, chapter 6 on page 85 considers some alternative solutions to overcome these limitations.

2 Fundamentals of InGaN Light-Emitting Diodes

In this chapter, the working principles, limitations and challenges of current state-of-the-art InGaN light-emitting diode (LED)-technology is discussed.

2.1 The III–Nitride Material System

The term group III–nitride (III–N) refers to three binary compounds InN, GaN and AlN, as well as the ternary and quaternary compounds that can be realized by mixing the group III metal atoms. Generally, growth of these materials will result in hexagonal (wurtzite) or cubic (zincblende) crystals[29], although the wurtzite phase is thermodynamically more stable. Here, the band gaps vary from the far infrared (InN, 0.7 eV[31–33]) over the near UV (GaN, 3.4 eV[34–36]) into the deep UV spectral range (AlN, 6.2 eV[37]). Consequently, band gaps corresponding to the whole visible spectrum are accessible with appropriate InGaN[38, 39], AlInN[40] or AlInGaN[41] alloy compositions. This tunability makes the III–N system a promising, and in some cases proven, candidate for optoelectronic applications. Among the realized applications are InGaN-based LEDs used for solid-state lighting (SSL)[42–45], AlGaN-based UV LEDs[46], InGaN-based laser diodes (LDs), emitting in the blue[47, 48], violet[49] and green[50–52], solar cells[53], sensors[54] and even photo-cathodes[55].

2.1.1 The Quantum-Confined Stark Effect

The wurtzite phase exhibits strong macroscopic polarization, in contrast to the cubic phase. This is a result of the lacking inversion symmetry, inherent to this hexagonal crystal structure. Therefore, the charge distributions for positive and negative charges are offset along the c-axis of the crystal (see figure 2.1 on the next page), which imparts a net spontaneous (also called pyro-) polarization on the crystal[56]. If stress is applied

to the crystal lattice, these charges shift, which leads to an additional, piezoelectric polarization[57]. This matter has serious implications on heterostructures grown along the c-direction. As the spontaneous polarizations of InN and GaN are significantly different, a polarization discontinuity develops at the interface of GaN and InGaN, if such layers are grown on top of each other. In addition, at least one of these

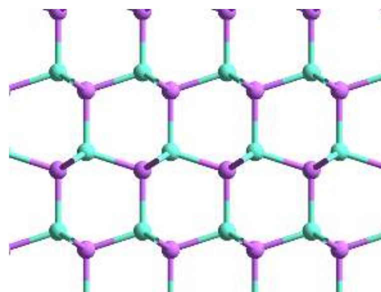

Figure 2.1: Sketch of the wurtzite crystal structure of GaN. The view direction is along the m-direction. The c-direction is towards the top of the image. Clearly, Ga and N atoms are ordered in c-planes consisting, purely, of the respective species. As the atoms are strongly charged, this leads to alternating space charges, i.e. dipoles are formed. In the bulk, these cancel each other, but with finite sizes and interfaces, strong piezoelectric charges result.

layers will be strained, if the growth is performed in a pseudomorphic way, as the lattice constants differ as well[29]. Such biaxial strain leads to additional, piezoelectric polarization charges at the interfaces[58]. In sum, the interfaces of an InGaN quantum well (QW) embedded in GaN are heavily charged. As a result the band structure of the heterostructure is significantly altered, bending conduction and valence bands - especially in the QW[59]. Electrons and holes populating the ground states in the QW are therefore coulombically attracted to the oppositely charged interfaces: The electron and hole wave functions are now separated, i.e. the electron-hole wave function overlap is reduced. Naturally, such overlap reduction decreases the matrix element and hence the rate of radiative recombination[60, 61]. Further, the coulomb interaction of the separated carriers leads to a reduction in emission energy, i.e. a shift to lower emission energies[62, 63], see figure 2.2 on the facing page. This redshift is - by analogy to the conventional shift of atomic transition energies in the presence of electric fields[64] - called the quantum-confined Stark effect (QCSE)[65].

In general, the QCSE in InGaN QWs, embedded in GaN barriers increases with indium composition[66, 67]. This is because both, the difference in spontaneous polarization - and hence interfacial charges, and the strain-induced piezoelectric polarization increase. In addition, the QCSE generally increases with the QW's thickness[62, 68],

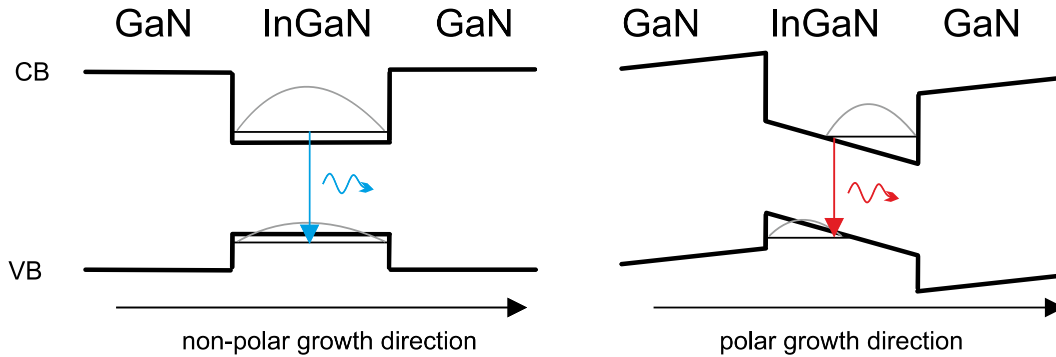

Figure 2.2: Sketch of the quantum-confined Stark effect (QCSE). Left: GaN/InGaN/GaN quantum well (QW) system in non-polar orientation. The blue arrow marks the ground state transition. Right: In polar orientation (i.e. c-direction), the conduction (CB) and valence bands (VB) are tilted. The electron and hole wave functions (grey lines) are separated, leading to a reduction of emission energy (red arrow)

as this naturally leads to a larger separation between electron and hole wave functions. Note that higher indium composition, and thicker QWs also lead to a deeper, and wider, respectively, potential in the electronic band structure. This leads to increasing, and decreasing confinement energies, respectively, also altering the emission energy. The confinement energy in such systems is, however, much smaller than the effects imparted by the QCSE, and is generally only notable in extremely thin, or non-polar QWs. For conventional structures such as those investigated in this work, one can usually assume that the difference between band gap energy of the InGaN alloy and emission energy of the InGaN QW is given by the QCSE. It can be estimated by considering not only the photon emission, but also the photon absorption. Here, the absorption edge remains near the band gap of the alloy, and the difference between absorption and emission (a Stokes-like shift[59, 69]), can be considered a measure of the QCSE.

2.1.2 Localization in InGaN Alloys

In an alloy, the structural, electrical and optical properties tend to develop in a continuous fashion from one material (i.e. GaN) to the other (i.e. InN). Macroscopically, properties like the band gap, the valence band ordering, the effective masses of the

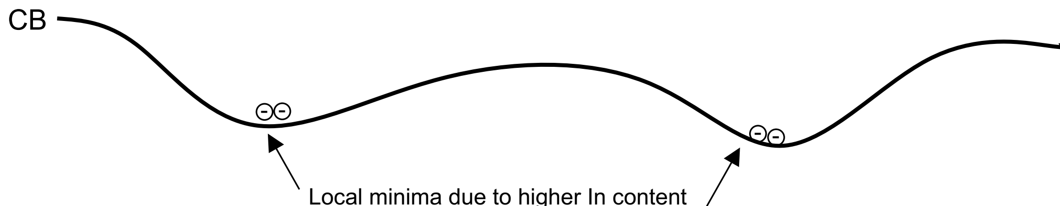

Figure 2.3: Sketched conduction band profile in an InGaN layer in real space. In regions with locally higher indium content, energy minima form, which capture carriers (in this case electrons). The thermal redistribution of these carriers leads to the characteristic S-shape of the emission energy.

carriers, etc, can be described by a – not necessarily linear – relationship as a function of the indium composition. Nevertheless, on a microscopic level, alloying obviously disturbs the crystal lattice, as it implies a substitution of a significant amount of atoms. For example, in $In_{0.2}Ga_{0.8}N$, 20% of the gallium atoms in the lattice are replaced by indium atoms. Indium on gallium site is an isoelectronic impurity. As the indium atom is much bigger than the gallium atom, this significantly alters the crystal lattice in the vicinity of such a "defect". Assuming a random distribution of the indium atoms, one may - depending on the wave function extent of the carriers or excitons, consider the crystal to be uniform again. Astonishingly, in InGaN even single indium atoms may provide a localization potential for holes[70]. Therefore, even random alloying, i.e. completely random replacement of gallium by indium atoms, leads to significant localization of hole states in InGaN[71, 72]. In addition, during the preparation of InGaN layers, the growth conditions can be such, that indium is preferentially incorporated close to other indium atoms, resulting in additional, macroscopic fluctuations of the indium composition[73], macroscopic clusters of higher indium content[74–76] or phase separation[77, 78]. In these cases, even deeper localization potentials are created, which may also bind electrons[79, 80]. In extreme cases, the localization centers may be considered to be quantum dots (QDs). The general principle is sketched in figure 2.3 for the conduction band. Local variations in indium content lead to local variations of the conduction and valence band energies, potentially allowing carrier capture. As a result, a characteristic "S-shaped" temperature dependence of the emission energy can be observed[81, 82]. At low temperatures, the observed emission stems, mostly, from localized carriers occupying random localization centers, and is therefore shifted to lower energies. With increasing thermal energy, such carriers can be redistributed

to the minima of the band structure (i.e. even deeper localization centers), shifting the emission further to lower energies. At higher temperatures, carrier delocalization results in a shift to larger emission energies, reaching the band-band transition energy (modified, if applicable, by the QCSE). From then on the emission follows the evolution of the band gap with temperature, which can be described by the Varshni equation[83]. This behavior is also expected for a purely random alloy[72], with localization energies in the range of several tens of meV, significantly contributing to the inhomogeneous broadening of the InGaN alloy emission, as well as reducing the radiative rate. Naturally, such localization centers will capture free carriers. On one hand this efficiently keeps the carriers away from non-radiative centers, explaining the unusually large radiative efficiency of bulk InGaN alloys[84]. On the other hand this leads to a locally increased carrier density, potentially enhancing high-carrier density losses (see section 2.2.5 on page 16).

2.2 Properties of InGaN Light-Emitting Diodes

In this section, general properties of InGaN LEDs will be described. First, a brief overview about the state-of-the-art design of such devices will be given. Then, an overview about the microscopic carrier recombination mechanisms in the device active region will follow, motivating the so-called ABC model, commonly used for evaluating device efficiency.

2.2.1 Design of Commercial InGaN Light-Emitting Diodes

Within SSL industry, a de-facto standard has developed regarding the device design for InGaN multiple quantum well (MQW) LEDs[26, 42, 44, 45]. The following points are by no means a complete description (or even growth recipe), but highlight the main choices made, which will be motivated in the following paragraphs.

Commonly, a c-plane (ii) sapphire (i) substrate is used. Using metal-organic vapor phase epitaxy (MOVPE) (iii) several μm (iv) of n-type GaN:Si (v) are deposited, followed often by an InGaN/GaN super-lattice (vi). InGaN QWs (vii) with a thickness of 1 to 3 nm (viii) are grown and repeated several (ix) times with GaN barriers in between (x). The stack is finished with p-type GaN:Mg (xi) in which an AlGaN electron blocking layer (EBL)(xii) is inserted. Such a structure is depicted in figure 2.4 on the next page. Final steps, like wafer processing and chip design go beyond the scope of this work.

i) As growing bulk InGaN layers of sufficient quality and doping the same are very difficult, the growth of the optically active InGaN QWs is almost always performed on a GaN buffer. Such buffers are in turn grown most often on three different types of substrate: silicon[85–90], sapphire (Al_2O_3)[91–96] and bulk-GaN[97, 98]. These are positioned with increasing cost, decreasing availability and decreasing wafer size. The quality of GaN layers grown on these substrates improves drastically along this series, as the lattice mismatch is decreased significantly. While all three substrates find use in industrial production, the vast majority of commercially available LED dies is produced on sapphire substrates, because the price of bulk-GaN substrates remains prohibitive, while the defect density generally found in GaN layers grown on silicon substrates is several orders of magnitude higher than on sapphire.

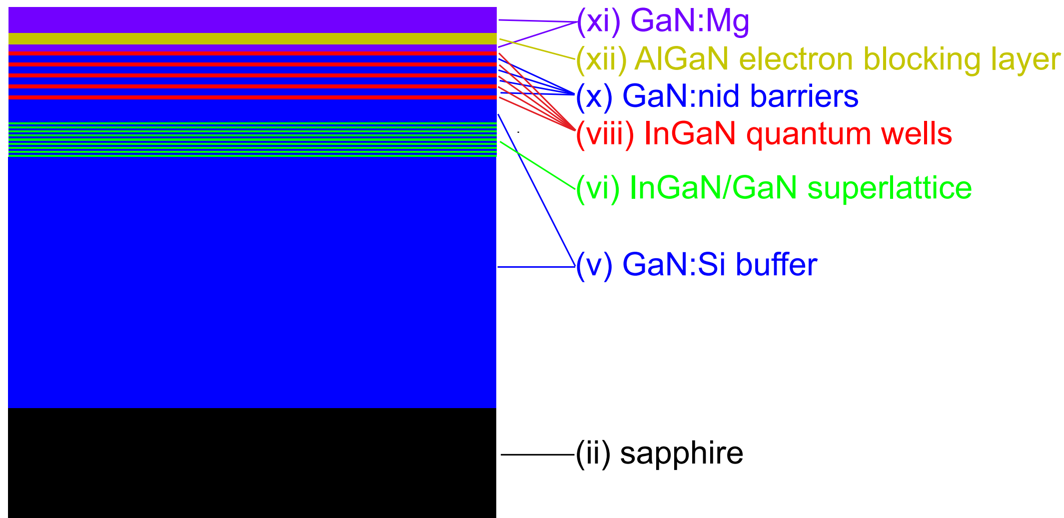

Figure 2.4: Sketch (not to scale) of a typical MQW LED growth sequence (see text)

ii) The sapphire substrates are generally oriented with c-plane surfaces, resulting in c-plane (+c growth direction) interfaces along the device structure. The main disadvantage originated from this choice is that the spontaneous and piezoelectric polarizations (section 2.1.1 on page 3) are the strongest in this direction, which means that the devices suffer from the QCSE. On the positive side, this orientation offers the highest growth rates, and the resulting layer structures have the highest epitaxial quality (planar interfaces, lowest defect density, etc). Nevertheless, much research effort is spent on improving growth in non- or semi-polar orientations in order to avoid the perils of the QCSE.

iii) For cost reasons, most device growth is performed by MOVPE (also called metal-organic chemical vapor deposition), rather than molecular beam epitaxy (MBE). MOVPE allows for much higher growth rates and larger wafer diameters, making such reactors far more productive in an industrial setting. Nevertheless MBE growth remains an important research tool[99–107], as it may allow higher structural quality, because no potentially contaminating carrier gas is required in the process.

iv) Starting the growth with a thick layer of GaN[36, 108] is necessary, in order to reduce the threading dislocation density, identified as a major limiting factor for

device lifetime and efficiency[80]. In addition, growth of a thick layer allows to obtain more or less relaxed GaN, despite the significant lattice mismatch to the sapphire substrate. The growth of such layers is usually started by the nitridation of the sapphire surface[109–111], a step also crucial for the control of the polarity of the GaN grown on top[112]. As the growth is performed at high temperatures (several hundred degrees Celsius), the different thermal expansion coefficients of the materials (sapphire, GaN, InGaN, AlGaN) have to be considered, i.e. some residual strain is desired during growth. For strain management and defect reduction, often layers grown at much lower temperatures are inserted into the GaN buffer[113, 114]. Further, the introduction of AlN interlayers (also grown at lower temperatures) has also been applied very successfully for the same purposes[35, 115–117].

v) Silicon is the most-commonly used n-type dopant in GaN[118–121]. On gallium-site it forms a shallow donor and can easily be incorporated to provide free carrier densities of the order of 10^{19}cm^{-3}. Some diligence is required, as the Si atom is much smaller than Ga and therefore leads to some strain which may lead to cracking or surface roughening[122, 123]. Here, germanium is a suitable alternative as the Ge atom is very similar to the Ga atom it replaces. GaN:Ge therefore offers superior crystalline quality and lower compensation, allowing up to 10^{20}cm^{-3} free carrier concentration[P4, 124, 125]. At the present time, Si remains the most popular n-type dopant, however.

vi) A short period superlattice consisting of GaN and InGaN layers with low indium composition is often inserted immediately below the active region, in order to manage the strain distribution.

vii) In principle, a LED might be realized as a simple p–n or p–i–n-junction. For efficient emission, however, it is necessary to make use of quantum confinement effects[126]. The restriction of the active region in at least one dimension to sizes below the Bohr radius, increases the electron–hole wave function overlap, and the density of states (DOS) in the ground states. While most commercial applications are realized with planar QWs, considerable research effort is and has been spent on different geometries, such as quantum wires[127–130], core-shell quantum rods[131–135] or quantum dots[136–140] (see also chapter 6 on page 85).

viii) In order to reach the desired emission wavelength for the LED, a specific combination of In composition and QW thickness must be chosen. Higher In composition leads to a narrowing of the band gap, as well as an increase in QCSE, both resulting in a shift to lower emission energy. In thicker QWs, the QCSE is increased, also shifting the emission towards longer wavelength (see section 2.1.1 on page 3 and section 2.2.4 on page 15). This design space is limited on one hand by the critical thickness of InGaN[141], reducing to a few nm as the indium composition is increased to around 20% and on the other hand by the so-called miscibility gap, a compositional range where spinodal decomposition is likely to occur at realistic growth temperatures[142], leading to phase separation of the alloy.

ix) As the production cost of LEDs basically scales with the device footprint, stacking multiple QWs is desirable, as this allows to obtain the same luminance from a smaller chip. The potential barriers between the QWs, however, reduce the mobility of the carriers, especially holes. Therefore only a limited number of QWs can be efficiently pumped electrically[A2, 143–146]. In practice the number of QWs tends to be between three and ten.

x) Generally, GaN is used as barrier material. Other barrier materials might offer some advantages: Using InGaN barriers with lower In composition than the QWs[146] results in lower lattice mismatch and reduced piezoelectric fields, AlGaN barriers[147] produce higher potential barriers and hence better carrier confinement, and AlInN barriers[148] may be used as a compromise. However, GaN barriers are naturally lattice matched to the underlying GaN buffer layer and can also be planarized relative easily, which significantly improves the interface quality towards the following QW.

xi) For a long time, the realization of efficient III–N–devices was precluded by the lack of sufficiently good p-type doping. The successful growth of GaN:Mg in the early 1990s[22–24] paved the way for all current applications and was awarded with the Nobel Prize in Physics in 2014. Nevertheless, p-type doping of GaN remains much more challenging than n-type. Mg on Ga-site is a relatively deep acceptor, and several compensation mechanisms are known [149–157], such that typically only a few percent of the incorporated Mg atoms are electrically active. Free hole densities are therefore always orders of magnitude lower than the Mg dopant

density, even after the usual thermal annealing step to get rid of hydrogen, which often forms compensating complexes with Mg in GaN. Because the Mg acceptor in AlN is even deeper than in GaN[158], p-type doping of AlGaN, as used in the EBL of LEDs or in the cladding layers of edge-emitting LDs is even more difficult, ultimately limiting the performance of GaN-based LDs[159].

xii) The mobility of the electrons in GaN is much higher than that of holes[29]. In consequence, even in a MQW stack, and despite the much larger band offset in the conduction compared to the valence band[160, 161], a significant part of the injected electrons would reach the p-side of the device[93, 162–164] and recombine there. Hence, the insertion of an AlGaN-EBL is necessary, providing a blocking barrier for electrons.

2.2.2 Efficiency of InGaN Light-Emitting Diodes

The figure of merit for a light emitter is the wall-plug efficiency, i.e. optical output power divided by electrical input power. This combines the quantum efficiency (QE) of the device with external factors, like the required power conversion (from 110/220V AC to 5V DC). Here, we will focus on the QE, which can be expressed in two forms. The first is called the external quantum efficiency (EQE). This is defined as the ratio of photons leaving the device (in the desired photon energy range) to injected electrons and holes. Here, different definitions exist, either counting carries entering the QWs, or carriers entering the doped layers. The scaling between these two quantities is the injection efficiency, i.e. the probability that an electron from the n-side and a hole from the p-side reach the QWs. Generally, for devices such as those described in section 2.2.1 on page 8, this can be assumed to be unity. A more fundamental quantity is the internal quantum efficiency (IQE), which is related to the EQE via the extraction efficiency η: $\mathrm{EQE} = \eta \mathrm{IQE}$. η is the probability that a photon generated in the active region of the LED leaves the device. It therefore includes losses from scattering and reabsorption. The IQE then describes the ratio of photons produced in the LED active region to electron–hole pairs inserted into the same. It can therefore be written as $\mathrm{IQE} = \frac{N_{rad}}{N_{rad}+N_{nonrad}}$, i.e. the number of processes leading to the emission of a photon as a fraction of the total number of processes, where an electron recombines with a hole.

2.2.3 Radiative and Non-Radiative Recombination Processes

The desired recombination process is the radiative one[165]. Here, an electron–hole pair annihilates producing a photon with the same energy according to Fermi's golden rule[166]. In a direct semiconductor such as InGaN, this process can, and usually does, happen without the help of phonons, as no momentum conversion is necessary. The rate of the radiative recombination depends on the matrix element of the transition, which is chiefly governed by the overlap between the electron and hole wave functions participating in the transition. It also depends linearly on the concentration of electrons n and holes p and can therefore be written as $R_{rad} = Bn^2$, if electron and hole densities are taken to be the same, where B is the radiative recombination coefficient.

The first non-radiative recombination process, which needs to be considered, is the Shockley-Read-Hall (SRH) recombination[167, 168]. Here, a charge carrier is captured by a trap state in the forbidden zone of the band gap and subsequently recombines with the other carrier type non-radiatively (i.e. emitting phonons) or radiatively (i.e. emitting photons with a much larger wavelength than desired). Such traps may be formed by defects in the crystal lattice. These can be native point defects, such as vacancies or interstitials, foreign point defects such as impurity or doping atoms, or extended structural defects, e.g. threading dislocations. The rate of SRH processes depends therefore on the density of trap states, on their capture cross section for the carriers and on the overlap necessary for the recombination leading to the depopulation of the trap. As trapped carriers are localized strongly the latter is rather low, which means that the lifetime of a carrier in such a trap is comparably large, typically in the μs range. The main process necessary for SRH recombination is the trapping of a specific charge carrier type (either electron or hole, depending on the trap), it goes linear with the charge carrier density, i.e, $R_{SRH} = An$, where A is the SRH recombination coefficient.

At higher carrier densities another non-radiative process needs to be considered, involving three particles - either two electrons and a hole or one electron and two holes: Auger recombination[169, 170], named after the eponymous effect in atoms[171]. Here, an electron–hole pair recombines (similar to radiative recombination), but the excess energy is transferred to another electron or hole, lifting it high up into the conduction or valence band, respectively. As three carriers are required for any Auger process, the Auger rate can be expressed as $R_{Auger} = Cn^3$, where C is the Auger recombination

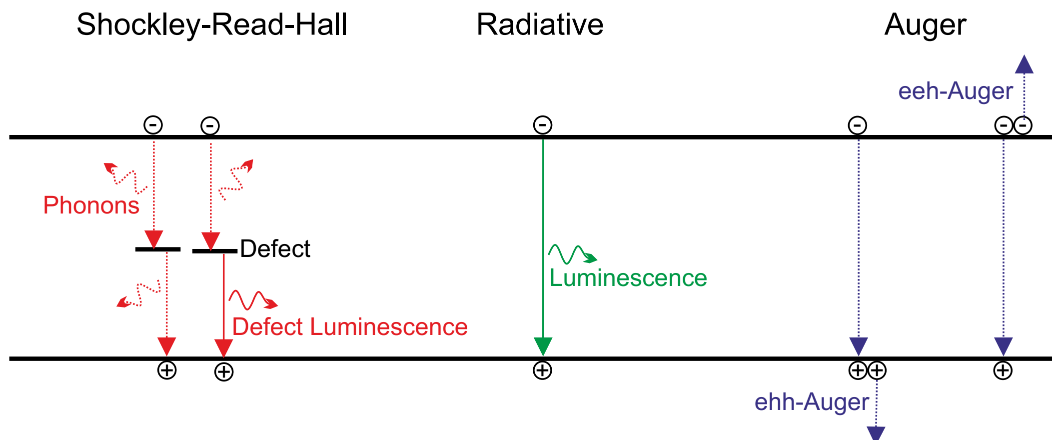

Figure 2.5: The principal recombination channels: SRH-recombination, involving a defect state in the forbidden zone of the band gap. Radiative recombination, producing a photon of the desired energy. Auger recombination, energy transfer to an additional hole (ehh) or electron (eeh).

coefficient.

These recombination channels are depicted schematically in figure 2.5. Other processes that one may consider, but have proven to be negligible in the context of the devices discussed here, are surface recombination[172], thermal escape of carriers (because of the large band offsets), or self-absorption (because of the Stokes-like shift between emission and absorption). Only taking into account the dominant recombination mechanisms mentioned above, the IQE can be written as:

$$\mathrm{IQE} = \frac{Bn^2}{An + Bn^2 + Cn^3} \tag{2.1}$$

This model is referred to as ABC-model in the literature[164, 173–175]. While being relatively simple, it adequately describes the IQE of state-of-the-art devices[176] over multiple orders of injected current, and hence carrier density. Section 5.1 on page 46 will show how this model can be reformulated in order to gain insight into the recombination coefficients with easily accessible physical quantities. This is important, as the carrier density n is hidden and can only be measured in indirect ways, such as integration over the whole emission of the device (Bn^2) in an Ulbricht sphere. In the following two sections, two phenomena commonly observed in InGaN LEDs' IQEs will be described. These limit the efficiency of existing III–N devices and hinder more

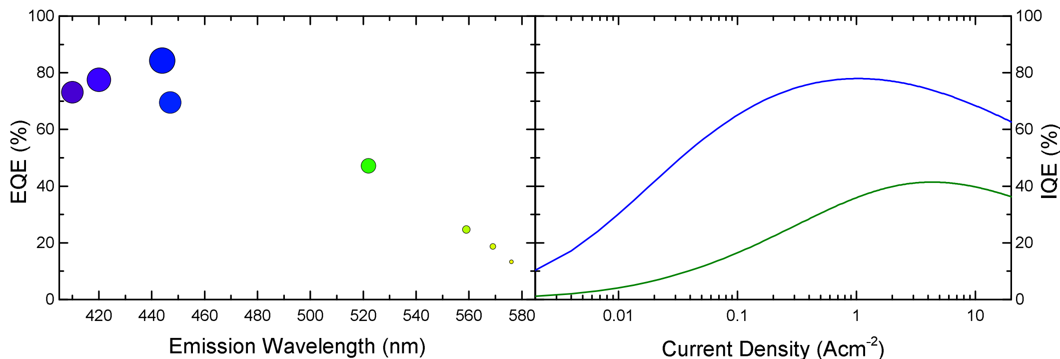

Figure 2.6: Left: The green gap: Evolution of recently reported[91, 177–179] peak EQE as a function of emission wavelength. Here, a strong reduction of efficiency towards the green spectral range is observed. Right: The droop: IQE as a function of drive current density for a typical blue- and green-emitting LED. At high current densities the IQE reduces due to Auger losses.

advanced applications, such as green-emitting LD.

2.2.4 The "Green Gap"

Phenomenologically, the IQE is observed to reduce very significantly as the emission is tuned from blue (420 nm) to green (530 nm)[26, 45]. This is visualized in figure 2.6a, where reported peak EQE values of state-of-the-art LEDs are plotted against the emission wavelength. Similarly, the efficiency of AlGaInP-based LEDs drops significantly, if the emission wavelength is tuned from red to green. This lack of highly efficient emitters in the green spectral region is called the "green gap". In contrast, commercial phosphor-based dyes have a conversion efficiency of close to 100%. If such phosphors are pumped by the much more efficient blue LEDs available today, the combined efficiency of blue InGaN LEDs and the blue-to-green converting phosphor is significantly higher than directly green-emitting InGaN LEDs, despite the inherent Stokes losses incurred. Here, it is noted that, despite the involvement of several large industrial corporations, no breakthrough in the IQE of green devices has been made in the last years, hinting that a fundamental limitation of the standard approach (section 2.2.1 on page 8) might be the origin. As a result, current white-light solutions, as used in SSL, do not employ green-emitting LEDs. Rather, they are build from blue-emitting In-

GaN chips, red-emitting InGaAlP chips and blue-absorbing and yellow-green-emitting phosphors. Sometimes, also the red part of the spectrum is produced by phosphors. A more efficient green emitter would immediately enable direct RGB (red, green and blue), all-LED solutions, promising much better color rendering[180].

In order to shift the emission of InGaN QWs into the green spectral region, one needs to increase the Indium content of the QWs, increase their thickness, or both. Both measures lead to an increase of the internal pyro- and piezoelectric fields, and therefore QCSE (section 2.1.1 on page 3). As a result, the electron-hole-overlap shrinks, decreasing the radiative recombination coefficient B, and finally IQE[59, 60, 68, 181, 182]. While some room for QW parameter variation exists (high In content, thin QW versus low In content, thick QW), the general effect cannot be avoided in the conventional c-plane orientation. Therefore, the solutions considered in the literature often entail more-or-less dramatic changes to the device concept (see chapter 6 on page 85 for a few examples), entailing different geometries or growth surfaces. Alternatively, one may also consider optimization of the existing, polar QW structures, with the explicit goal to decrease the QCSE, increase the electron-hole wave function overlap, or decrease the radiative lifetime. Unfortunately, such studies are often confined to theoretical considerations with little regard of the practical realization of the suggested improvements, or show, experimentally, improvements obtained by varying some parameter, without a state-of-the-art control structure. With this in mind, one aim of this thesis is to gain a more general understanding of the physical origin of the green gap.

2.2.5 The “Droop”

Another constantly observed phenomenon in InGaN MQW LEDs is the so-called “efficiency droop”, a reduction of IQE with increased drive current, seriously limiting the output power of such devices[92, 164, 173, 174, 183]. It follows from equation (2.1) on page 14, that the IQE depends strongly on the carrier density in the active region. As a function of drive current, and hence carrier density, the IQE first increases, as non-radiative SRH recombination is saturated and then decreases again. This is a clear sign of a non-radiative process, growing faster with carrier density than radiative recombination. This is displayed in figure 2.6b assuming recombination coefficients found in state-of-the-art blue- and green-emitting LEDs[A3]. Many processes, for example carrier leakage (i.e. escape of electrons from the active region), might be considered as

the origin of this phenomenon. A comparison between electrical and (resonant) optical excitation, which both show the droop effect, clearly identifies the droop mechanism to happen within the QW itself[92].

Hotly debated[90, 94, 96, 184], recent experimental evidence has confirmed Auger recombination to be the culprit. This finding was either achieved by direct detection of the hot electrons generated in the Auger process[185], or by conversion of the Auger-excited carriers to UV luminescence in purpose-grown structures [186]. A theoretical estimation of the Auger recombination coefficient is difficult, because many different processes may contribute to it. The processes can be of the electron-hole-hole (ehh) or electron-electron-hole (eeh) type. The final state of the third carrier may be in the same (intraband) or in a different (interband) band[187], and the transitions may also involve phonons, making this many-body-problem even more complicated[188]. From conventional expectations for direct semiconductors[164, 184], where Auger recombination coefficients decrease drastically as a function of band gap, C should be negligible in wide band gap materials and several orders of magnitude lower than commonly observed, or inferred from the droop behavior. This discrepancy can be resolved, if phonon-assisted (i.e. indirect) Auger processes are considered as well[188]. Nevertheless such calculations can only suggest that the observed Auger recombination coefficients are feasible and indeed originate from Auger processes, but they cannot reliably indicate which microscopic Auger processes are dominant. Meanwhile, some experimental evidence suggest that the dominant Auger processes are of the eeh-type[186, 189, 190] or even attempt to pin them to specific valence bands[191].

Similar to the situation with the green gap the literature is full of studies suggesting specific improvements to the device structure, but has failed to generate any breakthroughs in suppressing Auger recombination. On one hand this is because the microscopic Auger processes that dominate the droop are poorly understood, making it very difficult to combat them. On the other hand, the most obvious solution, reducing the carrier density, is both very easy as a concept and very difficult in reality.

2.3 Open Questions

In normal operating conditions of a LED, the droop phenomenon has been shown to originate from Auger processes. The limitations in high-power, and hence high-excitation, regimes are, however, less clear. This is of particular importance for LDs, where high carrier densities are required to obtain lasing and high gain. Strikingly, green InGaN LDs are even less successful than green InGaN LEDs, suggesting that further loss channels might exist and be relevant. Chapter 4 on page 29 will therefore investigate state-of-the-art InGaN/GaN QWs pumped resonantly with large excitation power densities. Here, a novel loss mechanism comprising excited, less-localized hole states is revealed.

While Auger recombination has been made responsible for the droop, the physical limit of current state-of-the-art LEDs in conventional power regimes is a matter of intense debate. In particular, the interplay between droop and green gap is not clear, even though they both rely on and influence the same measure - IQE. One may think that the increase of QCSE as the emission is tuned towards the green spectral region, or the increasing hurdles to obtain high quality material may be sufficient to explain the green gap. However, to truly understand the origin of this efficiency limitation, access to the recombination processes is vital. This is only possible by investigating the carrier recombination mechanisms within the device, e.g. by observing the carrier dynamics during operation. For this purpose, chapter 5 on page 45 will present a novel method to measure the differential lifetime (DLT) using an electro-optical pump-probe method. Combined with electroluminescence (EL) measurements, these can be used to determine the recombination coefficients corresponding to the principal recombination channels. These, in turn, allow to assess the causal connection between defect density (SRH recombination), conventionally blamed for the green gap, QCSE (reduction of the radiative rate), also made responsible for the green gap, and the magnitude of Auger recombination, usually only discussed in the context of the droop. As it turns out, the localization of holes, inherent to InGaN alloys, is a much neglected ingredient to the green gap.

3 Experimental Methods

3.1 Sample Growth

The samples presented in this work, were grown by metal-organic vapor phase epitaxy (MOVPE) at Osram Optosemiconductors GmbH. Two groups of samples were grown:

1) In order to investigate the optical properties of InGaN quantum wells (QWs), so-called quasi-single quantum wells (SQWs) were grown. Each of these samples consists of five InGaN QWs, which can be considered SQWs, as the GaN barrier between them is exceptionally large (around 17 nm), preventing any coupling between them. They are grown on standard c-plane templates and nominally undoped. Such a structure is sketched in figure 3.1 for a QW thickness of 3 nm. The thickness of the QWs is varied between 2.2 nm and 4 nm and the In content is generally around 20%. In particular, one series of samples with different thickness was grown with constant In content, while another was grown with varying In content, but the same emission wavelength, i.e. increasing In content with decreasing thickness. These samples are covered in chapter 4 on page 29. The findings presented therein are verified by investigating control samples, which feature either doped barriers, or no QWs at all.

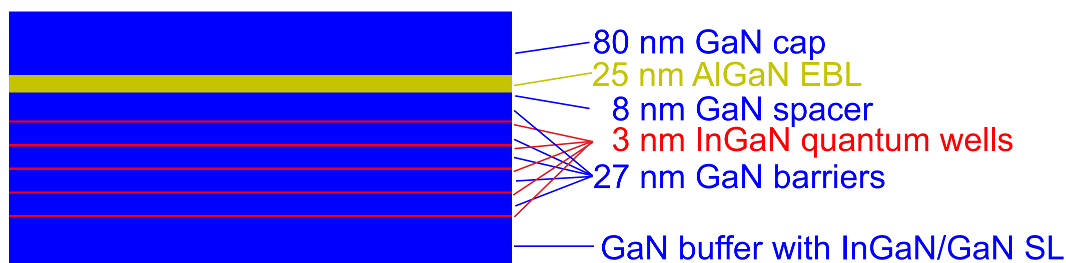

Figure 3.1: Schematic drawing of the active region of a a quasi-SQW sample with 3 nm QW thickness.

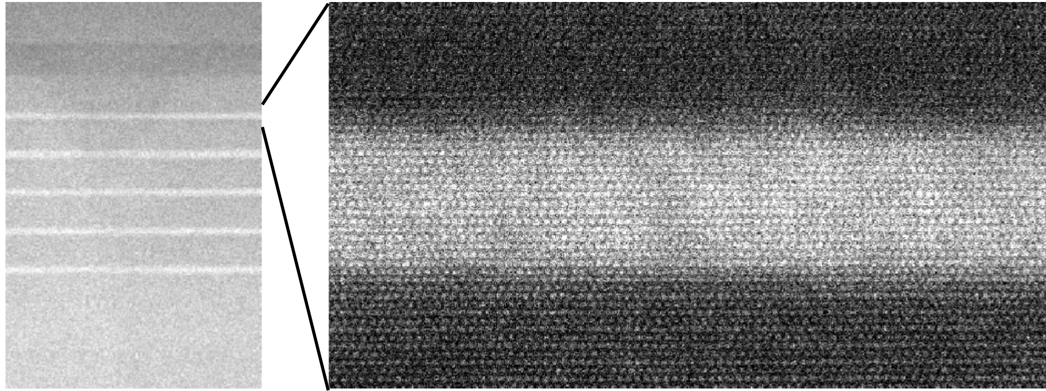

Figure 3.2: HRTEM micrograph (courtesy T. Schulz, IKZ Berlin) of a quasi-SQW sample with 4 nm thick QWs.

2) Investigations with the aim to obtain the recombination coefficients under realistic operating conditions are carried out on state-of-the-art light-emitting diode (LED) structures. The epitaxial structure is as described in section 2.2.1 on page 8, figure 2.4. The devices investigated consist of one to seven QWs with emission wavelengths in the blue (440 nm) to green (530 nm) spectral region. They are of the highest available epitaxial quality and packaged in a standard commercial package (Golden Dragon+), which easily allows to drive them electrically. The package features a large metallic back contact, which is also used to regulate the device temperature by bringing it into thermal contact with the cryostat. These samples are covered in chapter 5 on page 45.

The state-of-the-art epitaxial quality of the samples is confirmed by high-resolution transmission electron microscopy (HRTEM) measurements as shown in figure 3.2. In particular, no thickness fluctuations beyond a single monolayer are observed and no fluctuations of the indium composition of the quantum well can be detected, suggesting entirely random alloying. The interfaces are sharp and the density of V-shaped pits is low, implying almost perfect QWs.

3.2 Optical Spectroscopy

Various optical spectroscopy methods were applied or developed in the context of this work, which will be briefly outlined below.

3.2.1 Electroluminescence

Electroluminescence (EL) is a luminescent process (electron–hole recombination) which originates from carriers, which were inserted into the device by an applied bias. The method therefore requires an electrical device, such as a LED. For a LED, an EL-measurement is just the measurement of the emitted light during operation. For this work, EL was driven by either a DC current source, or alternatively a frequency generator. The latter was used to reduce the thermal load of the device during the EL measurement (pulsed EL[176]). The signal from the devices was collected through a μ-PL setup, dispersed through a 30 cm focal length Princeton Instruments monochromator, and detected by a Princeton Instruments charge-coupled device (CCD). For the purposes of characterizing the device's external quantum efficiency (EQE), the resulting spectra were integrated to obtain the total EL intensity.

3.2.2 Photoluminescence

In photoluminescence (PL), the carriers required for luminescence are generated by absorption of light[192], usually from a laser source. Several setups were used for such measurements, which will be described briefly below:

A) The most used setup in the frame of this work is sketched in figure 3.3 on the following page. It consists of a Spectra Physics Tsunami Ti:Sa laser, pumped by a frequency-doubled Nd:YAG. Optionally, the laser light can be directed through a Coherent Model 9200 Pulse Picker, allowing to reduce the repetition rate from 80 MHz into the kHz range. Subsequently, the laser beam is frequency-doubled by an APE HarmoniXX second harmonic generation system. The beam is then directed onto a beam splitter and enters a standard μ-PL setup in backscattering geometry. The samples were placed inside a Janis Helium flow cryostat, offering a temperature range of 10 to 350 K. Passing the beam splitter again, the PL signal enters a single stage 30 cm focal length SpectraPro 300i monochromator equipped

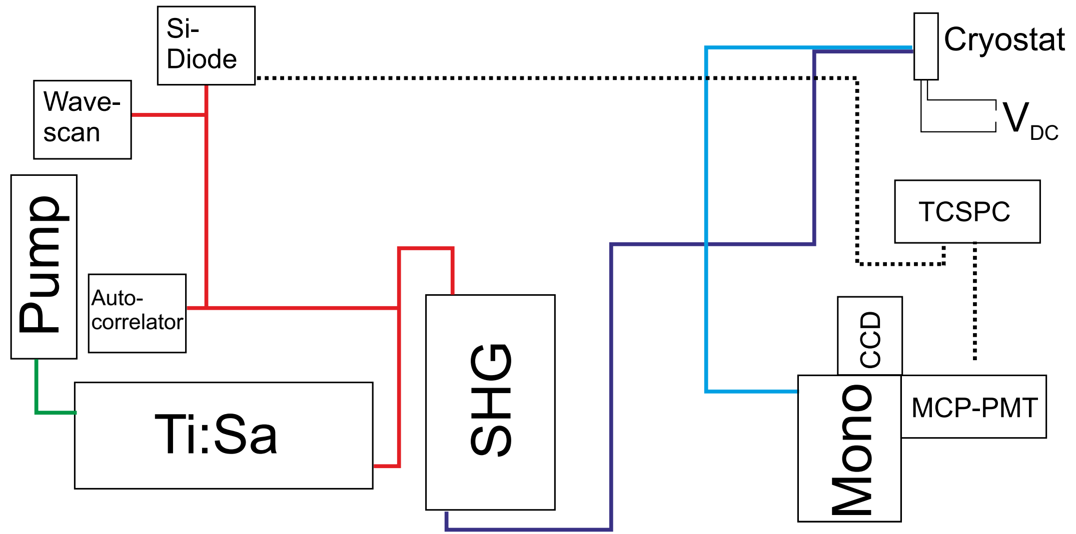

Figure 3.3: Sketch of PL setup A, used for resonant TRPL (ps-ns range), SSTRPL, EL

with 600, 1200 and 1800 lines/mm gratings. PL spectra were recorded utilizing a Princeton Instruments liquid nitrogen cooled, UV enhanced, Si-CCD. For time-resolved detection, a Peltier-cooled Hamamatsu multi-channel plate-photomultiplier tube (PMT) (S20 cathode) was used, whose single photon events were fed into a Becker&Hickl time-correlated single photon counting (TCSPC) measurement card (SPC-130), or were resolved by a PicoQuant PicoHarp300 system.

B) This second setup, shown schematically in figure 3.4 on the next page permits to use high excitation powers, as it features a Coherent Compex Pro XeCl Excimer laser, which pumps a Lambda Physics FL3001 dye laser. Employed dyes include 2-Methyl-5-t-Butyl-p-Quarterphenyl (DMQ) and Coumarin 102. The excitation light was reflected onto the sample by a small mirror, situated in the back scattering detection path. The sample was mounted either in a Oxford Instruments Helium flow cryostat, or in a custom Helium bath cryostat (i.e. situated in superfluid Helium at approximately 1.8 K). The PL signal was then dispersed by a SPEX 1404 0.8 m focal length additive double monochromator with 1200 lines/mm, 500 nm blaze gratings and detected by a TCSPC-able Hamamatsu Bi-Alkali PMT.

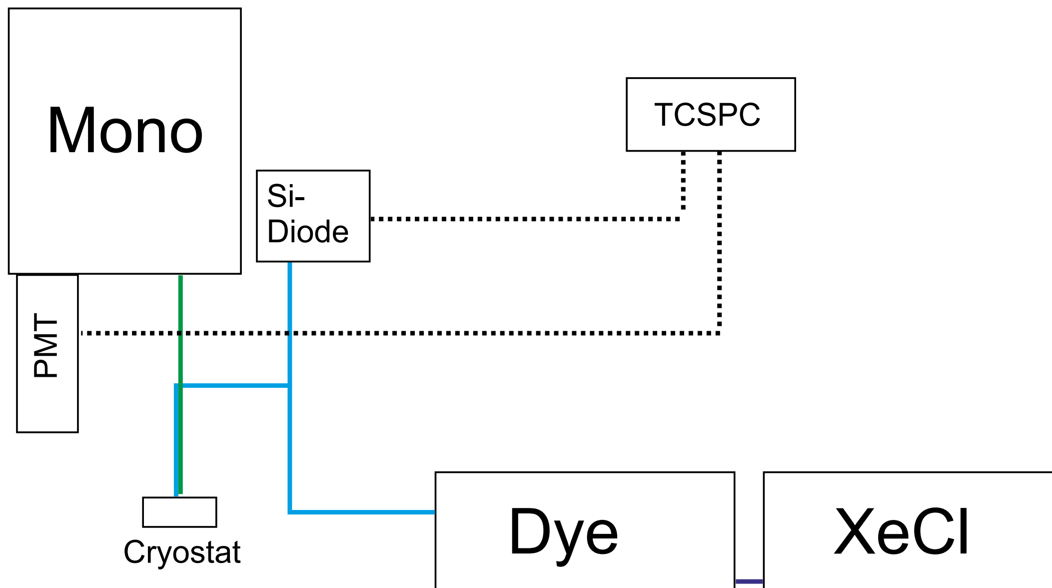

Figure 3.4: Sketch of PL setup B, used for resonant TRPL (ns-ms range), high-excitation PL

C) The third setup (figure 3.5 on the following page) was used for photoluminescence excitation spectroscopy (PLE). Here, a 500 W Xenon arc lamp was monochromatized by an additive double monochromator (Princeton Instruments SpectraPro 300i), and focused onto the sample, situated in a Janis Helium flow cryostat with an angle of 45°. The PL signal was then detected orthogonal to the sample surface and dispersed by a 1 m focal length SPEX 1704 single monochromator with a 1200 lines/mm, 300 nm blaze grating and recorded with a Princeton Instruments liquid nitrogen cooled, UV enhanced, Si-CCD.

3.2.3 Photoluminescence Excitation Spectroscopy

In a PLE measurement, the excitation wavelength is varied and the intensity of the emitted light is measured as a function thereof. The intensity then varies as a function of absorption of the material at the used wavelength and the transfer from the electronic states responsible for absorption to the electronic states responsible for luminescent emission. The combination of absorption and energy transfer is usually referred to as excitation channel of a specific luminescence.

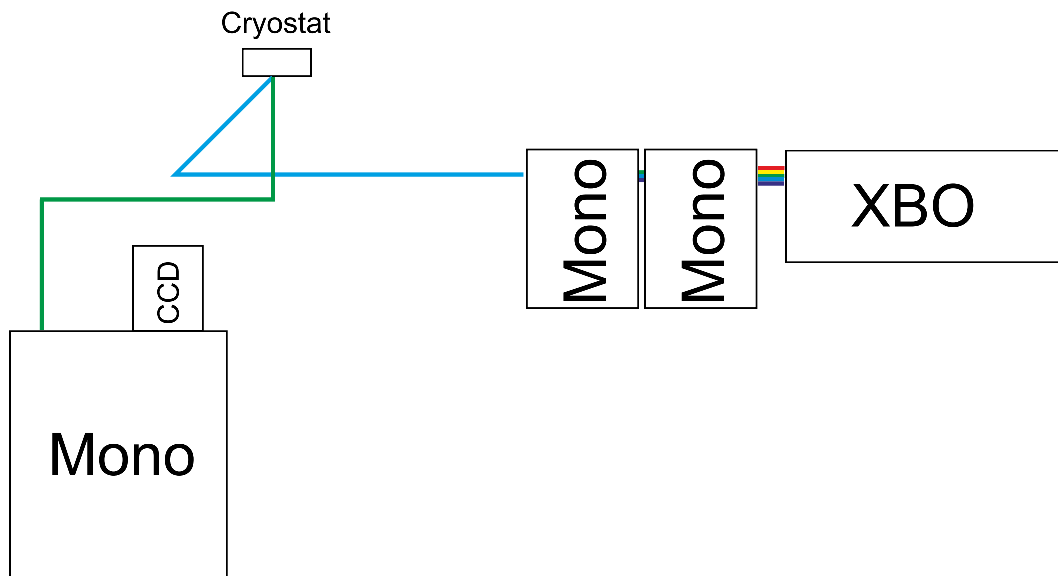

Figure 3.5: Sketch of PL setup C, used for PLE

3.2.4 Time-Resolved Photoluminescence

To study the dynamics of a system, it is very useful to use TRPL. Here, a time-modulated (in this case pulsed) light source is used, and the luminescence response of the system as a function of time delay is monitored. In the most simple case, one would expect an exponential decay following the excitation event, with the characteristic time of the decay corresponding to the carrier lifetime in the specific electronic states responsible for the PL transition. Obviously, in reality the picture is usually more complicated, as energy transfer processes (see PLE) and multiple competing decay channels make the dynamic processes more complex. TRPL was measured in setups A) and B). The excitation sources were A) a frequency-doubled Ti:Sa laser with a pulse duration of 2 ps and a variable repetition rate (utilizing a pulse picker) of up to 80 MHz and B) a XeCl-laser pumped dye laser with a pulse duration of around 15 ns and a repetition rate of 100 Hz. In combination, these setups allow the whole time range from a few ps to several μs to be covered. It should be noted here, that the high excitation power densities inherent to pulsed laser sources may lead to high excitation effects (see chapter 4 on page 29), which may be unwanted, for example if the pulsed source is used as a probe event (see section 5.2 on page 49). Therefore, careful tuning

of the excitation power density is often required.

3.2.5 Small-Signal Time-Resolved Photoluminescence

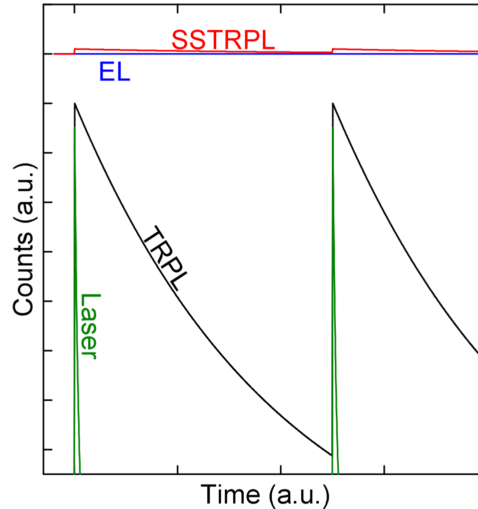

Figure 3.6: Sketch of the SSTRPL method: In conventional TRPL a pulsed laser (green) is used to excite electron-hole-pairs which then recombine with a specific lifetime (black). In EL, a constant current causes a constant signal (blue). Combining both methods, i.e. constant current and attenuated laser excitation, yields the SSTRPL signal.

SSTRPL[A2] combines EL with TRPL in order to measure the differential carrier lifetime, i.e. the lifetime of a carrier added to a steady-state carrier population. Here, the device is driven by a DC source, like in EL and additionally excited by the previously mentioned Ti:Sa laser, tuned into resonance (setup A)). This method is depicted in figure 3.6. Note that, as a small-signal method, the dynamic range of the signal is much reduced in comparison to conventional TRPL, making longer integration times necessary. Further, in this scheme confocal laser excitation and detection spots are absolutely vital to achieve acceptable signal-to-noise ratios. Details regarding the SSTRPL measurement procedure, developed during this work, can be found in section 5.1 on page 46.

3.2.6 Carrier Injection and Resonance Conditions

Please note the fundamental differences in the way carriers are injected into the active layers in the presented methods, sketched in figure 3.7 on the next page. Using EL (top left), electrons and holes are injected into the respectively doped GaN layers and transferred to the active region by the applied bias. In an ideal diode, no recombination

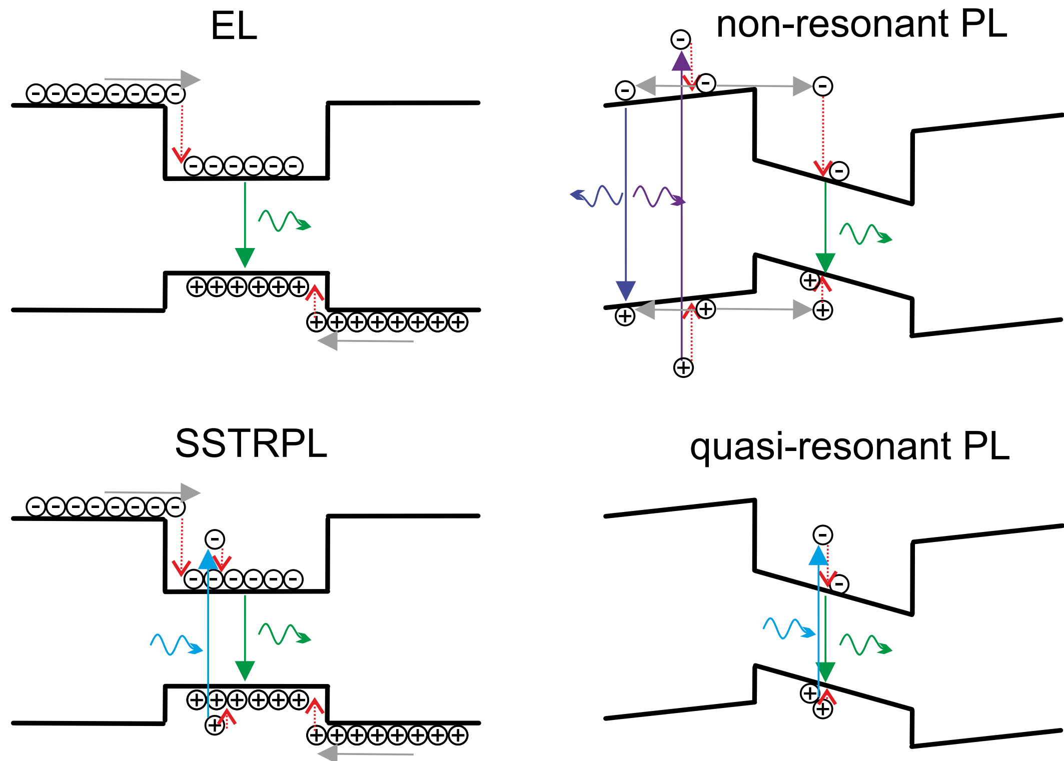

Figure 3.7: Schematic overview of the different excitation mechanisms. From top left clockwise: Electroluminescence, non-resonant photoluminescence, quasi-resonant photoluminescence, small-signal time-resolved photoluminescence. Red arrows show phonon-mediated relaxation processes, grey arrows carrier transport within the structure.

is possible outside of the p–n–junction, as the opposite charge carrier necessary for this process is not available. EL therefore guarantees recombination to stem from the active region. In PL, incident light is absorbed and creates electron–hole pairs. If the exciting photon energy is higher than the GaN band gap, the excitation is called non-resonant (top right). In this case, not only the InGaN QWs absorb the incident light, but also the GaN layers do, e.g. the capping layer. As a result, most of the electron–hole pairs are created in GaN and the carriers need to be transported to the InGaN QWs through carrier diffusion. They may, however, recombine before reaching the active layer, limiting the efficiency of this injection path. In order to guarantee optical absorption in the QWs a quasi-resonant excitation is necessary (bottom right). Here, the excitation photon energy is situated between the emission energy of the QW and the band gap of GaN. Therefore, the GaN layers are transparent for the incident light and the electron–hole pairs are created in the QWs only. In contrast to truly resonant excitation, the excitation and emission energies differ, which means that the carriers need to relax into the ground states with the help of phonons. As the density of states (DOS) rises with excitation energy, such quasi-resonant conditions offer higher absorption, and hence luminescence signal, than resonant conditions. Please note that under electrical injection, the carriers enter the InGaN QWs with an energy corresponding to the GaN band edges. This means that the optical excitation most resembling electrical injection is quasi-resonant, with a photon energy close, but slightly below the GaN band gap. For this reason, excitation wavelengths in the range of 370 to 400 nm were usually used within this work. A striking difference between such almost non-resonant excitation and EL, however is the lack of an applied voltage in the former. This is particularly notable, as the electric field counteracts the quantum-confined Stark effect (QCSE), i.e. the internal fields are reduced by biasing the device. For this reason, SSTRPL combines EL (internal field strength and carrier density as during operation) with quasi-resonant TRPL (direct injection into QW) in order to access the carrier dynamics in InGaN multiple quantum well (MQW) LEDs, see section 5.1 on page 46 for details.

4 Excited States in InGaN Quantum Wells

4.1 High-Excitation Effects in Semiconductors

Generally, one can distinguish three kinds of high-excitation effects often observed in optically-pumped semiconductors:

4.1.1 Heating

The most obvious effect is lattice heating. One cause for this is that the excitation photon energy is, for practical reasons, usually not exactly in resonance with the detection photon energy. The electron-hole-pairs are therefore not created in their ground states. The relaxation processes into these are usually mediated by phonons, i.e. heat. In the ground state, the carriers may recombine radiatively, but they may also recombine non-radiatively (see section 2.2.3 on page 13) - again emitting phonons and contributing to heating. Whether such lattice heating leads to a significant change in device temperature is determined by the ratio between heat generation and heat dissipation, where the latter is achieved by thermal or electronic transport. Note that the limiting factor for heat conductivity is not necessarily the investigated semiconductor, it might also be the interface to air, heat radiation into vacuum or the thermal contact to the cryostat. Therefore the individual heat conductivity of the whole arrangement (cryostat, sample, etc) limits the excitation power density achievable without local lattice heating.

4.1.2 Large Carrier Density

If high excitation power densities are used, this will, due to the finite lifetime of the carriers, usually result in an increased quasi-equilibrium carrier density. This leads to effects, which can also be observed in highly-doped semiconductors, such as band filling[193, 194], band gap renormalization and Burstein-Moss-Shift[193, 195]. Under

intense excitation, these effects are observed for both electrons and holes at the same time, rather than only for the carrier type originating from the doping. Here, the carriers start to occupy higher states in the conduction and valence bands (i.e. with $k \neq 0$), broadening the emission spectrum to higher energies. In addition, the coulombic interaction reduces the band gap slightly. As a result, the photoluminescence (PL) peak is observed to broaden with a characteristic shape, as the high-energy flank is given by the Fermi distribution of the carriers in the bands.

4.1.3 Excited States

In bulk materials, higher bands usually do not contribute significantly to the emission, as the interband relaxation into the lowest energy band is much faster than the recombination and the density of states (DOS) always provides states easily accessible via phonons. In lower dimensional material, this is not the case. Here, the ground states (i.e. the lowest bands of the band structure, restricted due to the dimensionality of the system), may be saturated if the generation of electron-hole-pairs overcomes the finite recombination rate. In this case, carriers relaxing into excited states may not be able to relax further into the ground state (Pauli blocking) and recombine in the excited states. Such recombination yields photons of higher energy, which may not be useful for the intended use of the device. In addition, the radiative lifetime of carriers in the excited states is usually much larger than the relaxation time into the ground state would be, i.e. the carriers spend more time in the excited state as compared to lower pump density conditions. In these states, the energetic separation from bulk barrier states is much lower than in the ground states, meaning that lower energies, potentially comparable to the thermal energy kT, are required to extract the carriers from the quantum wells (QWs). This gives rise to additional carrier losses[P1]. Generally, recombination of excited state carriers yields emission lines distinct from the ground state recombination. In the case of InGaN QWs, the peak may be less broad than the ground state transition, as the excited state wave functions are less influenced by the local indium composition (section 2.1.2 on page 5). The wave functions also provide more overlap, both because they are less localized in-plane and have a larger extent out-of-plane. As a result, the lifetimes are generally lower than that of the ground state transitions. Such excited state transitions can also be observed in absorption spectra, even at pumping levels where no emission from them is visible.

4.2 Optical Properties of High-Quality InGaN Quantum Wells

This section will briefly elaborate on the properties of the samples A) sketched in figure 3.1 on page 19. Comparing these samples to standard light-emitting diodes (LEDs), the difference are:

1. Lack of doped contact layers, as these may induce parasitic luminescences, associated with the doping impurities[151, 156, 157, 196].

2. With a thickness of 17 nm, the GaN barriers between the InGaN QWs are unusually large in order to avoid coupling effects between the QWs. The samples are therefore comparable to single quantum wells (SQWs), but with more active material.

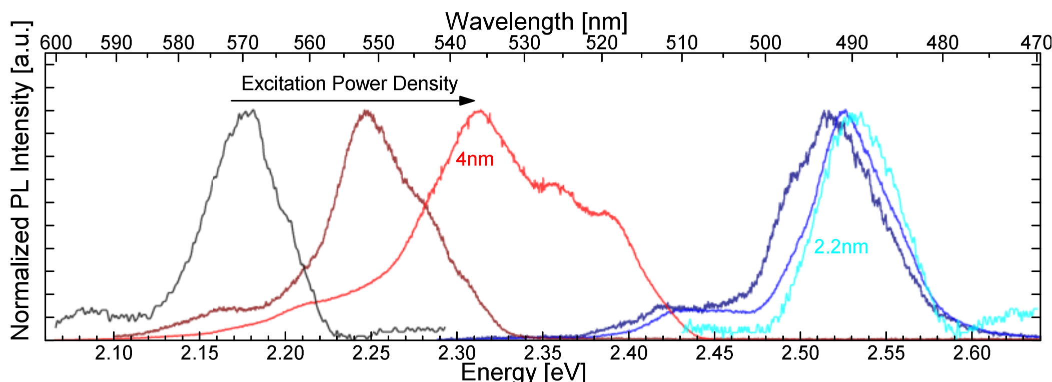

Figure 4.1: Typical PL spectra of quasi-SQWs. With increase of excitation power density (dark to light colors, Xe arc lamp, 325 nm line of a HeCd laser respectively) the PL signal obtained from a 4 nm (2.2 nm) thick QW sample shown in red (blue) shifts towards higher energies due to screening of the QCSE

Figure 4.1 shows typical PL spectra of such structures, obtained with different excitation power densities (either with a Xenon arc lamp or with the 325 nm line of a HeCd laser). Here, a strong shift of the emission towards higher energies is observed for a sample containing very thick (4 nm, red lines) quasi-SQWs. This is the signature of the QCSE, which is partly screened as the carrier density is increased in the active region by the pump laser. In contrast, for QWs with the same nominal In content and a thickness of only 2.2 nm, almost no shift is observed. This reduction in QCSE

is caused by the lower thickness of the QW layer, which does not allow for carrier separation, as it is comparable to the Bohr radius. Note that the QCSE is especially pronounced for these quasi-SQWs, as the samples are nominally undoped. In doped samples such as complete LED structures, the carrier density caused by the doping already screens part of the internal fields even without any pumping. In figure 4.2,

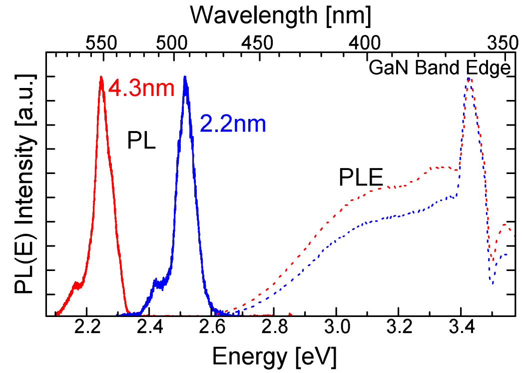

Figure 4.2: Typical PLE spectra of quasi-SQW structures. While PL emission from samples with similar In composition, but different QW thicknesses differs due to the QCSE, their absorption traces are almost identical.

the emission of these two samples is compared with the PLE signal obtained with a Xenon arc lamp. Please note that the absorption edges are basically identical, which is not surprising as the In composition is the same. The emission is shifted (in the case of the thicker QW, strongly), towards lower energies. This Stokes-like shift is a direct manifestation of the QCSE. The strong peak in the PLE spectrum is associated with the GaN band edge and corresponds to a charge transfer from the GaN barriers into the InGaN QWs. There are no signs of discrete excited electronic states in these PLE spectra. The stronger Stokes-like shift to longer wavelengths can be compensated by adjusting the In composition of the QWs. A series with the target wavelength of 510 nm is shown in figure 4.3 on the facing page. Note that this wavelength is reached only at moderate excitation power densities (achieved with a HeCd laser, figure 4.3b). At much lower excitation density (Xenon arc lamp, figure 4.3a), the unscreened QCSE leads to significant shift to lower energies for thicker QWs. Figure 4.3c shows PL spectra at room temperature, when subjected to the much more intense illumination of an XeCl-pumped dye laser, tuned below the GaN band edge (i.e. exciting only the QWs). Here, a very strong broadening to higher emission energies of several 100 meV is observed in all investigated samples. This behavior is fundamentally different than that described in section 4.1.3 on page 30: There are no traces of excited states in the absorption spectra (figure 4.2), and the emission is much broader than the ground

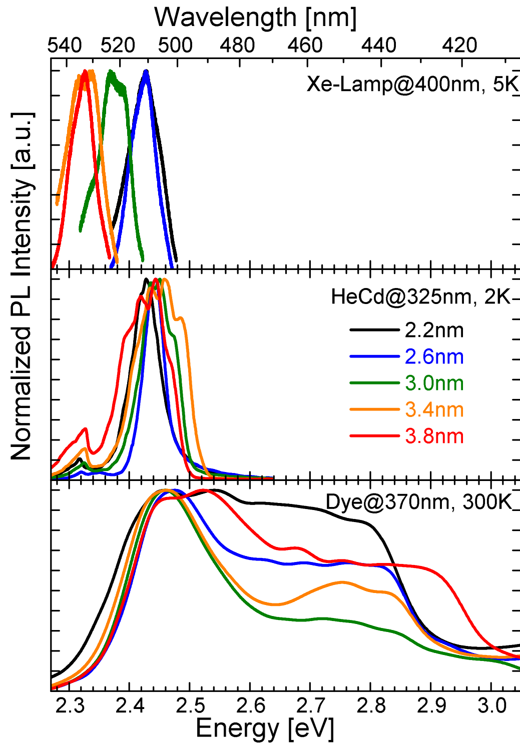

Figure 4.3: A series of quasi-SQWs samples with different QW thickness (but nominally the same emission wavelength of 510 nm) subjected to different excitation power densities provided by a) Xenon arc lamp b) HeCd laser c) XeCl-pumped dye laser. From a) to b) the QCSE is screened, while from b) to c) the CHC luminescence arises (see section 4.3 on the next page).

state transition. It is also noted that the broadening of the emission spectra cannot be explained by the shielding of the QCSE, as it extends far beyond the absorption edge. The origin of this phenomenon, which is obviously a high-excitation effect, will be discussed in detail in the following.

4.3 The Confined Hole Continuum

In order to explain this emission, one should consider the excitation mechanisms that may originate it. The excitation energy used lies below the band gap of the GaN barrier, and above the band gap of the InGaN QW. This guarantees that electron-hole pairs can only be generated within the QW. However, energetically, it does not guarantee that the excited carriers are confined in the QW itself. For example, counting from the electronic ground state (several hundred meV below the conduction band edge of GaN), hole states well below the InGaN QW valence band edge are accessible. Due to the internal electric fields (section 2.1.1 on page 3), the band profile is tilted. This is not only the case for the InGaN QW, but also for the GaN barriers. This results in a trigonal confinement potential encompassing a QW and a neighboring barrier, with energies below the GaN valence band edge. These states should be very similar to GaN bulk valence band states, i.e. quasi-continuous bands. These states will be called the CHC in the following.

The following work presents conclusive spectroscopic evidence that, indeed, the CHC is responsible for the observed high-energy, broad, fast-decaying luminescence under intense quasi-resonant excitation and was published as Ref. [A1]: F. Nippert, A. Nirschl, T. Schulz, G. Callsen, I. Pietzonka, S. Westerkamp, T. Kure, C. Nenstiel, M. Strassburg, M. Albrecht, and A. Hoffmann,
"Polarization-induced confinement of continuous hole-states in highly pumped, industrial-grade, green InGaN quantum wells",
Journal of Applied Physics **119**, 215707 (2016),
DOI: 10.1063/1.4953254

It also contains Refs. [A2, 26, 39, 44, 45, 59, 60, 63, 68, 73–75, 77–79, 82, 92, 181, 182, 185, 186, 193–195, 197–206]

The postprint version of this work is reproduced with the permission of AIP Publishing.

Polarization-induced confinement of continuous hole-states in highly pumped, industrial-grade, green InGaN Quantum Wells

Felix Nippert,[1, a)] Anna Nirschl,[2] Tobias Schulz,[3] Gordon Callsen,[1] Ines Pietzonka,[2] Steffen Westerkamp,[1] Thomas Kure,[1] Christian Nenstiel,[1] Martin Strassburg,[2] Martin Albrecht,[3] and Axel Hoffmann[1]
[1)] *Institut für Festkörperphysik, Technische Universität Berlin, Hardenbergstraße 36, 10623 Berlin, Germany*
[2)] *OSRAM Opto Semiconductors GmbH, Leibnizstraße 4, 93055 Regensburg, Germany*
[3)] *Leibniz-Institut für Kristallzüchtung, Max-Born-Straße 2, 12489 Berlin, Germany*

(Dated: 26 April 2016)

We investigate industrial-grade InGaN/GaN quantum wells (QWs) emitting in the green spectral region under high, resonant pumping conditions. Consequently, an ubiquitous high energy luminescence is observed, that we assign to a polarization field Confined Hole Continuum (CHC). Our finding is supported by a unique combination of experimental techniques, including transmission electron microscopy, (time-resolved) photoluminescence under various excitation conditions, and electroluminescence, which confirm an extended out-of-plane localization of the CHC-states. The larger width of this localization volume surpasses the QW thickness, yielding enhanced non-radiative losses due to point defects and interfaces, whereas the energetic proximity to the bulk valence band states promotes carrier leakage.

I. INTRODUCTION

InGaN/GaN quantum wells (QWs) are commonly applied in light emitting diodes (LEDs) and laser diodes (LDs) in the blue and even green spectral region[1–3]. However, both device types suffer from a distinct efficiency reduction towards the green spectral range, despite the better confinement properties of energetically deeper QWs. Established reasons for this matter include a reduced electron-hole-overlap in the QWs due to the quantum-confined Stark effect (QCSE)[4–8] and general difficulties in growing homogeneous InGaN material[9–15]. Also high pumping conditions are known to cause a further reduction of the efficiency that is attributed to Auger recombination[16–19]. In this Letter we report on an additional high excitation loss mechanism arising from confined hole continuum (CHC) states promoting carrier leakage, which is of utmost importance for the implementation of efficient, LDs emitting in green spectral region.

II. METHODS

A. Sample Growth

A large quantity of high quality InGaN QW samples with different structural parameters was investigated in order to support the generality of the presented findings. The growth was conducted by means of metal-organic vapor phase epitaxy on c-plane sapphire substrates. The active region was deposited on a 3 μm thick GaN buffer and consists of five identical InGaN QWs separated by 27 nm thick GaN barriers. Such thick barriers reduce the influence of the individual QWs onto each other, which means that they can be treated as uncoupled single QWs ("quasi-SQW"). Subsequently, the active region was overgrown with an $Al_{0.15}Ga_{0.85}N$ electron blocking layer (25 nm) and a GaN capping layer (80 nm). The samples analyzed are nominally undoped and the QWs have a nominal thicknesses between 2 nm and 3 nm and an Indium content of about 20%, resulting in emission wavelengths around 500 nm. Control samples with varying QW thicknesses (up to 4.3 nm), doping concentration in the barriers (up to $5 \cdot 10^{18} cm^{-3}$ Si), and emission wavelengths (485 to 570 nm) were grown in order to verify that the observed effects do not depend on the magnitude of the QCSE, a lack of free carriers, or any general QW property like thickness or composition. While all presented observations are valid for all of these samples, a particular set of samples was chosen exhibiting a weak QCSE-caused shift with excitation power density[5,7,8]. This choice eases an understanding of the reported phenomena, as none of the observations need to be uncoupled from additional dynamic processes imposed by the (de-)screening of the QCSE. In addition, a complete multi quantum well (MQW)-LED structure with n- and p-doped layers and commercial-grade QWs of similar thickness and composition was investigated. Consequently, the application of a DC bias to the sample becomes feasible in order to approve carrier localization. All samples represent the state-of-the-art in InGaN QW growth, with growth parameters kept to values as similar as possible to industrial mass production and are the brightest epitaxy-level structures ever investigated in our on spectroscopy focused laboratories.

B. Experimental Details

For photoluminescence (PL) measurements the samples were mounted in a Helium-flow cryostat. Continuous wave (cw) PL was measured using the 325 nm emis-

[a)] Electronic mail: felix@physik.tu-berlin.de

*Postprint reproduced from Ref. [A1]Nippert et. al, J. Appl. Phys. **119**, 215707 (2016) with permission of AIP Publishing. DOI: 10.1063/1.4953254*

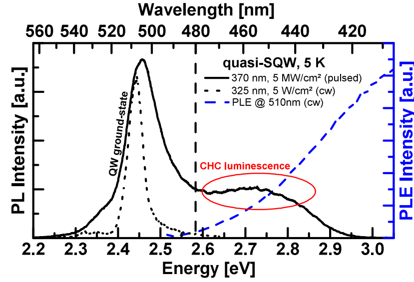

FIG. 1. Low temperature (5 K) photoluminescence spectra of a quasi-SQW, excited either non-resonantly (325 nm) with a HeCd laser (dashed, black line) or resonantly (370 nm) with a pulsed dye laser (solid, black line). A slight blue shift and a broadening of the emission peak towards higher energies (band-filling) is observed along with the drastically increased excitation power density. In addition, a broad luminescence band (the Confined Hole Continuum (CHC) luminescence) centered at around 2.75 eV is witnessed. The blue dashed line depicts a photoluminescence excitation spectrum with the detection centered at 510 nm. Here, no distinct excitation channels can be observed.

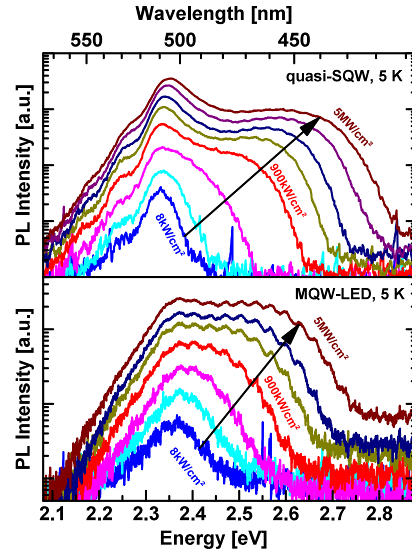

FIG. 2. Excitation power dependent series of low temperature (5 K) photoluminescence spectra comprising the same quasi-SQW depicted in Fig. 1 (top) and an additional MQW-LED (bottom). The highest excitation power density is equivalent to the black, solid line in Fig. 1. The broad CHC luminescence continuously shifts towards higher energies with rising excitation power density. The evolution of the spectra suggests a continuous density of states being involved in the overall luminescence process, well in agreement with the PLE results.

sion line of a HeCd laser. Resonant, high excitation PL and time-resolved PL (TRPL) were performed using a XeCl laser pumped dye laser operating with 2-Methyl-5-t-Butyl-p-Quarterphenyl (DMQ) tuned to 370 nm. The pulse duration of this system amounts to 10 ns with a repetition rate of 100 Hz. To access shorter time scales, a frequency-doubled Ti:Sa laser, also tunable around 370 nm, with pulse durations of 2 ps, and a repetition rate of 5 MHz was used. Photoluminescence excitation (PLE) spectra were excited with a monochromatized 500 W Xenon arc lamp. The luminescence signal was dispersed by a SPEX 1404 additive double monochromator (PL, TRPL), a SPEX 1702 single monochromator (PLE) or a McPherson 2035 subtractive double monchromator (TRPL), whereas the detection was achieved with either a Hamamatsu multi-channel plate photomultiplier (S20 cathode) detector (TRPL), a bi-alkali photomultiplier (TRPL, PL), or a Princeton Instruments charge coupled device (PLE). The structural properties of the samples were studied by a Titan scanning transmission electron microscope made by FEI (Field Emission Inc.) operated at 300 kV with a semi-convergence angle of 9.0 mrad using a high angle annular dark field detector (STEM-HAADF) for Z-contrast imaging.

III. RESULTS

Fig. 1 shows a low temperature PL spectrum of a quasi-SQW, that is non-resonantly excited at a moderate excitation power density of $5\,Wcm^{-2}$ (black, dashed line). A sharp emission peak of the QW ground-state transition is observed at an energy of around 2.44 eV. Repeating the same measurement under a much higher, resonant excitation with a power density of $5\,MWcm^{-2}$ (black, solid line) reveals two effects. First, the QW ground-state transition shifts by around 20 meV towards higher energies indicating a commonly reported weak QCSE[4–8]. At the same time a significant broadening and an apparent asymmetry of the emission band is observed, which indicates band-filling[20,21]. Second, an additional, broad peak is observed at much higher energies, which we call the Confined Hole Continuum (CHC) luminescence. This particular luminescence is not associated with any distinct excitation channel as the photoluminescence excitation (PLE) spectrum from Fig. 1 (blue dashed line) shows. Even though this PLE measurement was performed at low excitation power densities, the same result is obtained when the measurement is repeated at elevated excitation power densities with a dye laser (not shown). Fig. 2 illustrates PL spectra of the same quasi-SQW (top) and a MQW-LED (bottom) obtained under comparable, resonant excitation conditions as a function of excitation power density. The CHC luminescence significantly

*Postprint reproduced from Ref. [A1]Nippert et. al, J. Appl. Phys. **119**, 215707 (2016) with permission of AIP Publishing. DOI: 10.1063/1.4953254*

broadens towards higher emission energies with increasing excitation density for both specimens, and no appearance of any distinct, well-resolved PL feature can be observed. While the CHC luminescence shown in Fig. 1 and Fig. 2 (top) is still mimicking a separate luminescence band at high excitation power densities, its true continuous evolution towards higher energies with rising excitation power becomes straight-forwardly apparent in Fig. 2 (bottom). Owing to the vastly different time scales of the luminescence decays (later on introduced in Fig. 4) and the large temporal separation of the excitation pulses (10 ms), one always simultaneously records luminescence that corresponds to an entire range of excitation conditions. This leads to a large variety of luminescence signatures, which all continuously broaden towards higher energies, but must not be misinterpreted as a separate luminescence band. Please note that at a first glance this particular behavior of the CHC luminescence resembles a Burstein-Moss shift as commonly observed in highly excited bulk material[20,22]. We note that the reported phenomenon can be easily distinguished from the dynamic processes characteristic for the QCSE. Fig. 3 shows the temporal evolution of the PL signal in response to an optical pulse. The top panel shows the results for a thin (2.2 nm) quasi-SQW sample, while the bottom panel presents the same measurement for a thick (4 nm) quasi-SQW. In both cases two dynamic regimes can be observed. At low delay times, the CHC luminescence described above can be observed, whose dynamics will be analyzed in detail in the following section. At large time delays, the de-screening of the QCSE is visible with a characteristic shift to lower emission energies over time as the internal fields are reestablished. Naturally, the QCSE is much more pronounced in the thick quasi-SQW sample (bottom panel), motivating our focus on thin QW samples (top panel) for an analysis of the CHC luminescence. In addition, a similar, continuous trend is also observed in TRPL measurements. We have measured the temporal decay of several samples at cryogenic and room temperature over a broad range of detection energies comprising the QW ground-state transition and the CHC luminescence. All decays are mono-exponential[23] and the corresponding decay times that result from a deconvolution with the instrument response function[24] are plotted in Fig. 4 (red squares) as a function of detection energy. Here, the decay times decrease drastically towards high energies in a *continuous* manner, in accordance with the *continuous* evolution of the CHC luminescence, cf. Fig. 2. In addition, the time-resolution of our setup permits the extraction of rise times (green circles in Fig. 4) as soon as the frequency-doubled Ti:Sa excitation can be applied (please see the methods section for details). Again these time constants evolve in a similar way, i.e. they drastically and *continuously* decrease towards higher energies. In-line with PLE and PL results, the entire set of experimental trends shows no evidence for any kind of discrete state associated with the CHC luminescence. Fig. 5 introduces differential electroluminescence

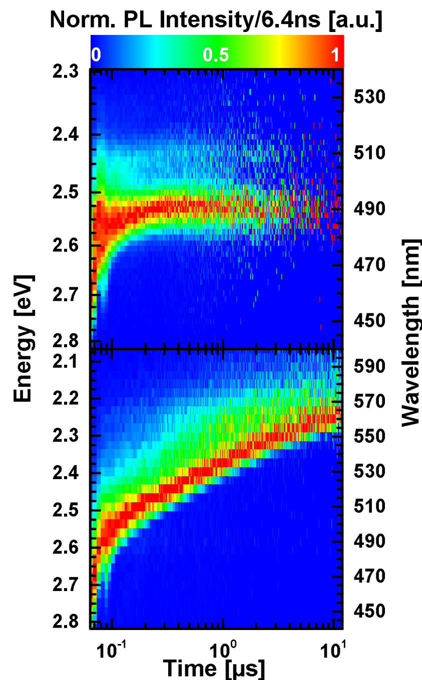

FIG. 3. Photoluminescence spectra as a function of delay time after excitation for a thin (2.2 nm, top) and thick (4 nm, bottom) specimen. The CHC luminescence at higher energies is observed to decay quickly, followed by a prolonged shift of the ground state luminescence due to de-screening of the QCSE. The latter is much more pronounced in the thicker sample.

(EL) spectra of a MQW-LED sample. We obtain such differential spectra by optically pumping the sample into the optimal excitation regime for the CHC luminescence, cf. Fig. 2 (bottom). Simultaneously we apply an electrical bias to the LED structure and acquire the total luminescence signal. The spectra from Fig. 5 finally depict the differences of spectra obtained either with or without an applied bias. Naturally, one can clearly observe an EL peak belonging to the QW ground-state transition once the LED is operating in above threshold conditions (green line). As the optical excitation pulses are temporarily well separated, this EL is mostly generated in between the optical excitation events. Nevertheless, the main observation of Fig. 5 is related to the high energy tail of the differential spectra. Here, it is clearly shown that the CHC luminescence is not at all affected by the applied bias proving that the contributing carriers are

Postprint reproduced from Ref. [A1]Nippert et. al, J. Appl. Phys. ***119****, 215707 (2016)*
with permission of AIP Publishing. DOI: 10.1063/1.4953254

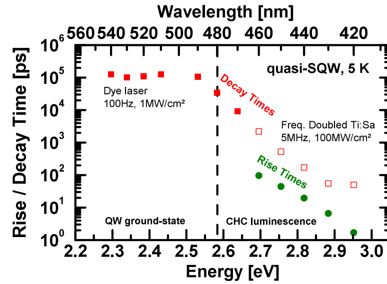

FIG. 4. Decay times (red squares) extracted from the mono-exponential decays observed at 5 K in a quasi-SQW. The filled, red squares correspond to excitation conditions as mentioned in the caption of Fig. 1, while the open, red squares were obtained with a frequency-doubled Ti:Sa laser, which also allowed the determination of the corresponding rise times (green circles). Please note the continuous evolution of the rise and decay times with rising detection energy, that encompasses the luminescence of the QW ground-state and the CHC luminescence.

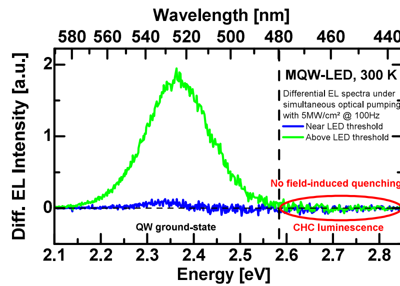

FIG. 5. Differential electroluminescence (EL) spectra of a MQW-LED sample, which is optically pumped similar to conditions shown in Fig. 2. Once the current flow is established, an EL peak is visible, originating from long times in between the optical excitation pulses. However, during the optical pulse, i.e. when the Confined Hole Continuum (CHC) luminescence is observed in photoluminescence, no effect of the applied bias on the CHC luminescence is observed, approving the confined nature of the CHC states. Please see the text for further details.

still well confined despite the continuous nature of the CHC luminescence.

To exclude parasitic effects, we have also investigated a variety of control samples with focus on the CHC luminescence. A sample exclusively containing GaN barrier material in the active region (no InGaN QWs) showed no trace of any CHC luminescence. This excludes barrier, cap, or buffer GaN material as the source of the CHC luminescence. Series of QWs with differing Indium compositions, QW thicknesses, and barrier doping concentrations as well as several production grade LED wafers have all shown the same luminescence characteristics described by Figs. 1-5. Interestingly, if the QW emission energy is tuned towards the blue spectral range (e.g. towards 450 nm), the overall effect of the CHC luminescence strongly diminishes. This observation can complementary be explained by an overlap of the QW ground-state and the CHC luminescence as well as an insufficient pump level. Here, in the blue spectral region, the reduced radiative lifetime of the QW ground state[23] must be counter-balanced by a drastic increase in excitation density, which naturally easily approaches excitation limitations governed by the samples' durability.

Subsequently, we can summarize the optical characteristics of the CHC luminescence as follows:

i) The CHC luminescence is universally found in all high-quality samples we have investigated. We do not observe this intriguing optical signature in samples of limited structural quality or lower Indium concentrations.

ii) The CHC luminescence only occurs at high carrier densities, which are easily reached under resonant, pulsed optical excitation.

iii) PLE spectra show no discrete excitation channel within the spectral range of the CHC luminescence. The absorption rather continuously increases towards the GaN band-edge. Power-dependent PL also shows a continuous broadening and a blue-shift of the high energy flank of the CHC luminescence.

iv) Within the CHC luminescence, the decay and rise times of the PL signal decrease continuously and drastically with increasing emission energy.

v) The CHC luminescence is robust against any temperature changes (not shown). It can be observed both at cryogenic as well as room temperature and the decay as well as the rise times do not significantly scale with temperature.

vi) The CHC luminescence is not suppressed by for LEDs commonly applied bias values pointing towards carrier localization despite its continuous experimental signature. Hence, we observe the rare case of a well-confined state-continuum that contradicts commonly applied textbook perceptions of QWs.

IV. DISCUSSION

Previous studies have attributed fast-decaying, high-energy shoulders[26] of InGaN QW emissions or even high energy peaks similar to the CHC luminescence[27] to in-plane, extended states, with main contributions arising from in-plane, localized QW states. In these models, such an in-plane localization arises from the potential minima created by In-rich regions in the QW. While this phenomenon can certainly describe high-energy shoulders with a certain ground-state separation, high-resolution transmission electron microscopy (HRTEM) measurements of our samples (see Fig. 6 for an example) preclude In-clusters and yield an In content of 19% with a com-

*Postprint reproduced from Ref. [A1]Nippert et. al, J. Appl. Phys. **119**, 215707 (2016) with permission of AIP Publishing. DOI: 10.1063/1.4953254*

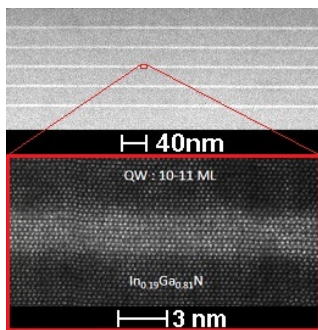

FIG. 6. Transmission electron micrographs of a typical quasi-SQW. The top panel shows an overview while the bottom panel depicts a high-resolution detail of one of the quantum wells. We observe abrupt InGaN/GaN interfaces and no thickness variations beyond a single monolayer. There is no evidence of phase separation in the InGaN quantum wells nor any composition fluctuations beyond the random distribution of In atoms[25]. Therefore, the optical properties of such a QW sample will not be dominated by any In-induced potential fluctuations.

pletely random distribution of the In atoms[25]. Please note that a pronounced In-clustering would be required in order to explain localization over the entire spectral range of the CHC luminescence reaching up to 0.4 eV above the QW ground-state transition. In addition such In-clustering would result in strong non-monotonicity of the observed transient decays. Also, we can exclude V-Pits[28,29] as the source of the CHC luminescence. Extensive micro-PL mapscans with a spatial resolution of around 300 nm[30] did not reveal any luminescence traces of the thinner QWs on the facets of V-Pits. Such luminescence contribution would appear as energetically sharp lines with a spot-like lateral distribution[28]. In addition, the well-known S-shape that can be observed in temperature-dependent PL measurements as a signature of in-plane localization[31] due to Indium fluctuations[10], is limited to less than 10 meV in all our samples (or does not exist at all in the case of thicker QWs). We can therefore also exclude any in-plane localization as the source of the CHC luminescence due to its large energetic separation from the QW ground-state transition. In order to coherently explain all our observations, we propose the model sketched in Fig. 7. As soon as the active region is highly pumped, the hole ground-states are increasingly saturated. The absorption below the GaN band edge, however, still allows the creation of electron-hole pairs, consisting for example of ground-state elec-

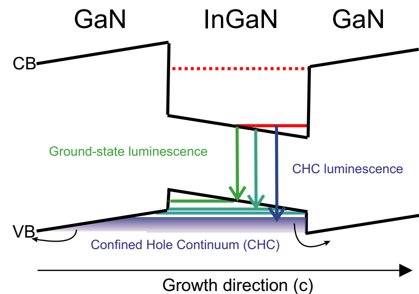

FIG. 7. Sketch of the proposed model for the observed Confined Hole Continuum (CHC) luminescence. Under high optical pumping the hole ground-states (green line) are saturated and excited hole-states (cyan lines) are populated. Once all discrete hole-states are filled, additional quasi-continuous hole-states below the GaN valence band edge (violet color gradient) are populated. These CHC states, despite their continuous nature, are still confined by the triangular potential arising from the internal polarization fields. Hence, the CHC states are more extended along the c-direction if compared to the ground and still confined excited states.

trons and highly excited holes. Naturally. these holes can still relax towards the QW. However, due to Pauli-blocking, this cascade ends in excited hole states (solid violet in Fig. 7) which lie energetically below the confinement potential of the QW, but still above the GaN band edge. These states are bulk-like, as they derive from GaN bulk valence band states in the adjacent barrier. Nevertheless, these states are still confined due to the tilted valence band edge in the barriers arising from polarization field discontinuities. Hence, in the depicted model, the holes are to some extent delocalized in the out-of-plane direction of the QW. Thereby the described model is consistent with all the characteristics of the CHC luminescence (i-vi). In particular this means:

I) The CHC luminescence will arise regardless of the precise properties of the individual InGaN QW. It is a general feature of InGaN/GaN heterostructures that the band offset in the valence band[32] is smaller in regard to the energetic difference between the excited and ground electron state. This general property enables hole states forming a quasi-continuum that protrudes out of the QW and is significantly populated well before all electron states within the QW are filled. We note that in principal the same quasi-continuum of states exists for electrons above the confined excited electron states. In contrast to the CHC states, these are not accessible by our excitation conditions, because the energetic difference between this Confined Electron Continuum and the hole ground states is larger than the energy of the pump photons.

II) The high energy CHC luminescence can only be observed once the ground hole states, as well as all truly

confined excited hole states have been filled. Due to inhomogeneous broadening of the ground state transiton and due to the energetic proximity of the ground and excited hole states, a direct observation of the excited hole state recombinations as distinct features in the spectrum is not possible. Therefore high excitation power densities and superior crystal quality are necessary to saturate the hole states in the QW, allowing the observeration of the CHC luminescence. We wish to remark that exactly this high excitation regime constitutes the basis for any high power LD applications, especially in the green spectral range.

III) Because of the continuous hole state density originating from the bulk GaN-like hole states of the CHC luminescence it is not surprising that the absorption and emission characteristics scale rather continuously upon variation of the excitation conditions as well. The excited electron state, marked with a dotted, red line in Fig. 7 may play a role as well at even further elevated excitation powers or under non-resonant pumping conditions, but all presented spectra are still dominated by the CHC states. Please note that any further contribution of excited electron states should show up as discrete luminescence features[33], however, any overlap with the CHC luminescence may spoil this observation.

IV) The rise times of the time-resolved photoluminescence decay can be attributed to the relaxation time of the excited holes. The corresponding values decrease towards higher emission energies, as the holes (excited into the bulk-like state continuum below the QW confinement potential) need to interact with a diminishing number of acoustic phonons in order to reach their final CHC states. The drastically reduced decay times across the CHC luminescence are related to the higher wave function overlap between the ground-state electrons (solid red line in Fig. 7) and the excited out-of-plane delocalized hole states (violet color gradient in Fig. 7) in contrast to the hole ground-states, which suffer from the QCSE (green line).

V) As soon as the excited hole-states become less localized within the QW, they are more prone to interact with point defects (at the InGaN-GaN interfaces or in the GaN barrier layers). In addition, the energy that is needed to overcome the remaining potential barrier is small enabling hole leakage under high excitation conditions (see curved black arrows in Fig. 7). The lack of a pronounced temperature dependence of the CHC luminescence's decay times, suggests that the decay is still dominated by non-radiative processes at cryogenic temperatures.

VI) The fact that the CHC luminescence does not diminish when a bias is applied to the sample proves that the holes involved are still sufficiently confined by the triangular potential, as otherwise they would be extracted from the active region, recombine elsewhere, and thus reduce the observed intensity. Hence, as indicated in Fig. 7, the tilted band structure in the active region still provides a confinement potential for hole states, which would otherwise be completely delocalized similar to bulk GaN valence band states.

V. CONCLUSION

The Confined Hole Continuum (CHC) luminescence, that we universally observe in all green-emitting, high quality InGaN QWs is the signature of a so far frequently neglected loss mechanism arising under high pumping conditions. As soon as the confined hole states are saturated, all additional holes introduced into the system relax into out-of-plane less localized states. In such states holes can interact with more non-radiative centers and the overall hole escape rate is enhanced. Obviously this phenomenon hinders any high power applications. Finally, we suggest two solutions in order to overcome the issue associated with the CHC luminescence:

A) The use of AlGaN barriers instead of GaN barriers would increase the valence band offset and shift the CHC luminescence to higher energies, while simultaneously increasing the number of confined hole states.[34]

B) The valence band offset can also be enlarged by incorporating higher amounts of Indium into thinner QWs[35], thus reducing the significance of CHC states.

Obviously, both of these solutions are technologically challenging and warrant further research. Additionally we wish to note that the growth on non-polar planes cannot offer a solution for this particular challenge. Close to any flat-band conditions, the excited hole states would not be additionally confined by any triangular potential and hole leakage would be expected to be increased even further under high-pumping conditions. The inceased electron-hole overlap in such non-polar structures, however, would help to reduce carrier lifetime and hence shift the excitation powers necessary to saturate the QW states to higher excitation power denisties.

In conclusion, we have identified a commonly neglected loss mechanism, which arises from a confined hole continuum (CHC). This loss occurs at high carrier densities constituting its importance for high power LEDs and LDs in the green spectral region.

We gratefully acknowledge the financial support of the European Union FP7-ICT Project NEWLED, No. FP7-318388 and the German Science Foundation within the Collaborative Research Center (CRC 787).

[1] S. Nakamura, M. Senoh, N. Iwasa, and S. Nagahama, Japanese Journal of Applied Physics **34**, L797 (1995).
[2] Y. Narukawa, J. Narita, T. Sakamoto, K. Deguchi, T. Yamada, and T. Mukai, Japanese Journal of Applied Physics **45**, L1084 (2006).
[3] M. R. Krames, O. B. Shchekin, R. Mueller-Mach, G. O. Mueller, L. Zhou, G. Harbers, and M. G. Craford, Journal of Display Technology **3**, 160 (2007).
[4] J. Im, H. Kollmer, J. Off, and A. Sohmer, Physical Review B **57**, 9435 (1998).
[5] L.-H. Peng, C.-W. Chuang, and L.-H. Lou, Applied Physics Letters **74**, 795 (1999).

*Postprint reproduced from Ref. [A1]Nippert et. al, J. Appl. Phys. **119**, 215707 (2016) with permission of AIP Publishing. DOI: 10.1063/1.4953254*

[6]F. Della Sala, A. Di Carlo, P. Lugli, F. Bernardini, V. Fiorentini, R. Scholz, and J.-M. Jancu, Applied Physics Letters **74**, 2002 (1999).
[7]J. Bai, T. Wang, and S. Sakai, Journal of Applied Physics **88**, 4729 (2000).
[8]T. Wang, J. Bai, S. Sakai, and J. K. Ho, Applied Physics Letters **78**, 2617 (2001).
[9]Y. Narukawa, Y. Kawakami, and S. Fujita, Physical Review B **55**, 1938 (1997).
[10]S. Chichibu and A. Abare, Applied Physics Letters **73**, 2006 (1998).
[11]N. Duxbury and U. Bangert, Applied Physics Letters **76**, 1600 (2000).
[12]P. Ruterana and S. Kret, Journal of Applied Physics **91**, 8979 (2002).
[13]H. K. Cho, J. Y. Lee, J. H. Song, P. W. Yu, G. M. Yang, and C. S. Kim, Journal of Applied Physics **91**, 1104 (2002).
[14]Y.-H. Cho, S. K. Lee, H. S. Kwack, J. Y. Kim, K. S. Lim, H. M. Kim, T. W. Kang, S. N. Lee, M. S. Seon, O. H. Nam, and Y. J. Park, Applied Physics Letters **83**, 2578 (2003).
[15]J. Jinschek, R. Erni, N. Gardner, a.Y. Kim, and C. Kisielowski, Solid State Communications **137**, 230 (2006).
[16]A. Laubsch, M. Sabathil, W. Bergbauer, M. Strassburg, H. Lugauer, M. Peter, S. Lutgen, N. Linder, K. Streubel, J. Hader, J. V. Moloney, B. Pasenow, and S. W. Koch, Physica Status Solidi (c) **6**, S913 (2009).
[17]M. Binder, A. Nirschl, R. Zeisel, T. Hager, H.-J. Lugauer, M. Sabathil, D. Bougeard, J. Wagner, and B. Galler, Applied Physics Letters **103**, 071108 (2013).
[18]J. Iveland, L. Martinelli, J. Peretti, J. S. Speck, and C. Weisbuch, Phys. Rev. Lett. **110**, 177406 (2013).
[19]F. Nippert, S. Karpov, I. Pietzonka, B. Galler, A. Wilm, T. Kure, C. Nenstiel, G. Callsen, M. Straßburg, H.-J. Lugauer, and A. Hoffmann, Japanese Journal of Applied Physics **55**, 05FJ01 (2016).
[20]E. Burstein, Phys. Rev. **93**, 632 (1954).
[21]H. C. Casey, J. Muth, S. Krishnankutty, and J. M. Zavada, Applied Physics Letters **68** (1996).
[22]B. E. Sernelius, K.-F. Berggren, Z.-C. Jin, I. Hamberg, and C. G. Granqvist, Phys. Rev. B **37**, 10244 (1988).
[23]P. Lefebvre, A. Morel, M. Gallart, T. Taliercio, J. Allegre, B. Gil, H. Mathieu, B. Damilano, N. Grandjean, and J. Massies, Applied Physics Letters **78**, 1252 (2001).
[24]D. V. O'Connor, W. R. Ware, and J. C. Andre, Journal Of Physical Chemistry **83**, 1333 (1979).
[25]T. Schulz, T. Remmele, T. Markurt, M. Korytov, and M. Albrecht, Journal of Applied Physics **112**, 033106 (2012).
[26]M. J. Davies, T. J. Badcock, P. Dawson, M. J. Kappers, R. a. Oliver, and C. J. Humphreys, Applied Physics Letters **102**, 022106 (2013).
[27]G. Sun, G. Xu, J. Yujie, H. Thao, G. Liu, J. Zhang, and N. Tansu, Applied Physics Letters **99**, 081104 (2011).
[28]A. Hangleiter, F. Hitzel, C. Netzel, D. Fuhrmann, U. Rossow, G. Ade, and P. Hinze, Phys. Rev. Lett. **95**, 127402 (2005).
[29]T. L. Song, Journal of Applied Physics **98**, 084906 (2005).
[30]J. S. Reparaz, G. Callsen, M. R. Wagner, F. Güell, J. R. Morante, C. M. Sotomayor Torres, and A. Hoffmann, APL MATERIALS **1**, 012103 (2013).
[31]Y.-H. Cho, G. H. Gainer, a. J. Fischer, J. J. Song, S. Keller, U. K. Mishra, and S. P. DenBaars, Applied Physics Letters **73**, 1370 (1998).
[32]P. G. Moses and C. G. Van de Walle, Applied Physics Letters **96**, 021908 (2010).
[33]T. Schulz, A. Nirschl, P. Drechsel, F. Nippert, T. Markurt, M. Albrecht, and A. Hoffmann, Applied Physics Letters **105**, 181109 (2014).
[34]Y.-D. Lin, S. Yamamoto, C.-Y. Huang, C.-L. Hsiung, F. Wu, K. Fujito, H. Ohta, J. S. Speck, S. P. DenBaars, and S. Nakamura, Applied Physics Express **3**, 82001 (2010).
[35]S.-M. Ko, H.-S. Kwack, C. Park, Y.-S. Yoo, S.-Y. Kwon, H. Jin Kim, E. Yoon, L. Si Dang, and Y.-H. Cho, Applied Physics Letters **103**, 222104 (2013).

*Postprint reproduced from Ref. [A1]Nippert et. al, J. Appl. Phys. **119**, 215707 (2016) with permission of AIP Publishing. DOI: 10.1063/1.4953254*

4.4 Conclusion

In conclusion, a broad, fast-decaying, high-energy luminescence in the blue spectral range was found in green-emitting QWs, pumped quasi-resonantly with very high excitation power densities. This CHC luminescence is explained to originate from excited quasi-continuous hole states, which are confined in the triangular potentials formed by QW-barrier pairs due to their polarization (QCSE). All observed properties of the CHC luminescence conform with this model:

1. The PL and PLE spectra show no distinct peaks, but a broad band, because the DOS is continuous - they are very similar to GaN bulk valence band states.
2. The CHC luminescence is only visible in high, quasi-resonant excitation conditions, as the ground states need to be saturated.
3. The decay of the CHC luminescence is in the ps-range and decreases for higher emission energies. At the same time, an observed rise time in the time-tesolved photoluminescence (TRPL) measurement also decreases. This suggests that the decay is dominated by relaxation of the holes within the quasi-bulk bands in the triangular potential.
4. The CHC luminescence is robust against applied bias, meaning that the carriers are sufficiently confined within the triangular potentials to not escape easily.
5. These optical properties do not change significantly as a function of temperature, they are the same at cryogenic temperatures and at room temperature. This suggests that the majority of recombinations is of non-radiative nature in any case. In particular, the carriers may more easily reach non-radiative centers (within the QW, the barrier, or their interface) or are more prone to thermalization due to the much smaller potential barrier.

In sum, the CHC luminescence is the fingerprint of a high-excitation density loss mechanism, which may inhibit the performance of green-emitting InGaN laser diodes (LDs). Any high-power application device design should therefore consider these states and try to minimize their impact, i.e. by band gap engineering in the active region. Naturally the effects discussed here are only relevant in high-pumping regimes, where the ground states can be satured. For example in LDs very high carrier densities

are desirable and necessary in order to achieve population inversion and high gain. In LEDs, however, high carrier densities do not come with the benefit of induced emission (and therefore shorter radiative lifetime). Here, the high-power efficiency is limited already by Auger recombination (see section 2.2.5 on page 16). The next chapter will take a look into the fundamental limitations of InGaN LED technology, unravelling the green gap and droop phenomena.

5 Recombination Coefficients in InGaN MQW LEDs

The quantum efficiency of InGaN light-emitting diodes (LEDs) is, at least for devices of sufficiently high epitaxial quality, accurately described by the so-called ABC-model. Here the recombination processes are characterized by the coefficients A, B, and C, corresponding to Shockley-Read-Hall (SRH), radiative, and Auger recombination, see section 2.2.3 on page 13. Reliable determination of these coefficients is important in order to understand the omnipresent efficiency reduction phenomena: the green gap (section 2.2.4 on page 15), and the droop (section 2.2.5 on page 16). A detailed knowledge of the recombination paths potentially allows to identify possible solutions to these problems. In the following, a novel method to determine the recombination coefficients in InGaN multiple quantum well (MQW) LEDs will be introduced (section 5.1 on the following page). This technique s applied to blue-emitting single quantum well (SQW) and MQW LEDs for demonstration purposes, highlighting the onset of non-uniform carrier distribution in MQW stacks (section 5.3 on page 55). The method is particularly suited for temperature-dependent measurements, which will be presented in section 5.4 on page 71. A determination of the recombination coefficients in blue and green-emitting MQW LED in a wide temperature range allows, finally (section 5.5 on page 81), to gain insight into the mechanisms responsible for the green gap.

5.1 Determination of the Recombination Coefficients

If we consider an electrically driven LED in equilibrium conditions, the number of injected carriers is equal to the number of recombining carriers in the active region, i.e. the steady-state carrier density n_0 is constant as a function of time ($\frac{dn_0}{dt} = 0$). Taking into account the three recombination mechanisms introduced in section 2.2.3 on page 13, we can formulate the rate equation[173, 174]:

$$\frac{j}{e} = An_0 + Bn_0^2 + Cn_0^3 \tag{5.1}$$

where j is the current density, and e is the elementary charge. Now, considering a small perturbation $\delta n(t)$ of the carrier density, i.e. $n(t) = n_0 + \delta n(t)$, with the initial perturbation $\delta n(t = 0) = \delta n_0$ the response of the system is given by:

$$\frac{dn(t)}{dt} = \frac{j}{e} - An(t) - Bn(t)^2 - Cn(t)^3 \tag{5.2}$$

which, using equation (5.1) can be written as:

$$\frac{d\delta n(t)}{dt} = -A\delta n(t) - 2Bn_0\delta n(t) - 3Cn_0^2\delta n(t) + O(\delta n(t)^2) \tag{5.3}$$

Here, higher orders of $\delta n(t)$ can be neglected, if $\delta n(t)$ is much smaller than n_0. This differential equation is solved by:

$$\delta n(t) = \delta n_0 e^{-\frac{t}{\tau}} \tag{5.4}$$

where the differential lifetime (DLT) τ is given by:

$$\frac{1}{\tau} = A + 2Bn_0 + 3Cn_0^2 \tag{5.5}$$

i.e. the response of the active region to a small, additional carrier population is a mono-exponential decay of the same depending only on the recombination coefficients A, B and C, and the equilibrium carrier density n_0. A second relationship, depending on the same parameters, was introduced earlier (equation (2.1) on page 14):

$$IQE(n_0) = \frac{Bn_0}{A + Bn_0 + Cn_0^2} \tag{5.6}$$

Solving for the maximum of this expression, one obtains the carrier density at $\mathrm{IQE}_{\mathrm{max}}$, $n_{max} = \sqrt{\frac{A}{C}}$. This gives the maximum IQE as:

$$\mathrm{IQE}_{\mathrm{max}} = \frac{Q}{Q+2} \tag{5.7}$$

where $Q = \frac{B}{\sqrt{AC}}$ is the so-called quality factor[175, 176]. If we now consider an external quantum efficiency (EQE) measurement performed in arbitrary units, the measured output power P is given by:

$$P(n_0) = \alpha\eta B n_0^2 \tag{5.8}$$

Here, η is the extraction efficiency, i.e. $\mathrm{EQE} = \eta\mathrm{IQE}$ and α is a dimensionless factor associated with the detection efficiency. This factor would be known in a calibrated measurement (such as in an Ulbricht sphere). The output power at IQE_{max} is then $P_{max} = P(n_{max}) = \alpha\eta B\frac{A}{C}$. Defining the normalized output power as $p = \frac{P(n_0)}{P_{max}} = n_0^2\frac{C}{A}$, the internal quantum efficiency (IQE) can be rewritten as:

$$\mathrm{IQE}(p) = \frac{Q}{Q + \sqrt{p} + \frac{1}{\sqrt{p}}} \tag{5.9}$$

and likewise for EQE. This means that Q can be extracted from a simple, arbitrary units, EQE measurement, as it is only determined by the shape of the EQE function, a parabola in logarithmic p coordinates. It follows for the DLT, that:

$$\frac{1}{\tau} = A(1 + 2Q\sqrt{p} + 3p) \tag{5.10}$$

which directly allows the extraction of SRH recombination coefficient A, provided Q is known. Finally, the radiative and Auger recombination coefficients can be evaluated, if the device geometry is known. Here, either 3D (per unit volume) or 2D (per unit area) coefficients may be computed. In the 2D case, the coefficients are given by:

$$B_{2D} = A^2 Q(Q+2)\frac{eS}{I_{max}} \tag{5.11}$$

and

$$C_{2D} = A^3(Q+2)^2(\frac{eS}{I_{max}})^2 \tag{5.12}$$

where I_{max} is the current where IQE_{max} is reached, i.e. the current corresponding to $p = 1$. Here, S is the area of the active region, which may be replaced by the volume V of the active region, to obtain the corresponding 3D values. In the standard, planar quantum well (QW) morphology, measuring the area S is straight-forward, while estimating the effective thickness of the (multiple) QWs might be very difficult. With these considerations in mind, the task to obtain the recombination coefficients has been reduced to a simple EQE measurement and a difficult DLT measurement, the latter of which will be discussed in more detail in the following section.

5.2 Differential Lifetimes

Section 5.1 on the preceding page has shown that a method to obtain the DLT is necessary, in order to estimate the recombination coefficients according to equation (5.10) on page 47. In particular, the requirements for this pump-probe measurement are that:

i) The experiment is performed while the device is as close as possible to normal operating conditions

ii) The additional, probe non-equilibrium carrier density δn_0 is small compared to the equilibrium carrier density n_0

iii) The temporal response of the system is known and allows evaluation of the DLT from the obtained data

Fulfilling these requirements at the same time is non-trivial and leads to the measurement method employed in this work, small-signal time-resolved photoluminescence (SSTRPL).

i) While the carrier density n_0 may be generated either with electrical injection or with optical injection, similarity with operating conditions can only be achieved by electrical pumping. This is because the applied bias associated with the required current density significantly alters the band structure in the active region, affecting electron–hole overlap and charge densities at the interfaces. Therefore, the device is operated with a DC current (pump) in SSTRPL.

ii) In principal, several approaches may be used to introduce the slight perturbation (probe) in carrier density required. Two main decisions need to be made here: a) optical or electrical injection b) pulsed or sinusoidal probe.

   a) Often, the electrical (DC) drive current is modulated slightly, in order to modulate the carrier density[94, 96, 207, 208]. One may then track the optical response, or (as is often done in electronics, or fast optical systems such as vertical cavity surface emitting lasers (VCSELs)) the electrical response (i.e. impedance). In both cases, the implicit underlying assumption is that the current modulation generated outside the device is transferred into the active region instantaneously. This means that the dominating contribution to

the device impedance is the active region, i.e. the transfer times for carriers from the contacts to the active region is small compared to the DLT. This assumption holds well for many device types (i.e. GaAs-based laser diodes) where such methods are used, but may fail for group III–nitride (III–N) LEDs, where the large interfacial charge densities at the InGaN/GaN interfaces can be considered to be two-dimensional electron and hole gases, and contribute significantly to the device capacitance. Also, the space-charge regions, which are modulated by the current modulation as well, extend far beyond the active region[A2]. Therefore it is necessary to inject the additional carriers optically, for example by pumping the QWs resonantly with laser light.

b) In principle, the optical pumping could be performed pulsed, or with a sinusoidal modulation. For a modulated probe excitation, the detected signal will be modulated with the same frequency, but shifted in time. This phase shift, recorded as a function of modulation frequency, can then be analyzed in order to extract the causal carrier lifetime[209]. Such a measurement is the optical equivalent of an electrical impedance measurement. The range of lifetimes accessible by this method depends on the frequency range of the setup. In addition, sinusoidal manipulation of the output power of the probe laser is only possible significantly above threshold, which means that the probe excitation never drops to zero, slightly changing the equilibrium carrier density n_0. This effect is, however, relatively small. In contrast, the response to a pulsed optical probe excitation is a mono-exponential decay in time (see equation (5.4) on page 46, superimposed with the cw electroluminescence (EL) signal of the pump. So in this instance, the signal processing is similar to conventional time-tesolved photoluminescence (TRPL), and the accessible lifetime range is limited by the time resolution of the setup and the pulse repetition rate[A2]. In principle, both methods yield comparable results[P8]. Here, a pulsed excitation, using a frequency-doubled Ti:Sa laser is used.

iii) An EL measurement as a function of current yields Q as well as the relation between the optical output power p and the current. Following this, SSTRPL transients can be recorded as a function of current, and hence p, allowing to obtain A via equation (5.10) on page 47. As the output power stemming from electrical injection is known, the optical excitation can be tuned to excite only

a negligible amount of additional carriers, in order to stay within small-signal conditions ($\delta n_0 \ll n_0$). This can be verified by changing the excitation power density. Within the small-signal regime, the measured DLT does not depend on the excitation power density - it is independent of δn_0.

While the measurement process is similar to conventional TRPL, the obtained result is very different, due to the dominating contribution of the constant, not time-correlated background caused by electrical injection (see figure 3.6 on page 25). Often, an assumption made in the evaluation of TRPL transients is that the dynamic processes causing the decay channels are independent of carrier density, i.e. the transient decay is the sum of multiple exponential decays and/or is fed by exponentially decaying processes (energy transfer). Generally, analyzing TRPL transients is only possible in a meaningful way, if the carrier density drops to zero at the end of the time window. The reason for this is that several orders of magnitude in signal dynamic are required in order to decide whether an observed decay is mono-, bi- or multi-exponential. Such dynamic is not possible if a steady luminescence background develops due to a too small time window. Obviously, this is also true for the SSTRPL case, where the intensity can never drop to zero, as the majority of photons detected is injected by the constant electrical pumping, and is therefore entirely uncorrelated to the optical probe pulses. In fact, this leads to a large constant background, and the dynamic of the signal is only a few percent of the total signal level. However, evaluation of the lifetime becomes possible nevertheless, because the dynamic is already known to be mono-exponential by definition. This fact also lifts the conventional restriction that the decay should be much faster than the accessible time window, as the result in the SSTRPL transient is exactly the same regardless: A large, constant background and a small mono-exponential decay. To make sure that carrier build-up due to incomplete decay is negligible, one can consider the contribution to the recorded signal ($I_0 e^{-\frac{t}{\tau}}$) from the n-th previous pulse, which is $I(t,n) = I_0 e^{-\frac{t+nT}{\tau}}$. Summing over all previous pulses, one obtains:

$$I(t) = \frac{I_0}{1 - e^{-\frac{T}{\tau}}} e^{-\frac{t}{\tau}} \tag{5.13}$$

i.e. the decay has the same time constant despite a residual density, and the

residual carrier density can be distinguished from the background caused by the equilibrium carrier density.

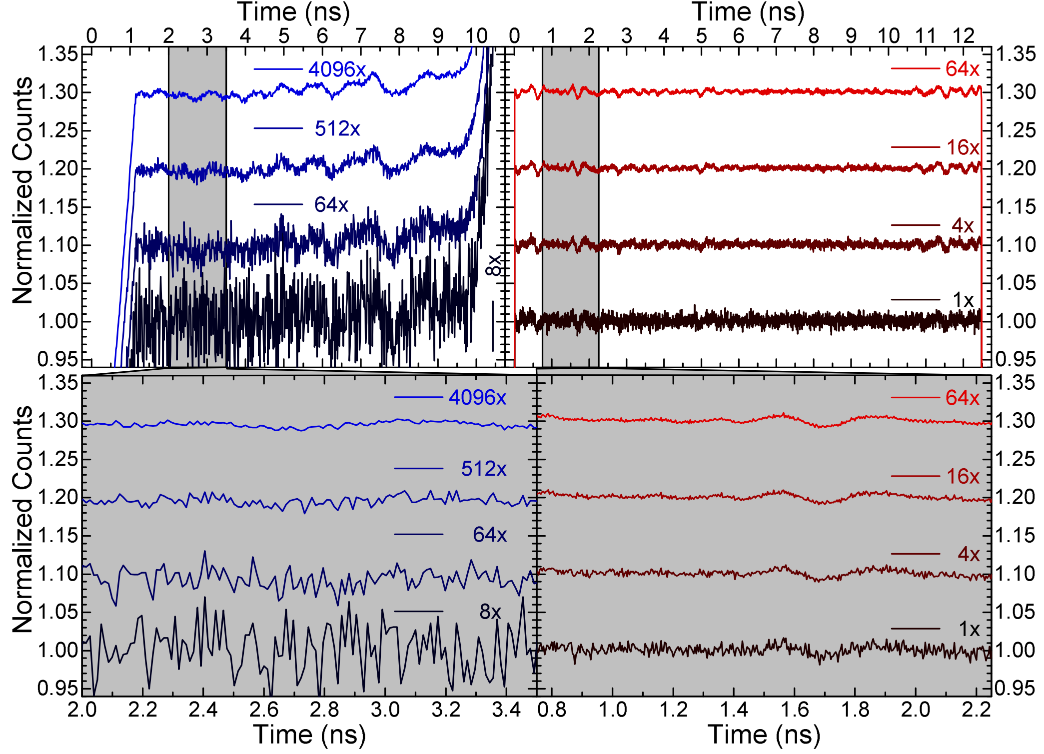

Figure 5.1: System responses to continuous wave illumination of the detector. Left: Becker&Hickl SPC–130. Right: PicoQuant PicoHarp 300. Different colors correspond to different number of cumulative transients. The transients have been normalized and offset to each other for clarity. The two lower panels show the marked regions in the upper panels in more detail to allow assessment of signal-to-noise ratios

To illustrate some of the hurdles present in such measurements figure 5.1 shows the continuous wave response of the two used detection systems. To obtain this response a LED was driven in continuous wave mode with the light directed onto the time-resolved detector. This signal was fed into the time-correlated single photon counting (TCSPC) electronics, either a Becker&Hickl SPC–130 (left) or PicoQuant PicoHarp 300 (right), with the mode-locking electronics of the Ti:Sa laser providing the necessary reference signal. Because the detected photons are causally uncorrelated to the synchronizing

laser, a constant TRPL trace would be expected, i.e. all histogram channels should, provided long enough integration time, tend to the same number. In practice, this is not the case, as the measurement electronics are subject to all kinds of external electric fields. For example, within the computer a multitude of oscillatory processes in the MHz range are present. As a result, the system response deviates from a constant one. In both systems, some characteristic deviations are visible, perturbing the base line of the signal by one (PicoHarp) or up to three percent (B&H). These deviations are of similar magnitude as the SSTRPL signal to be measured, which cannot be - by definition - stronger than a few percent. Therefore, data treatment has to correct for this system response. In addition, the B&H system shows some large artifacts at the edge of the measurement window. As a result, the useful range of data acquisition is reduced from the nominal 12.5 ns to around 9 ns. Further, it is also plagued by much lower signal-to-noise ratio (compare number of integrations necessary to resolve the systematic deviations in figure 5.1 on the preceding page). Note that knowledge of this continuous wave response is also crucial for other types of TRPL measurement, where small deviations from a constant (i.e. uncorrelated) stream of photons are considered, such as continuous wave auto- or cross-correlation measurements.

In principal, one would also need to consider the time resolution of the setup, i.e. the broadening of the measured decay, due to finite system response to the laser pulse. In our case, however, the system resolution (approximately 30 ps[A1]) is much better than the fastest observed decays (a few ns). A convolution with the system response to the excitation pulse is therefore not necessary.

Following these considerations, the continuous wave response of the system was measured for several days in order to obtain the smoothest possible response, which was then used to correct raw SSTRPL data. This is shown in figure 5.2 on the following page, where blue and red curves correspond to raw measurement data (integrated for several hours), obtained with the corresponding setups mentioned above. The green traces are the result of division by the continuous wave response shown in figure 5.1 on the preceding page. Here, decays void of any artifacts are observed, with the only difference between the two systems being the useful time range and signal-to-noise ratio. This proves that, as long as the system response to continuous wave illumination is reproducible, even very poor responses can still yield adequate SSTRPL transients. For longer time constants, as generally the case for green-emitting LEDs, low signal-

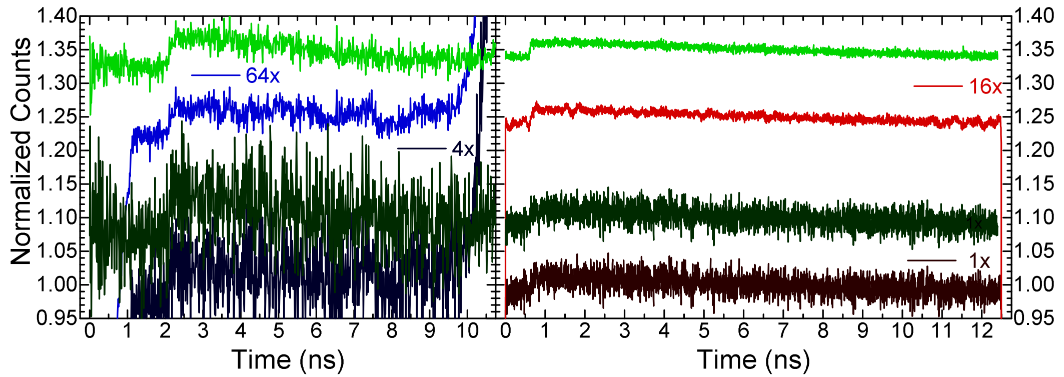

Figure 5.2: Blue (red) curves in the left (right) panel correspond to raw SSTRPL traces recorded with a Becker&Hickl SPC–130 (PicoQuant PicoHarp 300) with different number of cumulative, five minute integrations. The green curves show the corrected SSTRPL, obtained by dividing with the reference response, cf. figure 5.1 on page 52. Note that this removes most of the artifacts visible in the raw transients and allows evaluation of the decay. The transients have been normalized and offset to each other for clarity.

to-noise ratio and long time window are, however, crucial. Therefore, it was necessary to use the PicoHarp 300 system in those cases, while blue-emitting LEDs could be measured with either TCSPC system.

5.3 Carrier Distribution in Multi Quantum Well Stacks

One practical aspect warranting investigation in MQW LEDs, is the optimal number of QWs in the stack. On one hand, more QWs lead to higher active volume and, hence, reduced carrier density at the same operating current, which is beneficial as it reduces Auger losses (section 2.2.5 on page 16). On the other hand, more QWs imply more GaN barrier layers between them, which provide an obstacle for the carriers, which are injected from different sides of the p-n-junction. While the band offsets in the conduction band are much larger as compared to the valence band, the holes in III–N semiconductors posses a significantly larger effective mass than the electrons[210]. As a result, transport of holes along an InGaN/GaN MQW stack is more difficult than electron transport. Electrons and holes which occupy different QWs, obviously do not contribute to recombination, as their wave functions do not overlap. In principal, the optimal number of QWs can be found by trial-and-error (i.e. it is the structure with the best EQE), but in order to understand the physical limitations leading to this number, it is necessary to investigate the recombination processes.

The following work demonstrates the technique described in this chapter on a set of blue-emitting LEDs with differing QW number. As the QWs are nominally identical, this gives crucial insight into the carrier distribution in MQW LEDs. It was published as Ref. [A2]:
F. Nippert, S. Karpov, I. Pietzonka, B. Galler, A. Wilm, T. Kure, C. Nenstiel, G. Callsen, M. Straßburg, H.-J. Lugauer, and A. Hoffmann,
"Determination of recombination coefficients in InGaN quantum-well light-emitting diodes by small-signal time-resolved photoluminescence",
Japanese Journal of Applied Physics **55**, 05FJ01 (2016),
DOI: `10.7567/JJAP.55.05FJ01`

It also contains Refs. [26, 45, 90, 94, 96, 144–146, 155, 164, 175, 176, 185, 186, 189, 207, 208, 211]. In the following, the postprint version is reproduced with permission of The Japan Society of Applied Physics, who retain all copyrights.

Japanese Journal of Applied Physics REGULAR PAPER

Determination of Recombination Coefficients in InGaN Quantum-Well Light-Emitting Diodes by Small-Signal Time-Resolved Photoluminescence

Felix Nippert[1*], Sergey Karpov[2], Ines Pietzonka[3], Bastian Galler[3], Alexander Wilm[3], Thomas Kure[1], Christian Nenstiel[1], Gordon Callsen[1], Martin Straßburg[3], Hans-Jürgen Lugauer[3] and Axel Hoffmann[1]

[1] *Institut für Festkörperphysik, Technische Universität Berlin, Hardenbergstraße 36, 10623 Berlin, Germany*
[2] *STR Group Soft-Impact Ltd., P.O.Box 83, 27 Engels av. 194156 St. Petersburg, Russia*
[3] *OSRAM Opto Semiconductors GmbH, Leibnizstraße 4, 93055 Regensburg, Germany*

We suggest a novel technique for the evaluation of the recombination coefficients corresponding to Shockley-Read-Hall, radiative, and Auger recombination that occur in InGaN/GaN-based light-emitting diodes (LEDs). This technique combines the measurement of the LED efficiency as a function of LED drive current with a small-signal time-resolved photoluminescence measurement of the differential carrier life time (DLT). Using the relationships between the efficiency and DLT following from the empirical ABC-model, one can evaluate all three recombination coefficients. The suggested technique is applied to a number of single- and multiple-quantum well LEDs to gain a deeper insight into the mechanisms ultimately limiting their efficiency.

1. Introduction

While InGaN-based quantum well (QW) light emitting diodes (LEDs) can be considered a mature technology in the blue spectral region, they suffer from the "Droop", i.e. the reduction of efficiency with increasing drive current,[1,2] which has been discussed widely in literature and has been attributed to Auger recombination[3–5] experimentally. In addition, an extension of the emission wavelength into the "Green Gap"[1,6] has proven to be challenging. The origins of both phenomena are continuously debated and their detailed understanding requires deeper insight into the dominating loss mechanisms. For this purpose, the determination of the recombination coefficients corresponding to the principal channels, i.e. Shockley-Read-Hall (SRH), radiative, and Auger recombination is of utmost importance. Naturally, also a detailed analysis of their dependences on the

*E-mail address: felix@physik.tu-berlin.de

*Postprint reproduced from Ref. [A2]Nippert et. al, Jpn. J. Appl. Phys. **55**, 05FJ01 (2016)*
©2016 The Japan Society of Applied Physics. DOI: 10.7567/JJAP.55.05FJ01

LED structure design, InGaN composition, and temperature is quite desirable. First studies carried out in this direction[7–10] have reported on the recombination coefficients considered in terms of the commonly used ABC-model[2,11] and obtained by measuring the differential carrier lifetime (DLT) of non-equilibrium carriers by modulation of the LED operating current. Unfortunately, the recombination coefficients reported in the above studies poorly correlate with each other, which can be partly attributed to different experimental setups and to difficulties in the data interpretation for time-resolved current-modulation experiments (see Sec. 3.3).

In this paper, we suggest a novel technique for the determination of the recombination coefficients combining both, electrical and optical excitation of the LED active region. Our technique has certain advantages if compared to previously applied experimental approaches, since it avoids transient modifications of the LED band diagram, which interfere with the DLT measurements.

2. Theory

The so-called ABC-model is commonly used for interpreting the LED efficiency dependence upon variation of the operating current.[2,11] In this model, assuming an injection efficiency of 100% (i.e. in the absence of electron and hole leakage from the active region), the external quantum efficiency (EQE) of an LED is given by:

$$EQE = \eta \frac{Bn}{A + Bn + Cn^2}, \tag{2.1}$$

where n is the non-equilibrium carrier density assumed to be equal for electrons and holes, η is the light extraction efficiency, and A, B, and C are the SRH, radiative, and Auger recombination coefficients, respectively. Since EQE is usually derived from electroluminescence (EL) as a function of injection current, the number of degrees of freedom in Eq. 2.1 is too large for a meaningful determination of the recombination coefficients from the EL data.

The number of variables can be substantially reduced, if the equation is rewritten in terms of the normalized optical output power p, being the ratio between the LED output power P_{out} and the power P_m corresponding to EQE_{max}, the maximum of the measured EQE. In this case,

$$EQE = \eta \frac{Q}{Q + p^{1/2} + p^{-1/2}}. \tag{2.2}$$

Here, $Q = B/(AC)^{1/2}$ is the so-called quality factor[11] which is a dimensionless combination of the recombination coefficients relevant to the maximum value of internal

Postprint reproduced from Ref. [A2]Nippert et. al, Jpn. J. Appl. Phys. **55**, 05FJ01 (2016)
©2016 The Japan Society of Applied Physics. DOI: 10.7567/JJAP.55.05FJ01

quantum efficiency $IQE_{max} = EQE_{max}/\eta = Q/(Q+2)$. It is important that both values, EQE_{max} and P_m, can be derived directly from the measured EQE dependence on the LED operating current.

In order to evaluate Q, the EQE does not need to be measured in absolute units (e.g. in an Ulbricht sphere), which simplifies the measurements considerably. One can consider the ratio EQE_{max}/EQE depending on the normalized optical power p:

$$\frac{EQE_{max}}{EQE} = \frac{Q + p^{1/2} + p^{-1/2}}{Q+2}, \tag{2.3}$$

which allows finding the Q-factor and, hence, the IQE_{max} value.[12] Additionally, the light extraction efficiency η could be obtained from EQE_{max}/IQE_{max}, if the EQE measurement was performed in absolute units instead.

In addition to the quality factor Q, the parameter P_m can also be expressed in terms of the recombination parameters: $P_m = E_{ph}\eta V_r AB/C$, where E_{ph} is the energy of photons averaged over the LED emission spectrum and V_r is the recombination volume, which is the product of the active region area S and the effective active region width d. As P_m and E_{ph} are known from the EL measurements, η is evaluated by the procedure discussed above, and V_r is estimated from structural parameters. Therefore, the combination of the recombination coefficients $AB/C = P_m/(E_{ph}\eta V_r)$ can also be found from the EL data.

The above two combinations are insufficient for the unambiguous determination of the recombination coefficients. However, their determination becomes possible, if the measured DLT of non-equilibrium carriers is additionally involved. Starting from the rate equation for the unsteady carrier density $N = n + \delta n(t)$

$$\frac{dN}{dt} = j - AN - BN^2 - CN^3, \tag{2.4}$$

and considering $\delta n(t)$ to be a small perturbation of the steady-state carrier density n, one can show that the perturbation decays mono-exponentially with the DLT $\tau = (A + 2Bn + 3Cn^2)^{-1}$. In terms of the normalized optical power p the DLT can be expressed by

$$\tau = \frac{A^{-1}}{1 + 2Qp^{1/2} + 3p}. \tag{2.5}$$

Equation 2.5 shows that the measurement of the DLT corresponding to a certain steady-state non-equilibrium carrier density n (equivalent to a certain p) enables the direct evaluation of the SRH recombination coefficient A.

Postprint reproduced from Ref. [A2]Nippert et. al, Jpn. J. Appl. Phys. ***55****, 05FJ01 (2016)*
©2016 The Japan Society of Applied Physics. DOI: 10.7567/JJAP.55.05FJ01

With Q and A known, the coefficients B and C could be calculated, assuming that the active volume V_r is known. Generally this is not the case, because of the uncertainty in the estimation of the effective active region width d for multiple quantum wells[11] (MQW). Hence, we will use the corresponding sheet parameters: $B_{2D} = B/d$ and $C_{2D} = C/d^2$ instead. For the sheet recombination coefficients, the quality factor has the same form: $Q = B_{2D}/(AC_{2D})^{1/2}$. Another combination of the recombination coefficients, $AB_{2D}/C_{2D} = P_m/(E_{ph}\eta S)$ is now dependent on the active region area S which can be estimated unambiguously and is nearly equal to the LED chip area. Using both expressions, one can express the coefficients B_{2D} and C_{2D} via coefficient A and other experimentally determined parameters as follows:

$$B_{2D} = A^2 Q(2+Q)(qS/I_{max}) \quad , \quad C_{2D} = A^3(2+Q)^2(qS/I_{max})^2. \tag{2.6}$$

Here, q is the elementary charge and I_{max} the LED operating current corresponding to EQE_{max}, which is also found from the EL data without requiring any measurement in absolute units.

3. Experimental Details

As described above, only two spectroscopic measurements are necessary in order to obtain the recombination coefficients. Firstly, an EL measurement as a function of drive current in arbitrary units and secondly, one, preferably more, differential lifetime measurement(s) within this current range.

3.1 Samples

A number of state-of-the-art LED structures was grown by metalorganic vapor phase epitaxy on c-plane sapphire substrates in order to test the presented method. The active regions of the structures consist of one, three, or five InGaN quantum wells (QWs) with a nominal thickness of 3 nm sandwiched between GaN barriers. Standard Mg-doped p-GaN, AlGaN electron blocking layers, and Si-doped n-GaN ensure commonality with production devices. The emission wavelength of the samples is around 440 nm. Several LEDs in the commercial Golden Dragon+ package were produced from each wafer without epoxy casting, providing easy access for optical pumping.

3.2 Electroluminescence

In order to measure the EQE of the LEDs as a function of operating current and to obtain the respective Q-factors, the samples were mounted on a temperature-controlled

*Postprint reproduced from Ref. [A2]Nippert et. al, Jpn. J. Appl. Phys. **55**, 05FJ01 (2016)*
©2016 The Japan Society of Applied Physics. *DOI: 10.7567/JJAP.55.05FJ01*

heating element. The temperature of 350 K, resembling common operating conditions of LEDs, was confirmed to be large enough to avoid additional internal heating under variation of the LED operating current up to 500 mA. The LEDs were driven by a DC source over several orders of magnitude of injection currents and the EL was dispersed onto a Princeton Instruments charge-coupled device by a 30 cm SpectraPro monochromator. The resulting spectra were integrated in order to obtain the total EL intensity as a function of drive current. As a result the EQE as a function of optical output power can be derived.

3.3 Differential Carrier Lifetime

In literature, several methods exist to measure the DLT in electrically driven semiconductor heterostructures. For vertical cavity surface emitting lasers[13)] and edge emitting laser diodes[14)] a common method is to apply an AC-modulated DC bias to the device under test and to measure the impedance as a function of modulation frequency. Using a simplified model replacing the device region by an equivalent circuit consisting of series and p-n junction resistances, a capacitor, and a coil, one can then extract the differential carrier lifetimes from the measured capacitance of the device. While this method works well in some cases of semiconductor laser diodes made of conventional III-V compounds, its application to III-nitride LEDs is questionable. Indeed, AC modulation of the LED bias produces an electric current that is consumed not only for increasing carrier concentration in the active region but also for modulation of space-charge region widths. The DLT of non-equilibrium carriers can only be reliably extracted from the device capacitance, if the contribution of the space-charge regions to the capacitance is much less than that of the active region. The latter condition is satisfied in some laser diodes made of conventional III-V compounds. However, that is not the case for III-nitride LEDs for the following reasons. First, the conduction and valence band offsets in InGaN/GaN structures are much larger compared to other semiconductors, which produces extended space-charge regions beyond the active region. Second, polarization charges accumulated at the LED structure's interfaces provide a considerable contribution to the device capacitance via formation of two-dimensional electron and hole gases. Simulations of the capacitances of typical LED structures carried out with the modified simulator SiLENSe 5.2[15)] have shown that the capacitance originating from the space-charge regions dominates at low currents and becomes comparable with that of the LED active region at high currents. Therefore, the use of such AC-bias modula-

Postprint reproduced from Ref. [A2]Nippert et. al, Jpn. J. Appl. Phys. **55**, 05FJ01 (2016)

©2016 The Japan Society of Applied Physics. DOI: 10.7567/JJAP.55.05FJ01

tion techniques for the DLT evaluation in III-nitride LEDs may introduce considerable inaccuracies to the measurement results.

3.4 Small-Signal Time-Resolved Photoluminescence

To avoid the above mentioned uncertainty in DLT measurements, we optically injected the additional carriers into the QWs. To achieve a resonant excitation of the InGaN QWs exclusively, a frequency doubled Ti:Sa laser tuned to 400 nm was used. The small-signal time-resolved photoluminescence (SSTRPL) experiment consisted of a variable DC bias (tuned within the current range of the previous EL measurement) and a pulsed optical excitation (80 MHz repetition rate with a pulse length of around 2 ps). The samples were mounted and heated as described in Sec. 3.2. The combined PL and EL signal was dispersed by the same monochromator and detected with a Hamamatsu multi-channel plate photo-multiplier (S20 cathode). The recorded photon counts were evaluated with a Becker&Hickl time-correlated single photon counting (TCSPC) card. The time-resolution of this setup (50 ps) is well below all obtained lifetimes.

In order to ensure that all requirements for a differential lifetime measurement ($\delta n << n$) are fulfilled, the excitation power density of the laser was varied such that the contribution of the laser-induced PL is much smaller than the current-induced EL (<5%). It was verified that the variation of this ratio does not change the measured lifetimes. Because the vast majority of recorded photon counts are due to electrical injection and therefore not time-correlated with the laser pulses, long integration times of several hours are necessary to acquire enough signal. In addition great care is necessary to extract the underlying mono-exponential decay. For this purpose we have recorded the system response to uncorrelated EL signals, giving a reference response which is used to filter out artefacts that naturally occur in TCSPC electronics towards the edges of the time window, as the collection process is not time-symmetric.

The corrected transient decay traces finally consist of three components: The constant EL background, the dynamic PL decay, and additional contributions to the PL decay of previous pulses, if the injected carriers do not completely decay within the time window given by the laser repetition rate. Please note that in conventional TRPL experiments such residual carrier densities at the end of the time window should be avoided, because generally the decay times will vary as a function of excitation power density and hence will also vary as a function of residual carrier density. In the present specific case, however, such non-equilibrium effects can be neglected, as the optical excitation is

Postprint reproduced from Ref. [A2]Nippert et. al, Jpn. J. Appl. Phys. ***55****, 05FJ01 (2016)*
©2016 The Japan Society of Applied Physics. DOI: 10.7567/JJAP.55.05FJ01

always low enough that the carrier density is not altered significantly. A second reason to avoid carrier build-up in conventional TRPL is that it results in a rising baseline, which reduces the dynamic of the signal and can ultimately hinder its evaluation. For the case of SSTRPL measurements, the dynamic range is very limited in any recorded transient, due to the constant EL background. In addition the nature of the decay is known to be mono-exponential (Eq. 2.5). It would suffice to treat the residual carrier population as a small part of the constant, current-induced carrier density, but in order to assure that this carrier build-up does not endanger the conditions for a differential measurement we will include its effect in the fitting procedure as a small correction to the optical output power associated with the drive current.

3.5 Evaluation

The EL measurement is used in two ways. First, it proves that the sample under investigation can be treated by the ABC-model and that the currents applied in the DLT measurement do not cause significant internal heating, which would otherwise result in a reduction of the efficiency observed at high currents. Second, as described in Sec. 2, the measurement allows to determine the dimensionless quality factor Q. Figure 1 shows the result of this evaluation for a single quantum well LED at a temperature of 350 K. Applying Eq. 2.3 yields a quality factor of 4 corresponding to a peak IQE of 67 %. With this Q-factor, the ABC-model reproduces the LED efficiency behaviour over the entire current range.

In order to determine the entire set of recombination coefficients of the ABC-model, SSTRPL measurements at various drive currents above the current of peak efficiency were performed. This choice has been made on the basis of signal-to-noise ratio requirements, but generally the measurement can be performed at any current, which is approved by previous EL measurements to be within the ABC-model envelope. Once the raw SSTRPL transient decays have been treated in the manner described in Sec. 3.4, they can be fitted by a mono-exponential decay as detailed in Sec. 2. Generally, if I_0 is the peak intensity of a mono-exponential decay, the transient decay should have the form $I(t) = I_0 e^{-\frac{t}{\tau}}$, where τ is the decay constant. In order to account for the remaining carriers from the previous excitation pulses, which are separated by the repetition time T from each other, this equation becomes $I(t) = I_0 \sum_{n=0}^{\infty} e^{-\frac{t+nT}{\tau}} = I_0 \frac{e^{\frac{-t}{\tau}}}{1-e^{\frac{-T}{\tau}}}$. Adding the constant EL background originating from the current injection leads to the final

*Postprint reproduced from Ref. [A2]Nippert et. al, Jpn. J. Appl. Phys. **55**, 05FJ01 (2016)*
©2016 The Japan Society of Applied Physics. DOI: 10.7567/JJAP.55.05FJ01

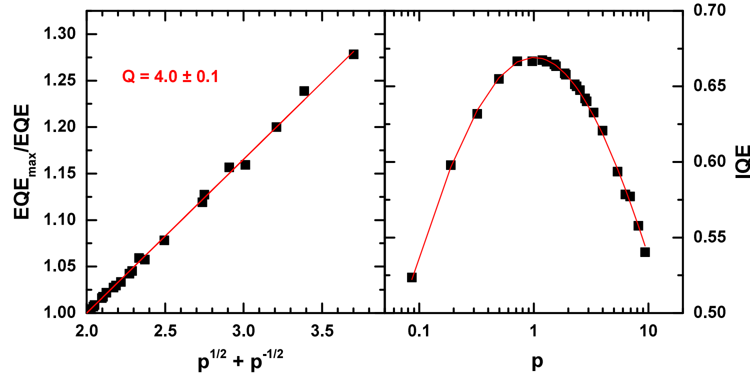

Fig. 1. (Color online) Left: EQE_{max}/EQE ratio as a function of $p^{1/2} + p^{-1/2}$ for a single quantum well LED at a temperature 350 K. Squared symbols are obtained by EL, while the solid line (red) is the linear approximation demonstrating, in particular, that the obtained data conform to the ABC-model.[12] Right: the implied IQE as a function of normalized optical output power for the same device. Squared symbols depict the data extracted from the EL measurements, while the solid line (red) illustrated the fitting with Eq. 2.3. The dimensionless quality factor $Q = 4.0 \pm 0.1$ corresponds to a peak IQE of 67 % at a current of 34 mA.

expression for the SSTRPL fitting function:

$$I(t) = EL + I_0 \frac{e^{\frac{-t}{\tau}}}{1 - e^{\frac{-T}{\tau}}}, \tag{3.1}$$

which is used to determine the DLT (τ). Figure 2 (right) shows an exemplary transient decay recorded for a SQW at a temperature of 350 K with an injection current of 148 mA, fitted with Eq. 3.1. While in principle such a measurement allows the extraction of the recombination coefficient A, the accuracy of the estimate can be improved significantly by varying the drive current and repeating this measurement. This leads to the dependence depicted by data points in Fig. 2 (left). The solid line is a fit of these data points according to Eq. 2.5 and yields a SRH recombination coefficient of $A = (4.46 \pm 0.04)10^6 s^{-1}$.

If, as it is the case here, the current at which the device efficiency is maximal (I_{max}) and the active area S is known, the sheet recombination coefficients B_{2D} and C_{2D} can now be evaluated using Eq. 2.6. This yields the values $B_{2D} = (2.31 \pm 0.04)10^{-5} cm^{-2} s^{-1}$ and $C_{2D} = (7.3 \pm 0.2)10^{-18} cm^{-4} s^{-1}$, which are well comparable to values found in

Postprint reproduced from Ref. [A2]Nippert et. al, Jpn. J. Appl. Phys. **55**, 05FJ01 (2016)
©2016 The Japan Society of Applied Physics. DOI: 10.7567/JJAP.55.05FJ01

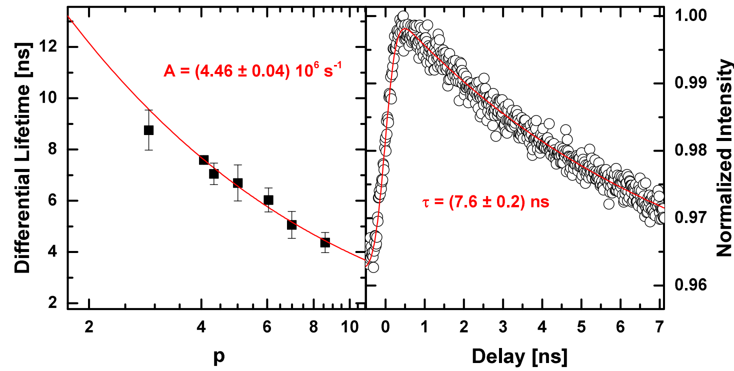

Fig. 2. (Color online) Left: Differential carrier lifetime as a function of normalized optical output power. The solid line represents a fit according to Eq. 2.5, yielding the SRH recombination coefficient $A = (4.46 \pm 0.04)10^6 s^{-1}$. Right: Acquired small-signal time-resolved photoluminescence transient decay for one of the single quantum well samples. The measurement was performed at 350 K with a drive current of 148 mA. The data points are corrected for the system response to a cw-signal and normalized. The dynamic in the PL signal is around 3% of the total signal, showing that the measurement was performed well within the differential regime. In this example, the extracted differential carrier lifetime is $\tau = (7.6 \pm 0.2)\, ns$.

literature.[10)]

4. Results

We have performed the measurements lined out in the previous section for various samples with one, three and five QWs in the active region, respectively. The results are summarized in Fig. 3, where multiple data points with the same number of QWs correspond to different chips manufactured from the same wafer. In particular, the quality factor (top left) increases drastically if the active region consists of multiple QWs. This is mirrored by a significant decrease in the A coefficient (bottom left). Both, Q-factor and A coefficient do not vary strongly if structures with three and five QWs are compared. In contrast, both the B and C sheet coefficients decrease continuously. We note that for a single QW with a nominal thickness of 3 nm the corresponding bulk coefficients B and C are of the order $10^{-11} cm^{-3} s^{-1}$ and $10^{-30} cm^{-6} s^{-1}$, respectively. While the sheet coefficients decrease with increased number of QWs, the corresponding bulk coefficients (assuming a nominally linearly increasing active volume) increase.

 Postprint reproduced from Ref. [A2]Nippert et. al, Jpn. J. Appl. Phys. ***55****, 05FJ01 (2016)*
©2016 The Japan Society of Applied Physics. DOI: 10.7567/JJAP.55.05FJ01

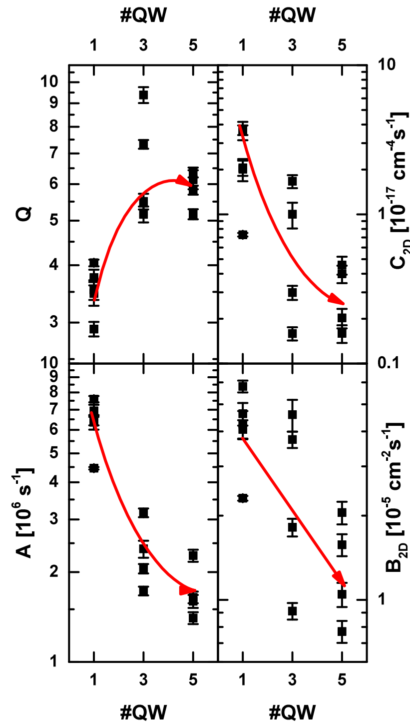

Fig. 3. (Color online) From top left counter-clockwise: quality factor (Q), SRH-recombination coefficient (A), sheet radiative recombination coefficient (B_{2D}) and Auger recombination coefficient (C_{2D}) for various LED devices as a function of the number of QWs. The determination of the parameters is described in Sec. 3.5. Multiple points at the same number of QWs correspond to different LED chips fabricated from the same wafer. Red arrows are guides to the eye.

5. Discussion

We note that the scatter of the obtained values for nominally identical chips is rather large. This is especially notable, because individual chips were not only taken from the same wafer, but also from adjacent positions. Such large scatter is not uncommon[10] and suggests a relatively large inhomogeneity in the material. The emission spectrum however, is basically identical. Therefore the large difference in recombination prop-

Postprint reproduced from Ref. [A2]Nippert et. al, Jpn. J. Appl. Phys. **55**, 05FJ01 (2016)
©2016 The Japan Society of Applied Physics. DOI: 10.7567/JJAP.55.05FJ01

erties arises from local differences in microscopic properties (e.g. point defect density, threading dislocation density) from chip to chip, rather than from more global properties such as QW composition and thickness, which may vary across the wafer and would cause varying EL spectra. This material inhomogeneity may originate from non-optimal growth-conditions of the LED structures studied here, which is also suggested by the relatively low quality factors compared to commercial blue LEDs, which show up to $Q = 8$ at 350 K.[12)]

The reduction of the SRH recombination parameter with QW number (M) is consistent with the assumption that all devices contain one highly defective QW[16)] and M-1 less defective QWs with a defect density ratio of approximately 7:1. The QW with a higher defect density is most likely the top-most QW, which suffers from an increased point defect incorporation due to Mg back diffusion during p-GaN growth.[16)]

The fact that the radiative and Auger sheet recombination coefficients do not scale with M^{-1} and M^{-2} respectively, strongly suggests that the effective active region width does not increase linearly with the number of QWs. Therefore not all of the QWs are efficiently pumped by the applied bias.[17–19)] As a result, any further addition of QWs does neither increase the Quality Factor (Fig. 3) nor shift the maximum of efficiency to higher currents. In this particular case, increasing the number of QWs beyond three has no positive effects on the overall efficiency of the LED.

6. Conclusion

We have demonstrated a novel technique that allows to directly measure the recombination coefficients corresponding to SRH, radiative, and Auger recombination in InGaN/GaN (multi) quantum well LEDs. This is achieved without requiring EQE measurements in absolute units and relies on the novel small-signal time-resolved photoluminescence (SSTRPL) approach. We have tested this method on a large quantity of SQW and MQW devices, where the determination of the recombination coefficients allows to pin the reduction in efficiency in SQW devices on an increased point defect density. In addition the lack of efficiency improvement from three to five QWs is shown to be caused by inhomogeneous pumping of the QWs. The suggested technique can be used for all devices (and in all operating regimes), which conform to the standard ABC-model. Therefore, SSTRPL will enable a deeper understanding of the underlying physical processes that limit device efficiency, providing a promising tool to analyse device shortcomings in the green spectral region.

*Postprint reproduced from Ref. [A2]Nippert et. al, Jpn. J. Appl. Phys. **55**, 05FJ01 (2016)*
©2016 The Japan Society of Applied Physics. DOI: 10.7567/JJAP.55.05FJ01

Acknowledgment

We gratefully acknowledge the financial support of the European Union FP7-ICT Project NEWLED, No. FP7-318388, and the German Science Foundation within the Collaborative Research Center 787 (CRC 787).

Postprint reproduced from Ref. [A2]Nippert et. al, Jpn. J. Appl. Phys. ***55****, 05FJ01 (2016)*
©2016 The Japan Society of Applied Physics. DOI: 10.7567/JJAP.55.05FJ01

References

1) M. R. Krames, O. B. Shchekin, R. Mueller-Mach, G. O. Mueller, L. Zhou, G. Harbers, and M. G. Craford, J. Disp. Technol. **3**, 160–175 (2007).
2) J. Piprek, Phys. Status Solidi A **207**, 2217–2225 (2010).
3) J. Iveland, L. Martinelli, J. Peretti, J. S. Speck, and C. Weisbuch, Phys. Rev. Lett. **110**, 177406 (2013).
4) M. Binder, A. Nirschl, R. Zeisel, T. Hager, H.-J. Lugauer, M. Sabathil, D. Bougeard, J. Wagner, and B. Galler, Appl. Phys. Lett. **103**, 071108–071108 (2013).
5) B. Galler, H.-J. Lugauer, M. Binder, R. Hollweck, Y. Folwill, A. Nirschl, A. Gomez-Iglesias, B. Hahn, J. Wagner, and M. Sabathil, Appl. Phys. Express **6**, 112101 (2013).
6) S. Nakamura, M. Senoh, N. Iwasa, and S. Nagahama, Jpn. J. Appl. Phys. **34**, L797–L799 (1995).
7) A. David and M. J. Grundmann, Appl. Phys. Lett. **96**, 103504 (2010).
8) W. G. Scheibenzuber, U. T. Schwarz, L. Sulmoni, J. Dorsaz, J.-F. Carlin, and N. Grandjean, J. Appl. Phys. **109**, 093106 (2011).
9) B. Galler, P. Drechsel, R. Monnard, P. Rode, P. Stauss, S. Froehlich, W. Bergbauer, M. Binder, M. Sabathil, B. Hahn, et al., Appl. Phys. Lett. **101**, 131111 (2012).
10) D. Schiavon, M. Binder, M. Peter, B. Galler, P. Drechsel, and F. Scholz, Phys. Status Solidi B **250**, 283–290 (2013).
11) S. Karpov, Optical and Quantum Electronics **47**, 1293–1303 (2015).
12) I. Titkov, S. Karpov, A. Yadav, V. Zerova, M. Zulonas, B. Galler, M. Strassburg, I. Pietzonka, H.-J. Lugauer, and E. Rafailov, IEEE J. Quantum Electron. **50**, 911–920 (2014).
13) G. Giudice, D. Kuksenkov, and H. Temkin, IEEE Photonics Technol. Lett. **10**, 920–922 (1998).
14) M. Shatalov, A. Chitnis, A. Koudymov, J. Zhang, V. Adivarahan, G. Simin, and M. Khan, Jpn. J. Appl. Phys. **41**, L1146 (2002).
15) `http://www.str-soft.com/products/SiLENSe/index.htm`.
16) K. Köhler, T. Stephan, A. Perona, J. Wiegert, M. Maier, M. Kunzer, and J. Wagner, J. Appl. Phys. **97**, 104914 (2005).

Postprint reproduced from Ref. [A2]Nippert et. al, Jpn. J. Appl. Phys. ***55****, 05FJ01 (2016)*
©2016 The Japan Society of Applied Physics. DOI: 10.7567/JJAP.55.05FJ01

17) A. David, M. J. Grundmann, J. F. Kaeding, N. F. Gardner, T. G. Mihopoulos, and M. R. Krames, Appl. Phys. Lett. **92**, 053502 (2008).
18) J. P. Liu, J.-H. Ryou, R. D. Dupuis, J. Han, G. D. Shen, and H. B. Wang, Appl. Phys. Lett. **93**, 021102 (2008).
19) Y.-K. Kuo, J.-Y. Chang, M.-C. Tsai, and S.-H. Yen, Appl. Phys. Lett. **95**, 011116 (2009).

Postprint reproduced from Ref. [A2]Nippert et. al, Jpn. J. Appl. Phys. ***55****, 05FJ01 (2016)*
©2016 The Japan Society of Applied Physics. DOI: 10.7567/JJAP.55.05FJ01

In this work, a novel measurement approach was demonstrated, which consists of a simple, arbitrary units EQE measurement to determine the Q-factor and a challenging SSTRPL pump-probe measurement to obtain the DLT and, finally, the recombination coefficients. This method was successfully applied to a range of blue-emitting MQW LEDs. Here, a strong decrease of the non-radiative SRH recombination for MQW, as compared to SQW devices is observed. This suggests a significant contamination in one of the QWs, likely the one closest to the p-side of the device, which may suffer from Mg diffusion during growth of the p-type GaN layer. Further, the efficiency of five QW LEDs is almost identical to that of three QW LEDs. Due to the determination of the recombination coefficients, this can be traced to inhomogeneous pumping of the five QW, i.e. the carriers are not equally distributed among the QWs, reducing radiative and Auger recombination. In other words, the effective active region thickness d, used to convert between sheet (B_{2D},C_{2D}) and volume (B_{3D}, C_{3D}) recombination coefficients does not scale linearly with the number of QWs in the device, limiting the maximum number of QWs such a device may contain.

Note that the measurements presented in this section were all performed at room temperature. In principal, other methods may also be used to obtain the DLT, for example the purely electrical methods usually used in VCSEL characterization. Such measurements are of questionable value, as described in section 5.2 on page 49, due to the inherent large polarization fields in InGaN/GaN heterostructures, which introduce significant, additional impedances into the system. At lower temperatures, where the conductivity of the devices is reduced, these effects should be even stronger, making SSTRPL necessary. Note also, that other, similar techniques[90, 94, 212], rely on absolute units EL measurements to obtain one of their input parameters for the rate equations. Performing such measurements (i.e. in an Ulbricht sphere) at lower temperatures is notoriously difficult[176], whereas in SSTRPL, the measurement works - in principle - just the same as at room temperature. In conclusion, the novel SSTRPL-based method to obtain the recombination coefficients has been demonstrated at room temperature with blue-emitting LEDs, but is also ideally suited to investigate as well green-emitting LEDs at lower temperatures, allowing to gain insight into the physical mechanisms at play. Such measurements will be presented in section 5.4 on the facing page

5.4 Temperature-Dependence of the Recombination Coefficients

One of the key questions that the solid-state lighting (SSL) industry faces today is the physical origin of the so-called green gap, the significant reduction in efficiency of green LEDs (section 2.2.4 on page 15). In particular, one may ask whether the green gap is the result of fundamental material parameters, or just a snapshot corresponding to the current level of technological expertise. Depending on the answer, it might be necessary to invest more heavily into unconventional approaches such as semi- or non-polar structures or nanostructures of reduced dimensionality such as nanowires or quantum dots. Obviously, in order to judge whether this, often observed, phenomenon is related to a fundamental physical issue, rather than e.g. suboptimal growth conditions, it is of paramount importance to carry out experiments on material of highest quality. For this reason, the following investigation is performed using state-of-the-art InGaN MQW LEDs, sourced from factory production runs. As has been alluded to in section 5.1 on page 46, the SSTRPL method provides direct access to the recombination coefficients. This section will show, that by measuring the temperature dependence of these recombination coefficients (and hence of the underlying radiative and non-radiative recombination processes), an understanding about the fundamental quantum efficiency limitations originating the green gap can be generated.

5.4.1 Potential Causes of the "Green Gap"

Generally, the assumed origin of the green gap phenomenon are challenging crystal growth at high indium composition and the quantum-confined Stark effect (QCSE):

a) Because the QCSE limits the QW thickness to around 3 nm, it is necessary to increase the In content in the InGaN QWs, in order to obtain green-emitting LEDs. In metal-organic vapor phase epitaxy (MOVPE), this is generally achieved by lowering the growth temperature[213]. At lower growth temperature, point defects are more likely to form, which may act as non-radiative centers, i.e. increase the A coefficient[214].

b) Further, InGaN with a higher In composition has a larger lattice mismatch to GaN, which means that the structures are affected by higher stress levels if grown

pseudomorphically. This reduces the critical thickness (before plastic relaxation occurs) of the layers, further limiting the design space (i.e. reducing the attainable QW thickness). If plastic relaxation occurs, the generated extended defects act as large non-radiative centers, drastically increasing the A coefficient.

c) Due to the large piezo-electric constants of III–N materials, and the larger amount of strain incorporated in InGaN/GaN heterostructures with higher In composition, the internal electric fields are magnified, pulling apart electron and hole wave functions more, even if the QW thickness is kept constant. Obviously this reduces the radiative B (and also the Auger C) coefficient.

d) Because the band offsets between InGaN and GaN increase with increasing In content, carrier transport along a MQW stack might be decreased, resulting in less homogeneous carrier distribution (section 5.3 on page 55), also reducing B and C.

5.4.2 Limitations of the ABC-model

The ABC-model is used regularly and with great success[30, 175, 176, 215], but hinges on a few assumptions, which need to be kept in mind:

1. There are no carrier losses other than SRH- and Auger recombination. In particular this implies that no carriers by-pass the active region. Such carrier leakage has been observed in LED structures, in particular if an electron blocking layer (EBL) is omitted[93, 162, 216]. In the present case, however, there is no sign of carrier leakage in the samples presented in this study and the IQE relation of blue devices follows the model almost perfectly at high temperatures, where such losses would be expected to play an important role.

2. The carrier injection is assumed to be homogenous in-plane. Considering that electrodes are usually manufactured in a way that they don't cover the whole chip (to reduce absorption), this is not entirely true[P8]. The measurements presented here were performed with low magnification, such that the values obtained represent average values for the chip.

3. The electron and hole concentrations are the same. This is assumed implicitly, as only the carrier concentration n is used in the formalism, generally. Assuming asymmetric carrier concentrations leads to a different behavior at low currents,

with the IQE tending towards a constant value, rather than decreasing towards zero[175].

4. The carriers are not "frozen out" due to localization. This assumption does not always hold for the samples presented in this study. As the temperature is reduced (especially for green-emitting devices), a higher than expected IQE is generally observed at low currents, because the carriers accumulate in local potential minima, where recombination is more efficient than in the "bulk" of the QW[92].As a consequence, EQE measurements at low temperatures (less than 150 K) cannot be analyzed properly, limiting the temperature range of the presented studies. While localization still plays a role at elevated temperature, as the following study will show, the LEDs conform to the ABC model for higher temperatures, allowing evaluation of the recombination processes with the presented method.

5. A further implicit assumption is that the recombination coefficients do not depend on the carrier density. Obviously, this is - strictly speaking - not the case, as the carrier density alters the charge distribution and subtly effects electron–hole wave function overlap and the state occupation. However, from an experimental point of view, this assumption holds very well, as the EQE can be approximated with constant recombination coefficients, i.e. constant Q, over several orders of magnitude[176].

6. The model only considers spontaneous emission, but not induced emission. It can therefore not be used in lasing structures.

5.4.3 Expectation

As a function of emission wavelength (i.e. with decreasing band gap) a decrease of the spontaneous radiative recombination coefficient (scaling with the band gap energy[217]) and an increase of the Auger recombination coefficient would be expected in bulk material[188]. Taking into account the increasing QCSE and therefore decreasing electron-hole wave-function overlap, however, a decrease of both coefficients can be expected[90]. With rising temperature one would expect SRH recombination to increase strongly, as such processes are usually associated with an activation energy. The radiative recombination rate, on the other hand, would be expected to decrease

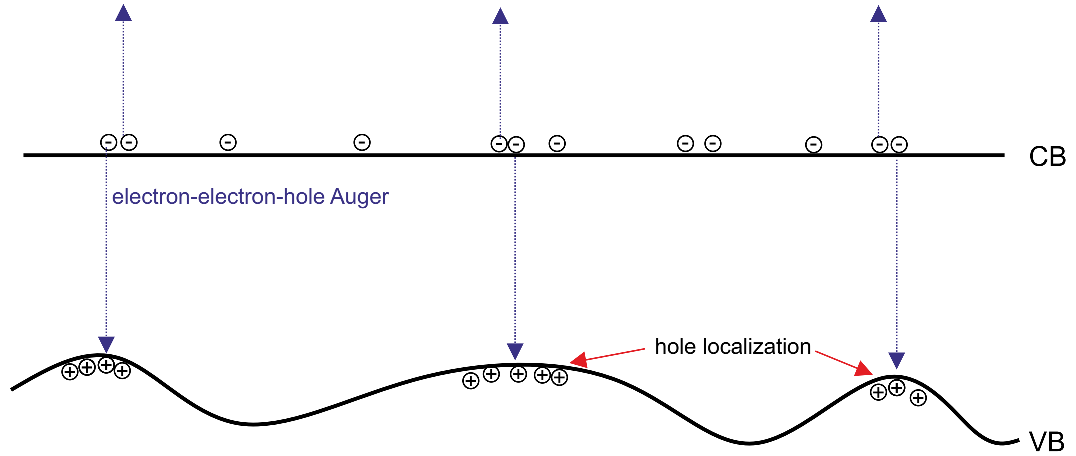

Figure 5.3: Sketch of the particular, dominant Auger process, consistent with all measurement results. In this electron-electron-hole process, a delocalized electron recombines with a localized hole and the energy is transferred to another electron. This process may be phonon-assisted. The sketch shows the band profiles in real space within the QW.

with T^{-1} in a QW[218–220]. For Auger processes, one might expect a similar behavior, however, if the majority of Auger processes is phonon-mediated[221], a strong increase with temperature would be plausible. In contrast to these expectations, the radiative recombination increases (in blue LEDs) or stays relatively constant (in green LEDs) as a function of temperature. This can be understood, if one considers the localization of holes, which is always present in InGaN alloys (see section 2.1.2 on page 5). Here, a simple model, considering holes to be localized (increasingly so for the green devices) in the local potential fluctuations of the alloy, while electrons are completely delocalized, can yield such behavior, consistent with measurement results. This process is sketched in figure 5.3. Such a model is reasonable, as it can be shown that random fluctuations of the In distribution can localize hole wave functions[70, 72, 222, 223]. In contrast, in order to create similar localization potentials for electrons, much higher variations of indium content, or fluctuations in the thickness of the quantum wells would be required[222, 223]. The samples used in this study are of sufficiently high quality, that such effects can be excluded.

The following work presents temperature-dependent recombination coefficients determined for blue- and green-emitting MQW LEDs. The results are discussed on the basis of this simple model of hole localization and allow to draw conclusions regarding the fundamental mechanisms responsible for the green gap. It was published as Ref. [A3]:

F. Nippert, S. Y. Karpov, G. Callsen, B. Galler, T. Kure, C. Nenstiel, M. R. Wagner, M. Straßburg, H.-J. Lugauer, and A. Hoffmann,
"Temperature-dependent recombination coefficients in InGaN light-emitting diodes: hole localization, Auger processes and the green gap",
Applied Physics Letters **109**, 161103 (2016),
DOI: `10.1063/1.4965298`

It also contains Refs. [A2, P5, 26, 30, 45, 60, 62, 68, 70–72, 90, 92, 96, 164, 173–176, 179, 181, 183, 185, 186, 189–191, 212–214, 218–221, 224–234]. In the following, the postprint version is reproduced with permission of AIP Publishing.

Temperature-dependent recombination coefficients in InGaN light-emitting diodes: hole localization, Auger processes, and the green gap

Felix Nippert,[1] Sergey Yu. Karpov,[2] Gordon Callsen,[1] Bastian Galler,[3] Thomas Kure,[1] Christian Nenstiel,[1] Markus R. Wagner,[1] Martin Straßburg,[3] Hans-Jürgen Lugauer,[3] and Axel Hoffmann[1]

[1)] *Institut für Festkörperphysik, Technische Universität Berlin, Hardenbergstraße 36, 10623 Berlin, Germany*

[2)] *STR Group – Soft-Impact Ltd., P.O.Box 83, 27 Engels av., 194156 St. Petersburg, Russia*

[3)] *OSRAM Opto Semiconductors GmbH, Leibnizstraße 4, 93055 Regensburg, Germany*

We obtain temperature-dependent recombination coefficients by measuring the quantum efficiency and differential carrier lifetimes in state-of-the-art InGaN light-emitting diodes. This allows us to gain insight into the physical processes limiting the quantum efficiency of such devices. In the green spectral range, the efficiency deteriorates, which we assign to a combination of diminishing electron-hole wave function overlap and enhanced Auger processes, while a significant reduction in material quality with increased In content can be precluded. Here, we analyze and quantify the entire balance of all loss mechanisms and highlight the particular role of hole localization.

Light-emitting diodes (LEDs) with InGaN/GaN multi quantum well (MQW) active regions are widely used as visible light emitters for solid-state lighting. However, such LEDs still suffer considerably from two phenomena: the so-called "green gap", i.e. LED efficiency reduction in the green/yellow spectral range[1,2], and efficiency droop[2–4] observed at high operating currents. The physical nature of the green gap is still debated extensively[5,6]. In order to shift the emission wavelength to the green/yellow spectral region, it is necessary to increase the In content in InGaN QWs. This may lead to stress relaxation via dislocation formation in the QWs, as a prominent lattice-mismatch with the surrounding GaN layers arises[7]. In addition, higher In content is normally achieved by lowering the InGaN growth temperature[8], which favors point defect formation[9]. Both, extended and point defects should promote Shockley-Read-Hall (SRH) recombination[10], thus reducing LED efficiency. Further, increased In content also gives rise to the quantum-confined Stark effect (QCSE)[11,12], which reduces the electron-hole wave function overlap, and hence the rate of radiative recombination[13,14]. Unfortunately, none of the above mentioned effects can explain quantitatively the magnitude of the reduction of LED efficiency[15], still observed even in devices of the highest quality[16]. For a long time, explanations for the efficiency droop were also controversial[4]. Hotly debated, the droop phenomenon has been assigned experimentally to (phonon-assisted) Auger recombination[17–19]. Deeper insight into the mechanisms critical for both, the green gap and the efficiency droop, may be achieved by measuring the recombination coefficients (RCs). Previous studies have considered room temperature RCs as a function of emission wavelength[10,20], or temperatures above room temperature[21]. Determination of the RCs over a larger temperature range permits to decouple temperature-independent factors, such as QCSE, from temperature dependent ones, e.g. carrier localization. In this Letter, we report on SRH, radiative and Auger RCs, measured in a wide temperature range for state-of-the-art blue- and green-emitting InGaN MQW LEDs. Our findings exclude inferior InGaN material quality from the list of potential causes for the green gap. In addition, we unravel and quantify the contributions of decreasing electron-hole wave function overlap and enhanced Auger recombination. Finally, we consider the increasing hole localization in InGaN alloys with higher indium composition in order to explain the temperature dependences of the RCs. For our study, MQW LEDs were grown by metal-organic vapor phase epitaxy on c-plane sapphire substrates. The devices emit at a wavelength of 445 nm (530 nm) and contain five (seven) QWs. The InGaN QWs were embedded in GaN barriers, comprising Si-doped n-GaN layers below the active region, Mg-doped p-GaN, and AlGaN electron blocking layers on top. The devices were packaged in OSRAM's commercial Golden Dragon+ package and represent the state-of-the-art epitaxial quality. Our method for an evaluation of the RCs is based on the ABC-model[22–24] considering the dependence of the LED external quantum efficiency (EQE) on the carrier concentration in the active region n in the form: $\mathrm{EQE} = \eta_{ext} Bn/(A + Bn + Cn^2)$. Here, η_{ext} is the light extraction efficiency, while the RCs A, B and C correspond to SRH, radiative, and Auger recombination, respectively. The method implies simultaneous measurements of the EQE and the differential carrier lifetime (DLT) by small-signal time-resolved photoluminescence (SSTRPL) *versus* LED operating current[25]. The EQE of our LEDs as a function of operating current was measured by integrating pulsed electroluminescence (EL), a standard method[26]. The EL spectra were recorded with a Princeton Instruments charge-coupled device through a 30 cm focal length SpectraPro monochromator. By evaluating the EQE as a function of normalized optical output power p (i.e. $p = 1$ at the maximum value of EQE – $\mathrm{EQE_{max}}$), the so-called quality factor $Q = B/(AC)^{1/2}$ can be found via the relationship[26]:

$$\frac{\mathrm{EQE_{max}}}{\mathrm{EQE}} = \frac{Q + p^{1/2} + p^{-1/2}}{Q + 2}. \tag{1}$$

Postprint reproduced from Ref. [A3]Nippert et. al, Appl. Phys. Lett. ***109****, 161103 (2016) with permission of AIP Publishing. DOI: 10.1063/1.4965298*

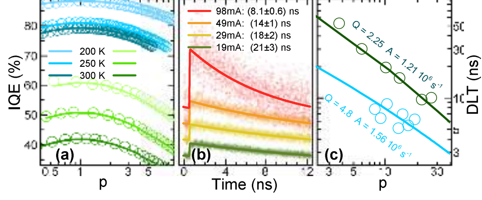

FIG. 1. (a) IQE as a function of p for a blue and a green MQW LEDs at different T. Circles correspond to data points, while solid lines are fits based on the ABC-model. (b) SSTRPL traces for one of the green devices at $T = 300\,\mathrm{K}$ at various currents. Circles correspond to data points and solid lines show mono-exponential fits (see Ref. [25] for details). (c) Exemplary evaluation of the SRH-RC A. Blue (green) points are measured DLTs of a blue (green) MQW LED at $T = 300\,\mathrm{K}$. Solid lines depict fits to the data based on Eq. 2.

For the DLT measurements,the LEDs were pumped electrically with a DC current and in addition optically with a frequency-doubled Ti:Sa laser tuned to 400 nm, guaranteeing optical absorption in the InGaN QWs exclusively. Details regarding the measurement procedure, data evaluation, and a discussion about the necessity of optical pumping for DLT measurements in InGaN structures can be found in Ref. [25]. From the measured DLT (τ), the SRH RC A can be found based on the following equation:

$$\tau = \frac{A^{-1}}{1 + 2Qp^{1/2} + 3p}, \tag{2}$$

Further evaluation of the sheet radiative [$B_{2D} = A^2Q(2+Q)(qS/I_{max})$] and sheet Auger [$C_{2D} = A^3(2+Q)^2(qS/I_{max})^2$)] RCs is straightforward[25]. Here, I_{max} is the current corresponding to the EQE maximum, S is the active region area, and q is the elementary charge. Note that both, A and Q, are independent of I_{max}; moreover, the Q-factor does not depend on whether bulk RCs B and C or sheet RCs B_{2D} and C_{2D} are used for its determination. As soon as the Q-factor is known, the maximum IQE value $\mathrm{IQE_{max}} = Q/(Q+2)$ can be easily estimated. Figure 1(a) shows the IQE of typical blue and green MQW LEDs as a function of normalized optical output power p. While the EQE datasets are measured in arbitrary units, their fitting by Eq. 1 allows the determination of the quality factor Q and, hence, the dependence of IQE on p in absolute units (solid lines in Fig. 1(a)). We wish to remark, that at low temperatures (<150 K) and low currents ($p < 1$), the behavior of green LEDs is found to deviate from the ABC model: The measured IQE is higher than predicted by theory. This implies that in this regime, the RCs are not independent of the injection level anymore, and the assumptions made to evaluate the RCs do not hold. Therefore, the presented study is confined to the temperature range where the LED efficiency can be well approximated by the ABC-

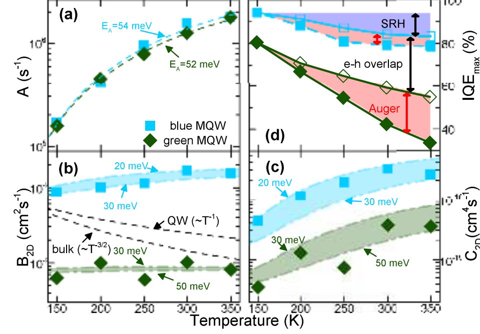

FIG. 2. Temperature dependence of the RCs corresponding to (a) SRH, (b) radiative, and (c) Auger recombination. Blue squares (green diamonds) refer to blue-emitting (green-emitting) MQW LEDs. The blue (green) shaded areas show theoretical estimates made for certain ranges of the hole localization energy (see text). (d) Temperature dependence of IQE. Open symbols represent values derived under the assumption that B_{2D} and C_{2D} would not vary with temperature above 150 K. The shaded areas demonstrate the impact of several mechanisms to IQE reduction (see text). Dashed lines in panel (a) and (b) show fits of the activation energy E_A of SRH recombination, and the expected temperature dependence of B in bulk and QW material, respectively.

model with constant RCs[26]. This also means that all DLT measurements are performed at $p > 1$ – a condition always fulfilled under real world operating conditions. Figure 1(b) displays exemplary SSTRPL traces obtained at 300 K at various currents. The transient decays are mono-exponential and the constant (EL) background has been subtracted for clarity. One can see that the DLTs decrease with rising LED drive current and, thus, with increasing carrier density in the active region. Using Eq. 2, these DLTs along with the Q-factors can be used to extract the SRH coefficient A. This is demonstrated in Fig. 1(c) for blue and green MQW LEDs at a temperature of 300 K. Here the measured DLT trends (circles) are approximated with Eq. 2 (solid lines) for unambiguous values of the A. Figure 2 summarizes the main results of our extended study. Filled blue squares (green diamonds) in Fig.2 correspond to blue (green) MQW LEDs. The IQE of green-emitting devices is found to be much lower than that of blue-emitting ones, cf. Fig.1(a), indicating the green gap behavior. Further, it can be observed that the efficiency of the green LEDs is lower than that of blue ones even at low temperatures and exhibits a more pronounced decline with temperature. Usually, the green gap is explained by a rise in the point/structural defect density in the InGaN QWs with high In content – an enhanced SRH recombination – or by a decreased overlap between electron and hole wave functions due to the QCSE, lowering the radiative recombination. Naturally,

also a combination of both factors seems plausible at first glance. In contrast, we have obtained almost identical SRH RCs A for our blue (445 nm) and green (530 nm) LEDs over the whole temperature range (see Fig. 2(a)). Consequently, very similar SRH-related activation energies E_A of 54 meV and 52 meV can be obtained. A similar result has been reported earlier for room temperature only[10,16]. In our case, the identical temperature dependence of the SRH RC over a wide temperature range provides strong evidence for a well-comparable crystal quality of the InGaN QWs for blue and green light emission, which is attained despite the very different compositions of the InGaN alloys. This means, that the observed IQE reduction towards longer emission wavelength cannot be associated with an assumed enhanced defect generation at higher In content in the QW active region. The radiative (B_{2D}) and Auger (C_{2D}) RCs are shown in Fig. 2(b) and (c). Both coefficients are reduced significantly for the green-emitting devices, if compared to blue-emitting ones. Whereas recalculation of the sheet RCs to the bulk ones is questionable because of uncertainty in the number of QWs participating effectively in recombination[25], the observed big difference in both RCs still suggests a substantial reduction in the overlap of electron and hole wave functions in green LEDs. This reduction cannot be, however, attributed entirely to the QCSE arising in the InGaN QWs due to polarization charges at the QW interfaces, which are enhanced with rising In content in the InGaN alloy. Indeed, both, B_{2D} and C_{2D}, are found to increase generally with T (see Fig. 2(b,c)). While the rise of the Auger RCs with T does not conflict qualitatively with available models considering phonon-assisted processes[27], a corresponding rise of the radiative RCs (blue LED) or an almost constant behaviour (green LED) is anomalous, as either a proportionality to $T^{-3/2}$ (bulk materials)[28,29], to T^{-1} (QWs)[30,31], or no temperature dependence (quantum dots)[32] is expected in semiconductors (compare with dashed lines in Fig. 2(b)). It should be noted that some traces of a synchronous variation of B and C with T, were previously reported[26,33], but attributing the anomaly just to the B coefficient has become possible only due to the direct determination of an independent set of the RCs in this study. In order to interpret the observed anomalous temperature dependence of B_{2D}, we consider that a few neighboring In atoms may provide effective carrier localization in InGaN[6,34,35]. Here, a simple model is used, assuming electrons to be completely delocalized and holes to be localized in the bulk of an InGaN alloy due to larger effective masses. The hole localization is characterized by the localization energy E_L counted from the top of the valence band, and the wave function localization radius $a_L = \hbar/(2m_h E_L)^{1/2}$ where $\hbar$ is the reduced Planck constant and m_h is the hole effective mass. Assuming the localized hole wave function to be hydrogen-like, one can calculate the radiative recombination constant[36]:

$$B = 64\pi\nu_B\langle a_{eff}\rangle^3, \nu_B = \frac{2\alpha n_r E_g E_P}{3\hbar m_0 c^2} \qquad (3)$$

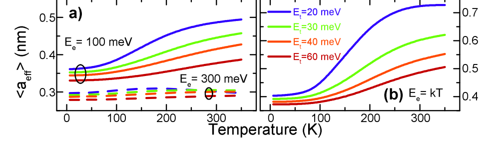

FIG. 3. Temperature dependence of the effective localization radius $\langle a_{eff}\rangle$ calculated for different energies E_t (characteristic for the localization strength) of the hole density of states tail. (a) For constant kinetic energies of electrons E_e, (b) for non-degenerate electrons ($E_e = kT$). A hole Fermi level of $F_p = 100$ meV is assumed for all calculations.

Here, $\alpha \approx 1/137$ is the fine-structure constant, n_r and E_g are the group refractive index and energy gap of the material, respectively, $E_P = 2m_0P^2/\hbar^2$ is the energy related to Kane's matrix element P[37], m_0 is the electron mass, and c is the velocity of light in vacuum. The effective localization radius $\langle a_{eff}\rangle$ in Eq. 3 is defined by the expression $\langle a_{eff}\rangle^3 = \rho^{-1}\int_0^\infty g(E_L)f(E_L)a_L^3(E_L)\xi^4(E_L)dE_L$ where $g(E_L)$ is the density of states (DOS) of localized holes, $f(E_L) = [1 + exp[(F_p - E_L)/kT]]^{-1}$ is the Fermi-Dirac distribution function of holes, $\xi(E_L) = m_hE_L/(m_hE_L + m_eE_e)$, m_e is the electron effective mass, and E_e is the mean kinetic energy of delocalized electrons, which is equal to kT in the case of non-degenerate carriers. Additionally, F_p is the quasi-Fermi level for holes, k is the Boltzmann constant, and the concentration of localized holes ρ is defined as: $\rho = \int_0^\infty g(E_L)f(E_L)dE_L$. As follows from Eq. 3, the temperature dependence of the radiative recombination constant B is mainly determined by that of the effective localization radius $\langle a_{eff}\rangle$. Assuming for simplicity the DOS of localized holes to have an exponential form[38], $g(E) = [1 + exp(E/E_t)]^{-1}$, with E_t being the specific energy of the DOS tail in the energy gap, and using typical values of $n_r = 2.9$, $E_g = 2.7$ eV, $E_P = 14$ eV, $m_e/m_h = 0.1$, $m_h = 2.0m_0$, one can obtain the temperature dependence of the effective localization radius $\langle a_{eff}\rangle$ shown in Fig. 3. Here, one can see that the variation of $\langle a_{eff}\rangle$ (and hence B) with temperature depends remarkably on the localization strength characterized by the parameter E_t and the electron kinetic energy E_e. For non-degenerate electrons (Fig 3(b)), $\langle a_{eff}\rangle$ increases monotonically, while the slope decreases with rising localization. If higher kinetic energies E_e are assumed (see Fig 3(a)), the overall, corresponding slope is reduced. With $E_e = 300$ meV, the effective localization radius is even found to increase at low temperatures, followed by a decrease towards higher temperatures ($E_t = 20$ meV) or to be practically independent of temperature ($E_t = 60$ meV). Generally, high-energy electrons possess a reduced overlap with the hole wave functions expressed by the factor ξ, thus causing a reduction of $\langle a_{eff}\rangle$ and, consequently, the radiative RC B. We note that in addition to the radiative RC B, where (temperature-independent) calculations have shown a re-

Postprint reproduced from Ref. [A3]Nippert et. al, Appl. Phys. Lett. **109**, 161103 (2016) with permission of AIP Publishing. DOI: 10.1063/1.4965298

duction due to random alloying[6], also the Auger RC C should scale with the electron-hole wave function overlap. C, corresponding to the process involving two delocalized electrons and a localized hole – in line with the experimentally identified dominant Auger process[19,39,40] – can be estimated as[41]:

$$C = \frac{(16\pi\sqrt{2})}{3}\langle a_L a_G\rangle^3 \frac{E_D}{\hbar}\frac{E_e}{E_g} \quad (4)$$

where $a_G = \hbar/\sqrt{2m_e(E_g - E_L)}$ and $\langle a_L a_G\rangle^3 = \rho^{-1}\int_0^\infty g(E_L)f(E_L)a_L^3(E_L)a_G^3(E_L)dE_L$. The shaded areas in Fig. 2(b) show the thermal evolution of the coefficient B calculated by Eq. 3. Here, good agreement can be reached with E_t in the range of 20-30 meV for blue and of 30-50 meV for green LEDs, values well comparable with the literature[6,34]. In order to achieve this direct comparison with the experimental sheet RC, the calculated B values were scaled with constant factors, to account for the uncertainty in the recombination volume and any additional electron-hole-overlap reduction caused by the QCSE. Here, Fig. 2(b) shows a good correlation of the theoretical temperature dependence with the data on the coefficients B_{2D}, directly suggesting stronger hole localization in green LEDs than in blue ones – as commonly expected[6]. Note that at even higher temperatures, once all holes are delocalized, the B coefficient reduces again[21]. Similarly, temperature-dependent C coefficients calculated for blue and green LEDs by Eq. 4 are presented by the shaded areas in Fig. 2(c) and also correlate with experimental data. The increase of Auger recombination with rising T is more significant than previously predicted in a much narrower temperature range[27]. Naturally not all possible Auger processes are considered in our model, motivating future examinations with focus on phonon-assisted processes. Nevertheless the steep rise of C can already be sufficiently explained by means of hole localization in our simplified model. Based on the determined RCs, we can distinguish between various factors contributing to the green gap. In addition to the observed IQEs (filled symbols), Fig. 2(d) also shows hypothetical IQEs, assuming that their temperature-dependence is determined by the rise in SRH recombination only (open symbols) yielding, e.g., $Q(T) = B(150\text{K})/\sqrt{A(T)C(150\text{K})}$. Consequently, the violet-shaded area indicates the IQE reduction due to SRH recombination that rises with T (150-350 K). The mostly temperature-independent difference between the hypothetical IQE trends for blue and green LEDs (marked by an arrow in Fig. 2(d)) is associated with the different magnitudes of the B and C RCs and therefore originates from the decreasing electron-hole-overlap towards the green spectral range, compared to blue LEDs, due to the QCSE and hole localization, as discussed above. The overlap decrease is responsible for about half of the total green gap IQE reduction towards operating temperature (350 K). The red-shaded areas in Fig. 2(d) mark the additional IQE losses due to the specific temperature dependence of the B and C coefficients. As the temperature dependence of B is minor, cf. Fig. 2(b), Auger recombination is the major contributor to such kind of losses. We have found the efficiency losses to be much more pronounced for green LEDs, meaning that the contribution of Auger recombination to the green gap is most significant. The difference between the Auger losses in blue and green LEDs suggests that the more pronounced thermal activation of Auger processes directly correlates with the stronger localization occurring in green InGaN alloys. Naturally, any rise in charge carrier localization enhances the electron-phonon-coupling[42–45] favoring phonon-assisted Auger processes and their impact on the IQE reduction. In conclusion, we have observed close to identical SRH RCs over the entire temperature range for blue- and green-emitting MQW, ruling out defect generation in InGaN with high In content as principal cause of the green gap. In contrast, the radiative and Auger RCs were found to decrease significantly in green-emitting LEDs, because of a reduced overlap between electron and hole wave functions. The anomalous temperature dependence of the radiative recombination allows us to attribute a part of this reduction to hole localization induced by fluctuations of the InGaN composition, while the temperature independent reduction stems from the QCSE. Here, even a simplified model for all recombination processes, involving delocalized electrons and localized holes, suffices to interpret the data. In addition, the strong rise with temperature of the Auger RC leads to a further reduction of quantum efficiency with temperature. This is especially true for green-emitting LEDs, where holes are still substantially localized at operating temperatures.

We acknowledge financial support from the European Union FP7-ICT Project NEWLED (FP7-318388), and the German Science Foundation (CRC 787).

[1] S. Nakamura, M. Senoh, N. Iwasa, and S. Nagahama, Jpn. J. Appl. Phys. **34**, L797 (1995).
[2] M. R. Krames, O. B. Shchekin, R. Mueller-Mach, G. O. Mueller, L. Zhou, G. Harbers, and M. G. Craford, J. Disp. Technol. **3**, 160 (2007).
[3] A. Laubsch, M. Sabathil, W. Bergbauer, M. Strassburg, H. Lugauer, M. Peter, S. Lutgen, N. Linder, K. Streubel, J. Hader, J. V. Moloney, B. Pasenow, and S. W. Koch, Phys. Status Solidi C **6**, S913 (2009).
[4] J. Piprek, Phys. Status Solidi A **207**, 2217 (2010).
[5] Y. Jiang, Y. Li, Y. Li, Z. Deng, T. Lu, Z. Ma, P. Zuo, L. Dai, L. Wang, H. Jia, W. Wang, J. Zhou, W. Liu, and H. Chen, Sci. Rep. **5**, 10883 (2015).
[6] M. Auf der Maur, A. Pecchia, G. Penazzi, W. Rodrigues, and A. Di Carlo, Phys. Rev. Lett. **116**, 027401 (2016).
[7] A. Lobanova, A. Kolesnikova, A. Romanov, S. Y. Karpov, M. Rudinsky, and E. Yakovlev, Appl. Phys. Lett. **103**, 152106 (2013).
[8] S. Keller, B. P. Keller, D. Kapolnek, A. C. Abare, H. Masui, L. A. Coldren, U. K. Mishra, and S. P. Den Baars, Appl. Phys. Lett. **68**, 3147 (1996).
[9] S. Hammersley, M. J. Kappers, F. C.-P. Massabuau, S.-L. Sahonta, P. Dawson, R. A. Oliver, and C. J. Humphreys, Appl. Phys. Lett. **107**, 132106 (2015).
[10] D. Schiavon, M. Binder, M. Peter, B. Galler, P. Drechsel, and F. Scholz, Phys. Status Solidi B **250**, 283 (2013).

Postprint reproduced from Ref. [A3]Nippert et. al, Appl. Phys. Lett. **109**, 161103 (2016) with permission of AIP Publishing. DOI: 10.1063/1.4965298

[11] T. Takeuchi, S. Sota, M. Katsuragawa, M. Komori, H. Takeuchi, H. Amano, and I. Akasaki, Jpn. J. Appl. Phys. **36**, L382 (1997).
[12] J. Bai, T. Wang, and S. Sakai, J. Appl. Phys. **88**, 4729 (2000).
[13] J. S. Im, H. Kollmer, J. Off, A. Sohmer, F. Scholz, and A. Hangleiter, Phys. Rev. B **57**, 9435 (1998).
[14] F. Della Sala, A. Di Carlo, P. Lugli, F. Bernardini, V. Fiorentini, R. Scholz, and J.-M. Jancu, Appl. Phys. Lett. **74**, 2002 (1999).
[15] K. Bulashevich, O. Khokhlev, I. Y. Evstratov, and S. Y. Karpov, in *SPIE OPTO* (International Society for Optics and Photonics, 2012) pp. 827819–827819.
[16] S. Saito, R. Hashimoto, J. Hwang, and S. Nunoue, Appl. Phys. Express **6**, 111004 (2013).
[17] J. Iveland, L. Martinelli, J. Peretti, J. S. Speck, and C. Weisbuch, Phys. Rev. Lett. **110**, 177406 (2013).
[18] M. Binder, A. Nirschl, R. Zeisel, T. Hager, H.-J. Lugauer, M. Sabathil, D. Bougeard, J. Wagner, and B. Galler, Appl. Phys. Lett. **103**, 071108 (2013).
[19] B. Galler, H.-J. Lugauer, M. Binder, R. Hollweck, Y. Folwill, A. Nirschl, A. Gomez-Iglesias, B. Hahn, J. Wagner, and M. Sabathil, Appl. Phys. Express **6**, 112101 (2013).
[20] A. David and M. J. Grundmann, Appl. Phys. Lett. **97**, 033501 (2010).
[21] B. Galler, P. Drechsel, R. Monnard, P. Rode, P. Stauss, S. Froehlich, W. Bergbauer, M. Binder, M. Sabathil, B. Hahn, and J. Wagner, Appl. Phys. Lett. **101**, 131111 (2012).
[22] H.-Y. Ryu, H.-S. Kim, and J.-I. Shim, Appl. Phys. Lett. **95**, 081114 (2009).
[23] Q. Dai, Q. Shan, J. Wang, S. Chhajed, J. Cho, E. F. Schubert, M. H. Crawford, D. D. Koleske, M.-H. Kim, and Y. Park, Appl. Phys. Lett. **97**, 133507 (2010).
[24] S. Karpov, Opt. Quant. Electron. **47**, 1293 (2015).
[25] F. Nippert, S. Karpov, I. Pietzonka, B. Galler, A. Wilm, T. Kure, C. Nenstiel, G. Callsen, M. Straßburg, H.-J. Lugauer, and A. Hoffmann, Jpn. J. Appl. Phys. **55**, 05FJ01 (2016).
[26] I. Titkov, S. Karpov, A. Yadav, V. Zerova, M. Zulonas, B. Galler, M. Strassburg, I. Pietzonka, H.-J. Lugauer, and E. Rafailov, IEEE J. Quant. Electron. **50**, 911 (2014).
[27] E. Kioupakis, Q. Yan, D. Steiauf, and C. G. Van de Walle, New J. Phys. **15**, 125006 (2013).
[28] G. Lasher and F. Stern, Phys. Rev. **133**, A553 (1964).
[29] G. W. t Hooft and C. van Opdorp, Appl. Phys. Lett. **42**, 813 (1983).
[30] Y. Arakawa, H. Sakaki, M. Nishioka, J. Yoshino, and T. Kamiya, Appl. Phys. Lett. **46**, 519 (1985).
[31] T. Matsusue and H. Sakaki, Appl. Phys. Lett. **50**, 1429 (1987).
[32] L. V. Asryan, Quant. Electron. **35**, 1117 (2005).
[33] J. Hader, J. Moloney, and S. Koch, Appl. Phys. Lett. **99**, 181127 (2011).
[34] L. Bellaiche, T. Mattila, L.-W. Wang, S.-H. Wei, and A. Zunger, Appl. Phys. Lett. **74**, 1842 (1999).
[35] A. Reznitsky, A. Klochikhin, S. Permogorov, L. Tenishev, W. Lundin, A. Usikov, M. Schmidt, and C. Klingshirn, Phys. Status Solidi C **0**, 280 (2003).
[36] A. Levanyuk and V. Osipov, Phys. Usp. **24**, 187 (1981).
[37] E. O. Kane, J. Phys. Chem. Solids **1**, 249 (1957).
[38] M. Jacobson, D. Nelson, O. Konstantinov, and A. Matveentsev, Semiconductors **39**, 1410 (2005).
[39] A. Nirschl, M. Binder, M. Schmid, I. Pietzonka, H.-J. Lugauer, R. Zeisel, M. Sabathil, D. Bougeard, and B. Galler, Opt. Express **24**, 2971 (2016).
[40] K. W. Williams, N. R. Monahan, D. D. Koleske, M. H. Crawford, and X.-Y. Zhu, Appl. Phys. Lett. **108**, 141105 (2016).
[41] S. Y. Karpov, in *SPIE OPTO* (International Society for Optics and Photonics, 2016) pp. 97680C–97680C.
[42] E. Rashba and G. Gurgenishvili, Phys. Solid State **4**, 759 (1962).
[43] J. Feldmann, G. Peter, E. O. Göbel, P. Dawson, K. Moore, C. Foxon, and R. J. Elliott, Phys. Rev. Lett. **59**, 2337 (1987).
[44] A. V. Kavokin, Phys. Rev. B **50**, 8000 (1994).
[45] G. Callsen, G. M. O. Pahn, S. Kalinowski, C. Kindel, J. Settke, J. Brunnmeier, C. Nenstiel, T. Kure, F. Nippert, A. Schliwa, A. Hoffmann, T. Markurt, T. Schulz, M. Albrecht, S. Kako, M. Arita, and Y. Arakawa, Phys. Rev. B **92**, 235439 (2015).

Postprint reproduced from Ref. [A3]Nippert et. al, Appl. Phys. Lett. ***109****, 161103 (2016) with permission of AIP Publishing. DOI: 10.1063/1.4965298*

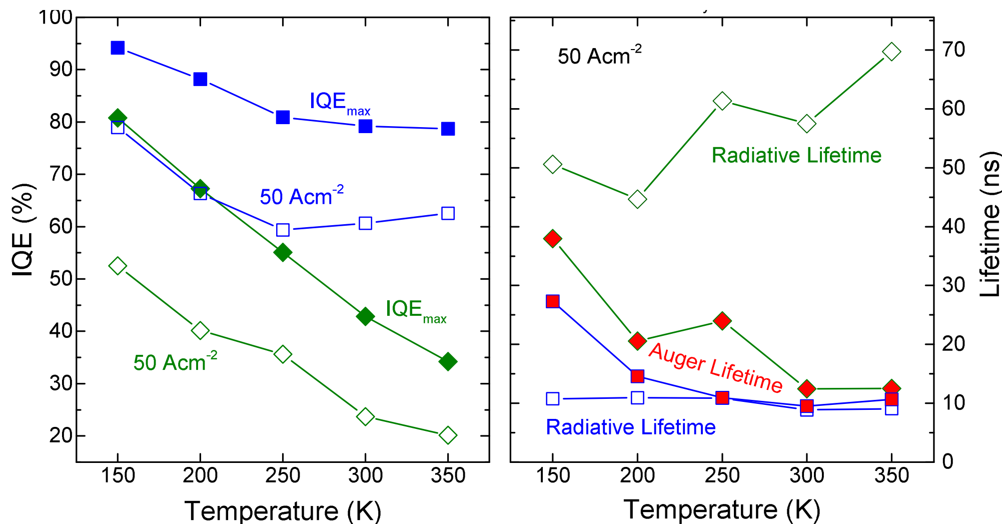

Figure 5.4: Left: Internal quantum efficiency of blue and green MQWLEDs determined by the presented measurements and analysis[A3]. Filled (open) symbols correspond to current densities corresponding to the maximum of efficiency and standard operating conditions, respectively. Right: Contributions to the differential carrier lifetime at standard operating conditions for blue and green LEDs. Open (red filled) symbols show the radiative (Auger) differential carrier lifetime, respectively.

5.5 Conclusion: Origin of the "Green Gap"

The preceding publication shows that the determination of the recombination coefficients as a function of temperature gives direct access to the different physical processes limiting the quantum efficiency. In particular, of the suggested explanations (section 5.4.1 on page 71) for the green gap, a) and b) can be excluded. The growth of InGaN QWs with high In content, as required for green emission wavelengths, is certainly challenging[74, 75, 77, 78], and many groups observe higher defect densities[214, 235–238]. Nevertheless it is in principle possible to produce material with a similar crystal quality as in the blue (lower indium composition) spectral region. This is attested by the almost identical magnitude and thermal evolution of the SRH recombination coefficient A.

Despite such successful technology transfer from blue to green, the typical green gap IQE reduction is found in these samples as well, and is therefore not related to the

density of non-radiative centers. This is shown in figure 5.4a, where filled symbols show the maximum of IQE as a function of temperature for blue and green devices. The open symbols show the IQE at an injection current density of 50Acm^{-2}, representing common operating conditions. Note that at large operating current the efficiency is much reduced due to the droop phenomenon, i.e. additional Auger losses. Nevertheless the observed trends are qualitatively the same as for the efficiency maximum: The IQE is continuously reduced with rising temperature for green devices, while in blue MQW LEDs the IQE stabilizes at around 250 K.

The radiative B and Auger C coefficients are significantly reduced in magnitude in green-emitting devices, as compared to blue-emitting ones, proving lower electron-hole-overlap, due to both, QCSE (c) and hole localization. However, only around 50% of the observed IQE loss from blue- to green-emitting LEDs can be associated with this overlap reduction. The other part is strongly thermally activated, influenced by the hole localization. This is also visualized in figure 5.4b. Here, open symbols show the differential radiative lifetime at an injection level of 50Acm^{-2}, while red filled symbols represent the corresponding Auger lifetime. While, in the case of both blue- and green-emitting LEDs, an increase of Auger processes can be seen, there is also a marked difference: the radiative lifetime is relatively constant for blue MQWs, but even increases in green devices. In addition, the balance between the two processes (SRH not shown as it is orders of magnitude weaker at such higher current) is very different. In blue LEDs, radiative and Auger recombination are balanced, while in green LEDs, Auger recombination is clearly the dominant recombination process at such current densities.

An alternative representation is shown in figure 5.5 on the next page. Here blue and green symbols show the total radiative rates for blue and green devices, respectively, while red symbols show the total non-radiative rate. Filled and open symbols again represent operating conditions at the maximum of efficiency and at a current density of 50Acm^{-2}. Note that the carrier density at the maximum of efficiency is just $\sqrt{\frac{A}{C}}$ and therefore the SRH rate An and the Auger rate Cn^3 are the same – half of the total non-radiative rate. In contrast, at large currents - and therefore larger steady-state carrier density, almost all non-radiative losses are Auger losses.

The hole localization manifests itself in the observed temperature-dependence of the radiative recombination coefficient B, which rises with temperature (see also blue

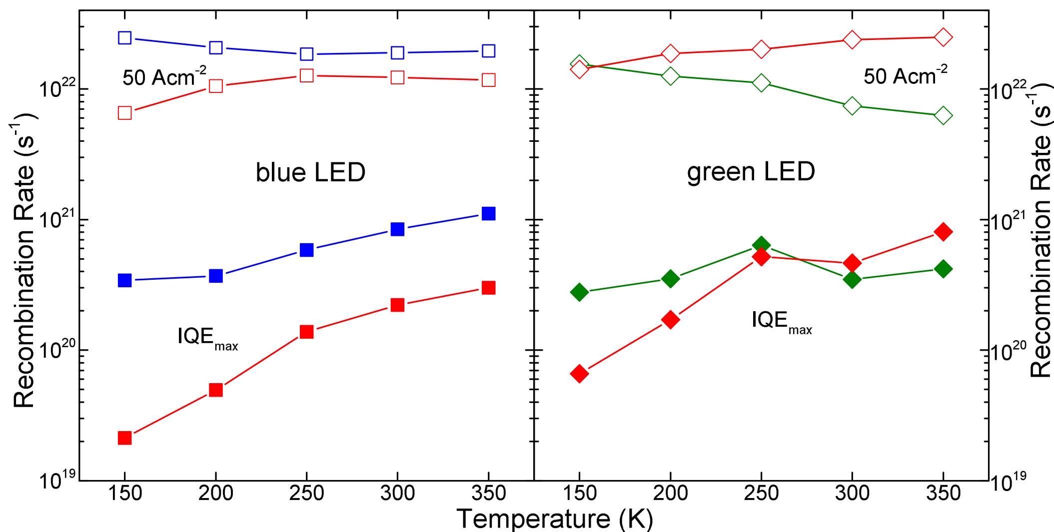

Figure 5.5: Total radiative (blue/green) and non-radiative (red) recombination rates determined for blue and green MQW LEDs at the operation point of maximum efficiency (filled) and at a standard injection current density (open).

solid points in figure 5.5a) – in contrast to the generally expected behavior. Here, using a simplified model of the recombination assuming holes to be localized, and electrons to be delocalized, sensible localization depths in the order of 25 meV (for blue-emitting LEDs) to 40 meV (for green-emitting LEDs) can be approximated. As these localization energies are in the order of kT at room temperature, the holes become increasingly, although not completely, delocalized as the samples are heated towards operating temperature. This increases their wave functions' overlap with the electron wave functions, resulting in the observed rising trend in the radiative recombination.

Due to the different localization depth, caused by the different stoichiometry of the alloys, the delocalization of localized holes requires much higher temperatures in the green spectral range. This is evident by comparing the temperature dependence of the B coefficients[A3], or the corresponding radiative rates (figure 5.5). Naturally, this effect also influences Auger recombination processes, as these also rely on electron–hole recombination and therefore scale with the electron–hole wave function overlap. In this case, however, a rising trend for the Auger recombination coefficient C with temperature is not unexpected, as the majority of Auger processes is thought to be

phonon-mediated and therefore also scales with the phonon population – which of course also increases with temperature. Nevertheless, in the simple model presented, also the temperature-dependence of the Auger recombination can be adequately reproduced.

In sum, the temperature dependencies of the radiative and Auger recombination processes develop in an unfavorable way, i.e. if one ignores the temperature-dependence of the non-radiative A coefficient, the IQE still diminishes both as a function of increasing temperature and with the emission of the devices shifted into the green spectral region. These losses, which make up approximately 50% of all losses contributing to the green gap, are therefore proven to be, exclusively, Auger losses, enhanced due to the localization of holes in the InGaN alloy. This directly links the green gap to the droop – two phenomena commonly considered separately.

In conclusion, the presented studies highlight the crucial role of hole localization for the green gap. Here, convincing experimental evidence is given, that the majority of the green gap IQE reduction is neither caused by increased defect density, nor the QCSE – but rather because the delicate balance between radiative and Auger recombination tips towards Auger recombination as the indium composition of the alloy, and therefore the hole localization, is increased. This finding strongly suggests that the decade-long observed practical limitation of the IQE of green-emitting InGaN-based devices is, in fact, quite fundamental, rather than merely technological.

Note that, while in principal the observed amount of localization is compatible with uniform random alloying, there is no straight-forward experimental method to distinguish uniform from slightly non-uniform random alloying. Careful tuning of the growth parameters might still improve the uniformity of the alloy and therefore soften the detrimental effect of hole localization observed in this work. However, even the perfectly uniform random alloy is expected to show some localization. It is therefore the opinion of the author of this thesis, that - in addition to further work on improving current technology - more exotic approaches, circumventing, rather than solving this problem, are required, if green-emitting InGaN structures are supposed to pass the threshold set by phosphor-converted blue light sources. In this spirit, chapter 6 on the next page presents a few select approaches considered and trialled within the community.

6 Alternative Approaches: Pitfalls and Perspectives

While the physical reasons, underlying the droop and the green gap phenomena were a matter of intense debate, it was still obvious that - if possible - the quantum-confined Stark effect (QCSE) and higher carrier densities should be avoided, in order to increase the radiative rate, and decrease the Auger rate, respectively. Notwithstanding the findings in the previous chapters, these are still useful goals in order to increase quantum yield. In the following, the most common concepts to this end will be briefly discussed.

6.1 Growth in semi- and non-polar directions

From a conceptual point of view, the easiest way to get rid of the QCSE (see section 2.1.1 on page 3), is to leave the conventional, c-plane, polar growth direction, and instead grow the devices on non-polar or at least semi-polar orientations. Much effort is spent on growth on semi- or non-polar direction[239–246] but so far the efficiencies of the resulting devices are far from reaching that of polar ones - despite vanishing QCSE. One problem is strain relaxation, which has so far been shown to be difficult to control. Plastic relaxation via misfit dislocations has been shown to occur quickly[247–249], even on GaN substrates. Further, point defect densities are often found to be much higher than in polar material. In order to illustrate this, samples grown at CNRS-CRHEA on c-plane and m-plane substrates are compared in the following. Here, an m-plane growth geometry is obtained by growing on stripe-patterned r-plane sapphire substrates[250]. Initially the GaN growth proceeds in c-direction, on the facets of the pattern. At later growth stages the different growth fronts coalesce leading to an m-plane surface, which serves as a base for the active layers[251]. The structural parameters of the patterned substrate can also be tuned in such a way, that

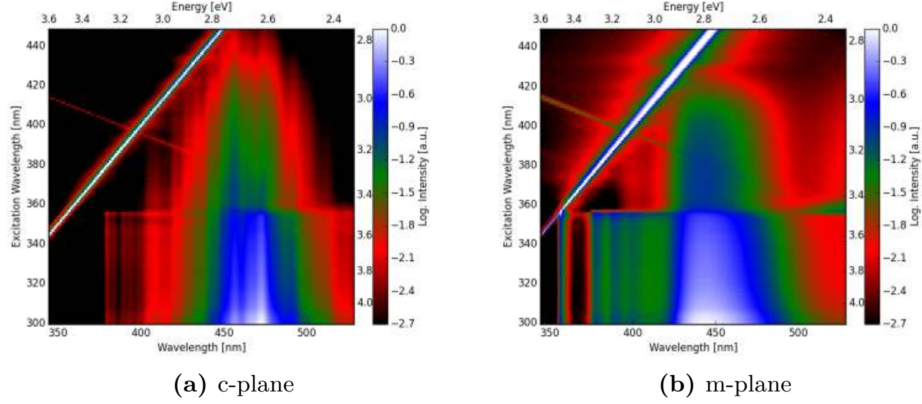

(a) c-plane

(b) m-plane

Figure 6.1: Photoluminescence excitation maps of blue-emitting InGaN quantum wells grown on different crystallographic orientations at 10 K. The plots show PL spectra on the x-axis as a function of excitation (Xe-arc lamp) wavelength on the y-axis as logarithmic color contrast. The bright white line corresponds to the excitation, while the other straight line is due to a monochromator reflex. See text for more detail.

a significant amount of stacking faults can be blocked[252, 253].

In contrast to the conventional, c-plane, sample (figure 6.1a), the semi-polar sample's luminescence is shifted to higher energies (figure 6.1b). This shift is the result of both, reduced QCSE and lower In composition, as indium incorporation is inhibited on this growth plane. Further (not shown), the overall emission intensity is significantly lower, suggesting lower quantum efficiency. The reason for this is a significantly enlarged amount of point defects, as testified by this measurement. Both photoluminescence excitation spectroscopy (PLE) maps can be divided into two excitation regimes: below and above the GaN band gap.

Above the band gap, the majority of light absorption occurs in the GaN barrier and capping layers of the structure, which is also why the PLE signal is enhanced. A first striking difference is the observation of band edge and donor-acceptor-pair (DAP) (blue) luminescences, only possible in the m-plane sample. This suggests, that a large quantity of carriers generated in the GaN layers do not reach the (energetically more favorable) InGaN quantum wells. In the polar sample, the opposite observation can be made: Most carriers recombine in the InGaN quantum wells (QWs), despite being created in the GaN layers, i.e. the mean free path is significantly larger on c-plane.

The reduced energy transfer in semipolar orientation - and the occurrence of the DAP luminescence[196] - strongly suggest a much higher point defect density in the GaN barriers, impeding carrier transport throughout the structure.

Exciting below the band gap, only the InGaN QWs can be excited, as testified by the lack of blue DAP luminescence in this regime (figure 6.1b on the preceding page). In turn, a yellow luminescence, also characteristic for point defect-rich material[196], starts to appear - again only for the m-plane sample. In contrast to the above mentioned defects, these point defects must exist in the QWs themselves. In sum, it can be concluded that all layers of the active region are significantly more defective, if grown in semi-polar direction, compared to polar. This observation is also commonly found in the literature [254], in particular in association with p-GaN overgrowth, and is one of the major reasons why non- and semi-polar orientation approaches remain challenging.

6.2 Cubic InGaN

Another strategy to circumvent the QCSE is to work with the cubic zincblende phase of GaN[255–257], which does not exhibit this effect to start with. Unfortunately, the zincblende phase is thermodynamically less stable than the wurtzite phase. This makes growing high-quality cubic GaN very challenging, as hexagonal inclusions need to be avoided. Cubic group III–nitride (III–N) layers have only been achieved in molecular beam epitaxy (MBE), on a variety of substrates, e.g. SiC[258], r-plane sapphire[259] or even GaAs[256, 257], making this approach potentially very cost-efficient, if the process can be transferred to metal-organic vapor phase epitaxy (MOVPE). While light-emitting diodes (LEDs)[260] and advanced nanostructures[261, 262] have been fabricated, mass production of high-quality cubic GaN currently remains elusive.

6.3 Quantum Dots

Instead of preventing the polarization fields from forming, one may also consider to prevent the fields from tearing apart the electron and hole wave functions. To this end, a further increase of the confinement by forming InGaN quantum dots (QDs) is an option. Also, one could consider a QD to be an extremely deep localization potential, preventing the carriers from diffusing within the active layer, where they may encounter

non-radiative centers (thus reducing the A coefficient, although potentially increasing Auger recombination as found for QW structures in section 5.5 on page 81).

Such InGaN QDs may be obtained by the Stranski-Krastanow method[263], where the strain induced by the large lattice-mismatch ultimately leads to a transition from a 2D to a 3D growth mode, forming QDs embedded in a wetting layer. Such growth is commonly employed in the GaAs system[264, 265], with the QD layer used as gain material for e.g. vertical cavity surface emitting lasers (VCSELs)[266]. In the III–N system, similar approaches have also been used to fabricate GaN/AlN QDs[267]. While the internal electrostatic fields are generally found to be weaker than in planer structures, they still exist. As a result, small changes in QD geometry may lead to large changes in the optical properties of the QDs[268, 269]. Variation in the QD geometry, i.e. a distribution of height, composition, and shape of the QDs, occurs naturally in such a self-assembled growth approach[270, 271]. Further, the remaining QCSE, and resulting electron–hole wave function separation implies an electric dipole moment for excitons in the QDs, drastically enhancing their coupling to the environment[140, 269, 272], partly compensating the shielding from structural defects aimed for.

Naturally, such effects are enhanced significantly, if the QD is composed of a ternary alloy such as InGaN, increasing the degrees of freedom for QD morphology. Such growth[136–139, 273] hence displays large variations in emission energy on a single QD basis, resulting in very broad ensemble luminescence. Incorporation of such inhomogeneous InGaN QD layers into LEDs is possible[274, 275], and may appear even desirable in the context of solid-state lighting (SSL) (where in principal, broad band sources are preferred). However, the lack of controllability of the emission properties makes the integration into white light sources very difficult. A further issue that warrants investigation in this context is the control over carrier injection, as only carriers reaching the QDs should recombine, while the wetting layer should only act as a carrier transport layer. Naturally, the current paths in a QD device, especially with randomly distributed and more or less randomly shaped QDs, are rather more complicated than in a planar device.

6.4 Microrods

Instead of changing the orientation of the sample surface, one may also consider changing the orientation of the growth front. A prominent example is the growth of quantum

wells on the sidewalls of GaN nano- or microrods[131–134]. For rods grown on c-plane, these facets are non-polar. This geometry has the added benefit of increasing the active area, which is now a function of the rods' dimensions and pattern. As such, the carrier density at a given current density (per device area) is reduced, suppressing Auger losses. Further, because the rods can expand into free space, strain is not an issue in this geometry, enabling growth on cheap substrates such as silicon. Naturally, as the growth of the active layers is in non-polar direction, similar problems arise as in conventional non-polar growth (see section 6.1 on page 85). Here, a benefit compared to 2D layers is that strain can be compensated by lattice expansion into the free space between the rods, such that some of the issues present in planar non-polar geometries are prevented.

Nevertheless, the growth procedure is significantly more complex than conventional designs. In particular the poor p-type conductivity in GaN means that current spreading along the outer p-GaN shell of such devices is very difficult, a problem that is solved by covering the whole rod with a thin metal layer. Another critical issue is the light outcoupling. The density of rods cannot be increased arbitrarily, as the light emitted from one rod is scattered multiple times from the surrounding rods, potentially being reabsorbed. This effect is especially pronounced as, due to the lack of QCSE, emission and absorption of the wires are not shifted to each other – the rods are not transparent for the emission wavelength. Naturally this means that a very high IQE is critical in order to efficiently recycle reabsorbed photons[276]. In addition, a device consisting of such microrods is essentially a huge quantity of single-rod-LEDs in parallel. Therefore, any failure in the form of a current breakthrough in a rod reduces the overall efficiency of the device, meaning that the manufacturing processes need to be very reliable. Another problem that arises with this approach is sidewall contamination during growth, increasing series resistance. Nevertheless, competitive blue-emitting LEDs have been fabricated with this approach[135], suggesting that further pursuit of this strategy is worthwhile.

6.5 Lasing

A more radical solution to Auger losses at high carrier densities is to enhance radiative recombination to be an efficient competitor to Auger recombination. This is possible by using stimulated rather than spontaneous emission, as is the case in laser cavities.

To date GaN-based laser diodes (LDs) still trail LEDs in peak wall plug efficiency, but reach this maximum of efficiency at much higher current densities[159]. The reduction in wall plug efficiency is mostly related to electrical losses, which arise as laser structures require much thicker p-type AlGaN layers. Doping AlGaN with magnesium is even more challenging than GaN and usually results in poor hole mobilities. Nevertheless, in principle a LD with similar efficiency as LEDs (usually operated significantly above the current of maximum efficiency) can be produced. In comparison to the LED, this device has much more luminance per chip area and a significantly better directed beam. As such, it may be a good alternative to conventional LEDs for applications which require directed light, such as halogen spot replacements or automotive headlights. Here, two main problems arise: First, the directionality is partly lost, if a phosphorous conversion layer is required for white light generation, but at the same time lasing in the green spectral range is very challenging. Second, LEDs are already limited by the heat dissipation of the package (i.e. requiring expensive materials as heat sinks in conventional sockets), but a LD - even if it had the same efficiency - would produce not only orders of magnitude more light but also orders of magnitude more waste heat.

6.6 Outlook

In conclusion, all of the suggested approaches require extensive research work in the coming decade. The growth on semi- and non-polar planes is still not sufficiently controllable to be a viable alternative for the industry. Here, research activities need to focus on figuring out whether the observed growth problems (defect incorporation, stress relaxation, indium incorporation) are solvable or not. For cubic nitrides, more work needs to be spent on the ability to control phase purity. Ideally, ways to grow cubic GaN in MOVPE would be found, making the system more attractive for mass production. The growth of QDs will likely stay poorly controllable such that the only way forward here seems to be to embed the QD in other quantum structures, such as positioned quantum wires. Such structures would probably not be used in lighting applications, but may be useful for quantum communication. Microrods appear to be closest to commercial realization, but so far no significant gains in comparison to conventional designs have been reported. Here, more work on optimization should quickly show the merits of this path. In the pursuit of LDs for SSL, breakthroughs in p-type AlGaN layer conductivity are required. This requirement is shared with UV LEDs and LDs, where hole conductivity is also one of the bottlenecks preventing efficient devices.

7 Conclusion

This thesis investigated the major loss mechanisms in InGaN/GaN quantum well (QW) optoelectronic devices. Here, two power regimes can be distinguished.

1. The high-power regime is important for laser diodes (LDs), where high carrier densities are required to obtain lasing. This regime was accessed by quasi-resonant, pulsed optical excitation. In such excitation conditions, excited states play an important role[P1]. Within the frame of this work, extensive studies of high-excitation photoluminescence of InGaN/GaN quasi-single quantum well (SQW) led to the first description of the confined hole continuum (CHC)[A1]. This observation hinges on the extremely high crystalline quality of the samples investigated, allowing to reach the high carrier densities required. The luminescence arising from the CHC was characterized to be extremely broad and featureless - in contrast to excited electron states. It decays with drastically decreasing time constants towards higher emission energies, reaching less than 30 ps at 3 eV – orders of magnitude faster than the ground state transitions. In conjunction with extremely fast, and also decreasing, rise times, this decay was attributed to hole relaxation within the CHC band. Utilizing several sets of purpose-grown control structures, as well as biased multiple quantum well (MQW) light-emitting diode (LED) structures, the CHC luminescence was shown to occur universally in high-quality samples. Further, a model for its origin was developed. Here, the CHC is identified as bulk GaN valence-band like states situated in the triangular potential, created at the InGaN/GaN interface due to piezoelectric fields[A1].
2. The conventional power regime includes the operating conditions of state-of-the-art MQW LEDs. In this regime, two well known phenomena were investigated: the green gap and the droop. Utilizing the ABC-model, commonly used to describe the quantum efficiency of such devices, a methodology to gain access to

the recombination coefficients was developed[A2]. It consists of a simple external quantum efficiency (EQE) measurement (not requiring an Ulbricht sphere), and a novel pump-probe technique called small-signal time-resolved photoluminescence (SSTRPL). Here LEDs are driven with a constant bias, and additionally pumped quasi-resonantly with a pulsed laser. The temporal response to the laser pulse can then be used to obtain the differential lifetime (DLT), and ultimately, the recombination coefficients. With this method, the physical origin of the green gap was elucidated. By comparing the temperature-dependence of the recombination coefficients in blue- and green-emitting MQW LEDs, some common assumptions regarding the green gap's cause could be (dis)approved[A3]. First, non-radiative Shockley-Read-Hall (SRH) recombination was shown to be independent of emission wavelength ($A \approx 10^6 s^{-1}$), which implies similar epitaxial quality of InGaN QWs with different composition. Second, radiative and Auger recombination are drastically reduced in the green spectral range, as the electron–hole wave function overlap is reduced. This is both, due to the expected increase in quantum-confined Stark effect (QCSE), and due to localization effects. In fact, the temperature dependencies of the radiative recombination coefficient, shown to increase with T, directly attest the influence of localization. Considering that the InGaN alloy is expected to cause hole localization even if random indium distribution is assumed, a simple model was developed, in which electrons are delocalized, while holes are localized by local In fluctuations. This model is in line with all experimental findings. Finally, knowledge of the recombination coefficients as a function of temperature in the green gap, and outside of the green gap, allowed to pin point the physical mechanism originating the green gap. The quantum efficiency of green devices is not only lower than for blue devices in general, it also decreases more significantly with rising temperature. As the SRH losses are the same for both, this is caused by the balance between radiative and Auger recombination paths. This means that the larger hole localization inherent to InGaN alloys with higher In composition, i.e. in the green spectral range, is associated with enhanced Auger recombination[A3]. The microscopic interaction between localized holes and delocalized electrons which may lead to such higher Auger coefficients remains an open question motivating future work.

7.1 Outlook

In order to overcome the green gap efficiency reduction, two paths can be suggested based on the findings in this work:

1. Hole localization has been shown to be a decisive ingredient limiting current c-plane technology. While the localization depths necessary to explain the experimental data are compatible with random alloying, there may still be some room for improvement. Already small improvements in the uniformity of the InGaN alloy, reducing the localization depth perhaps by a few meV, could improve the thermalization of localized holes at operating temperature, thereby also improving internal quantum efficiency (IQE) in the green spectral region. Along this road, progress can be monitored by the novel method presented in this work (SSTRPL), which has been shown to give invaluable insight into the recombination processes. In addition, atomic-scale structural investigations will be vital in order to quantify the degree of non-uniformity in high-quality InGaN alloys.

2. Alternative approaches, which reduce the QCSE and/or the carrier densities - and therefore Auger recombination - should be persued further. In particular, the research in these areas should be focused on the green spectral range. With the results of this work in mind, it will not suffice to reduce the QCSE, one will also need to consider the uniformity of the employed InGaN layers in order to control localization.

Publications

Authored Articles

This cumulative thesis is based on the following pre-publications:

[A1] F. Nippert, A. Nirschl, T. Schulz, G. Callsen, I. Pietzonka, S. Westerkamp, T. Kure, C. Nenstiel, M. Strassburg, M. Albrecht, and A. Hoffmann,
"Polarization-induced confinement of continuous hole-states in highly pumped, industrial-grade, green InGaN quantum wells",
Journal of Applied Physics **119**, 215707 (2016),
DOI: 10.1063/1.4953254.

[A2] F. Nippert, S. Karpov, I. Pietzonka, B. Galler, A. Wilm, T. Kure, C. Nenstiel, G. Callsen, M. Straßburg, H.-J. Lugauer, and A. Hoffmann,
"Determination of recombination coefficients in InGaN quantum-well light-emitting diodes by small-signal time-resolved photoluminescence",
Japanese Journal of Applied Physics **55**, 05FJ01 (2016),
DOI: 10.7567/JJAP.55.05FJ01.

[A3] F. Nippert, S. Y. Karpov, G. Callsen, B. Galler, T. Kure, C. Nenstiel, M. R. Wagner, M. Straßburg, H.-J. Lugauer, and A. Hoffmann,
"Temperature-dependent recombination coefficients in InGaN light-emitting diodes: hole localization, Auger processes and the green gap",
Applied Physics Letters **109**, 161103 (2016),
DOI: 10.1063/1.4965298.

Co-Authored Articles

The following works were co-authored during the same time. Some of them are related to this work (see comments).

[P1] T. Schulz, A. Nirschl, P. Drechsel, F. Nippert, T. Markurt, M. Albrecht, and A. Hoffmann, "Recombination dynamics in InGaN quantum wells – Contribution of excited subband recombination to carrier leakage", *Applied Physics Letters* **105**, 181109 (2014), DOI: 10.1063/1.4901256
Relevance: In contrast to Ref. [A2], this work focuses on excited electronic states, which are shown to contribute to carrier leakage out of the quantum wells.

[P2] N. Ledentsov, V. Shchukin, J. Lyytikäinen, O. Okhotnikov, Y. M. Shernyakov, A. Payusov, N. Y. Gordeev, M. Maximov, S. Schlichting, F. Nippert, and A. Hoffmann, "Green (In, Ga, Al) P-GaP light-emitting diodes grown on high-index GaAs surfaces", *Applied Physics Letters* **105**, 181902 (2014), DOI: 10.1063/1.4900938
Relevance: The phosphide material system is situated on the other side of the green gap. While it is the standard material system for red-emitting LEDs, it also suffers from reduced efficiency towards the green spectral region, as AlGaInP becomes indirect. Here, variations of the growth direction (changing the microstructure) is shown to improve efficiency.

[P3] G. Callsen, M. Wagner, J. Reparaz, F. Nippert, T. Kure, S. Kalinowski, A. Hoffmann, M. Ford, M. Phillips, R. Dalmau, R. Schlesser, R. Collazo, and Z. Sitar, "Phonon pressure coefficients and deformation potentials of wurtzite AlN determined by uniaxial pressure-dependent Raman measurements", *Physical Review B* **90**, 205206 (2014), DOI: 10.1103/PhysRevB.90.205206
Relevance: The elastic properties of AlN, one of the building blocks in the III–N material system are investigated in this work.

[P4] C. Nenstiel, M. Bügler, G. Callsen, F. Nippert, T. Kure, S. Fritze, A. Dadgar, H. Witte, J. Bläsing, A. Krost, and A. Hoffmann, "Germanium–the superior dopant in n-type GaN", *physica status solidi (RRL)-Rapid Research Letters* **9**, 716 (2015), DOI: 10.1002/pssr.201510278
Relevance: Germanium is a promising alternative to the conventional silicon donor in GaN, potentially enabling higher free carrier concentrations and mobilities, vital for low resistance.

[P5] G. Callsen, G. M. O. Pahn, S. Kalinowski, C. Kindel, J. Settke, J. Brunnmeier, C. Nenstiel, T. Kure, F. Nippert, A. Schliwa, A. Hoffmann, T. Markurt, T. Schulz, M. Albrecht, S. Kako, M. Arita, and Y. Arakawa,
"Analysis of the exciton–LO-phonon coupling in single wurtzite GaN quantum dots",
Physical Review B **92**, 235439 (2015),
DOI: `10.1103/PhysRevB.92.235439`
Relevance: As both dominant non-radiative losses, Shockley-Read-Hall and Auger recombination, are mediated by phonons, an understanding of the coupling between the electronic and phononic systems in the III–nitrides is very important.

[P6] S. Freytag, M. Feneberg, C. Berger, J. Bläsing, A. Dadgar, G. Callsen, F. Nippert, A. Hoffmann, P. Bokov, and R. Goldhahn,
"Unintentional indium incorporation into barriers of InGaN/GaN multiple quantum wells studied by photoreflectance and photoluminescence",
Journal of Applied Physics **120**, 015703 (2016),
DOI: `10.1063/1.4955426`
Relevance: Clean interfaces between InGaN QWs and GaN barriers are highly desirable in order to provide the best confinement. In reality, however, growing such sharp interfaces is challenging, and some unintentional In incorporation may spoil the sample quality.

[P7] E. M. Sala, G. Stracke, S. Selve, T. Niermann, M. Lehmann, S. Schlichting, F. Nippert, G. Callsen, A. Strittmatter, and D. Bimberg,
"Growth and structure of InGaSb quantum dots on GaP(001)",
Applied Physics Letters **109**, 102102 (2016),
DOI: `10.1063/1.4962273`
Relevance: Unrelated to this work.

[P8] I. Reklaitis, F. Nippert, R. Kudžma, T. Malinauskas, S. Y. Karpov, I. Pietzonka, H.-J. Lugauer, M. Straßburg, P. Vitta, R. Tomašiūnas, and A. Hoffmann,
"Differential carrier lifetime in InGaN-based light-emitting diodes obtained by small-signal frequency-domain measurements: Advantages and limitations of the technique",
Journal of Applied Physics **121**, 035701,
DOI: `10.1063/1.4973903`
Relevance: This paper compares SSTRPL with the corresponding frequency-domain measurement, where the optical probe excitation is modulated rather than pulsed. Both methods are shown to yield comparable results.

Unpublished Articles

[U1] C. Nenstiel, G. Callsen, F. Nippert, T. Kure, M. R. Wagner, S. Schlichting, N. Jankowski, M. P. Hoffmann, S. Fritze, A. Dadgar, A. Krost, A. Hoffmann, and F. Bechstedt, "Electronic excitations stabilised by a degenerate electron gas in semiconductors",

arxiv: 1610.01673
Relevance: In continuation of Ref. [P4], it is shown that, due to the similarity of Ge and Ga atoms, very high doping concentrations with low compensation can be reached - even enabling the observation of novel quasi-particles.

Conference Contributions

Some of the results were also presented at international conferences.

[C1] F. Nippert, A. Nirschl, I. Pietzonka, H.-J. Lugauer, T. Kure, C. Nenstiel, M. Bügler, G. Callsen, M. Straßburg, and A. Hoffmann,
"Radiative and non-radiative processes in InGaN/GaN quantum wells for green LED structures",
E-MRS Spring Meeting, Strasbourg, France (2013).

[C2] F. Nippert, A. Nirschl, I. Pietzonka, H.-J. Lugauer, T. Kure, C. Nenstiel, M. Bügler, G. Callsen, M. Straßburg, and A. Hoffmann,
"Radiative and non-radiative processes in green InGaN/GaN quantum wells",
International Nano-Optoelectronics Workshop, Cargese, France (2013).

[C3] F. Nippert, T. Schulz, S. Westerkamp, A. Nirschl, I. Pietzonka, A. Franke, T. Kure, C. Nenstiel, G. Callsen, M. Albrecht, H.-J. Lugauer, M. Straßburg, and A. Hoffmann,
"Origin of non-radiative losses in thick InGaN/GaN QWs",
SPIE Photonics West, San Francisco, USA (2014).

[C4] F. Nippert, S. Westerkamp, A. Nirschl, I. Pietzonka, T. Schulz, M. Albrecht, A. Franke, T. Kure, C. Nenstiel, G. Callsen, M. Straßburg, and A. Hoffmann,
"QCSE and excited states in thick InGaN/GaN QWs",
E-MRS Spring Meeting, Lille, France (2014).

[C5] F. Nippert, A. Hoffmann*, A. Nirschl, M. Binder, I. Pietzonka, B. Galler, H.-J. Lugauer, and M. Straßburg,
"Internal losses and droop in InGaN/GaN quantum wells",
Solid State Lighting Symposium, Lund, Sweden (2014).

[C6] F. Nippert, T. Kure, C. Nenstiel, S. Westerkamp, G. Callsen, A. Hoffmann, A. Nirschl, I. Pietzonka, M. Straßburg, T. Schulz, and M. Albrecht,
"Blue luminescence in green InGaN/GaN quantum wells",
SPIE Photonics West, San Francisco, USA (2015).

[C7] F. Nippert, I. Pietzonka, B. Galler, A. Wilm, S. Y. Karpov, T. Kure, C. Nenstiel, G. Callsen, M. Straßburg, H.-J. Lugauer, and A. Hoffmann,
"Determination of recombination coefficients in InGaN QW LEDs by small-signal TRPL",
6th International Symposium on Growth of III-Nitrides, Hamamatsu, Japan (2015).

[C8] F. Nippert, T. Kure, C. Nenstiel, G. Callsen, A. Hoffmann*, S. Y. Karpov, I. Pietzonka, B. Galler, A. Wilm, M. Straßburg, and H.-J. Lugauer,
"Radiative and non-radiative processes in InGaN quantum well LEDs",
SPIE Photonics West, San Francisco, USA (2016).

[C9] F. Nippert, S. Y. Karpov, B. Galler, G. Callsen, T. Kure, C. Nenstiel, M. Straßburg, H.-J. Lugauer, and A. Hoffmann*,
"Recombination coefficients in InGaN quantum well light-emitting diodes",
International Workshop on Nitride Semiconductors, Orlando, USA (2016).

*presenting author, if not myself

Bibliography

[1] K. Lehovec, C. A. Accardo, and E. Jamgochian,
"Injected light emission of silicon carbide crystals",
Physical Review **83**, 603 (1951),
DOI: 10.1103/PhysRev.83.603.

[2] L. Patrick,
"Structure and characteristics of silicon carbide light-emitting junctions",
Journal of Applied Physics **28**, 765 (1957),
DOI: 10.1063/1.1722851.

[3] R. M. Potter, J. M. Blank, and A. Addamiano,
"Silicon carbide light-emitting diodes",
Journal of Applied Physics **40**, 2253 (1969),
DOI: 10.1063/1.1657967.

[4] K. Weiser, and R. S. Levitt,
"Electroluminescent gallium arsenide diodes with negative resistance",
Journal of Applied Physics **35**, 2431 (1964),
DOI: 10.1063/1.1702875.

[5] H. Rupprecht, J. M. Woodall, K. Konnerth, and D. G. Pettit,
"Efficient electroluminescence from GaAs diodes at 300°K",
Applied Physics Letters **9**, 221 (1966),
DOI: 10.1063/1.1754721.

[6] K. K. Shih, and G. D. Pettit,
"Properties of GaP green-light-emitting diodes grown by liquid-phase epitaxy",
Journal of Applied Physics **39**, 5025 (1968),
DOI: 10.1063/1.1655918.

[7] R. H. Saul, J. Armstrong, and W. Hackett,
"GaP red electroluminescent diodes with an external quantum efficiency of 7%",
Applied Physics Letters **15**, 229 (1969),
DOI: 10.1063/1.1652980.

[8] Y. Park, C. Geesner, and B. Shin,
"Yellow-light-emitting ZnSe diode",
Applied Physics Letters **21**, 567 (1972),
DOI: 10.1063/1.1654259.

[9] R. J. Robinson, and Z. K. Kun,
"P-n junction zinc sulfo-selenide and zinc selenide light-emitting diodes",
Applied Physics Letters **27**, 74 (1975),
DOI: 10.1063/1.88358.

[10] H. Katayama, S. Oda, and H. Kukimoto,
"ZnS blue-light-emitting diodes with an external quantum efficiency of 5x10-4",
Applied Physics Letters **27**, 697 (1975),
DOI: 10.1063/1.88350.

[11] A. Suzuki, M. Ikeda, N. Nagao, H. Matsunami, and T. Tanaka,
"Liquid-phase epitaxial growth of 6H-SiC by the dipping technique for preparation of blue-light-emitting diodes",
Journal of Applied Physics **47**, 4546 (1976),
DOI: 10.1063/1.322428.

[12] L. Hoffmann, G. Ziegler, D. Theis, and C. Weyrich,
"Silicon carbide blue light emitting diodes with improved external quantum efficiency",
Journal of Applied Physics **53**, 6962 (1982),
DOI: 10.1063/1.330041.

[13] J. Ren, K. A. Bowers, B. Sneed, D. L. Dreifus, J. W. Cook, J. F. Schetzina, and R. M. Kolbas,
"ZnSe light-emitting diodes",
Applied Physics Letters **57**, 1901 (1990),
DOI: 10.1063/1.104006.

[14] M. A. Haase, J. Qiu, J. M. DePuydt, and H. Cheng,
"Blue-green laser diodes",
Applied Physics Letters **59**, 1272 (1991),
DOI: 10.1063/1.105472.

[15] H. Jeon, J. Ding, A. V. Nurmikko, W. Xie, M. Kobayashi, and R. L. Gunshor,
"ZnSe based multilayer pn junctions as efficient light emitting diodes for display applications",
Applied Physics Letters **60**, 892 (1992),
DOI: 10.1063/1.106496.

[16] M. C. Tamargo, M. J. S. P. Brasil, R. E. Nahory, R. J. Martin, H. H. Farrell, T. J. Gmitter, D. E. Aspnes, A. L. Weaver, Y. Zhang, and B. J. Skromme,
"ZnSe/ZnCdSe quantum well light emitting diodes",
Journal of Vacuum Science & Technology B **10**, 692 (1992),
DOI: 10.1116/1.586433.

[17] W. Xie, D. C. Grillo, R. L. Gunshor, M. Kobayashi, H. Jeon, J. Ding, A. V. Nurmikko, G. C. Hua, and N. Otsuka,
"Room temperature blue light emitting p-n diodes from Zn(S,Se)-based multiple quantum well structures",
Applied Physics Letters **60**, 1999 (1992),
DOI: 10.1063/1.107123.

[18] J. M. Gaines, R. R. Drenten, K. W. Haberern, T. Marshall, P. Mensz, and J. Petruzzello,
"Blue-green injection lasers containing pseudomorphic Zn1-xMgxSySe1-y cladding layers and operating up to 394 K",
Applied Physics Letters **62**, 2462 (1993),
DOI: 10.1063/1.109319.

[19] S. Guha, J. M. DePuydt, M. A. Haase, J. Qiu, and H. Cheng,
"Degradation of II-VI based blue-green light emitters",
Applied Physics Letters **63**, 3107 (1993),
DOI: 10.1063/1.110218.

[20] G. C. Hua, N. Otsuka, D. C. Grillo, Y. Fan, J. Han, M. D. Ringle, R. L. Gunshor, M. Hovinen, and A. V. Nurmikko,
"Microstructure study of a degraded pseudomorphic separate confinement heterostructure blue-green laser diode",
Applied Physics Letters **65**, 1331 (1994),
DOI: 10.1063/1.112042.

[21] J. Pankove, E. Miller, D. Richman, and J. Berkeyheiser,
"Electroluminescence in GaN",
Journal of Luminescence **4**, 63 (1971),
DOI: 10.1016/0022-2313(71)90009-3.

[22] H. Amano, M. Kitoh, K. Hiramatsu, and I. Akasaki,
"Growth and luminescence properties of Mg-Doped GaN prepared by MOVPE",
Journal of the Electrochemical Society **137**, 1639 (1990),
DOI: 10.1149/1.2086742.

[23] I. Akasaki, H. Amano, M. Kito, and K. Hiramatsu,
"Photoluminescence of Mg-doped p-type GaN and electroluminescence of GaN p-n junction LED",
Journal of Luminescence **48**, 666 (1991),
DOI: 10.1016/0022-2313(91)90215-H.

[24] S. Nakamura, M. Senoh, and T. Mukai,
"Highly p-typed Mg-doped GaN films grown with GaN buffer layers",
Japanese Journal of Applied Physics **30**, L1708 (1991),
DOI: 10.1143/JJAP.30.L1708.

[25] S. Nakamura, M. Senoh, and T. Mukai,
"High-power InGaN/GaN double-heterostructure violet light emitting diodes",
Applied Physics Letters **62**, 2390 (1993),
DOI: 10.1063/1.109374.

[26] S. Nakamura, M. Senoh, N. Iwasa, and S. Nagahama,
"High-brightness InGaN blue, green and yellow light-emitting diodes with quantum well structures",
Japanese Journal of Applied Physics **34**, L797 (1995),
DOI: 10.1143/JJAP.34.L797.

[27] I. Akasaki, S. Sota, H. Sakai, T. Tanaka, M. Koike, and H. Amano,
"Shortest wavelength semiconductor laser diode",
Electronics Letters **32**, 1105 (1996),
DOI: 10.1049/el:19960743.

[28] S. Nakamura, M. Senoh, S.-i. Nagahama, N. Iwasa, T. Yamada, T. Matsushita, H. Kiyoku, and Y. Sugimoto,
"InGaN-based multi-quantum-well-structure laser diodes",
Japanese Journal of Applied Physics **35**, L74 (1996),
DOI: `10.1143/JJAP.35.L74`.

[29] S. Strite, and H. Morkoç,
"GaN, AlN, and InN: A review",
Journal of Vacuum Science & Technology B **10**, 1237 (1992),
DOI: `10.1116/1.585897`.

[30] S. Y. Karpov,
"Light-emitting diodes for solid state lighting: searching room for improvements",
in *SPIE OPTO*, **9768**, pp. 97680C–97680C
International Society for Optics and Photonics (2016),
DOI: `10.1117/12.2207265`.

[31] T. Matsuoka, H. Okamoto, M. Nakao, H. Harima, and E. Kurimoto,
"Optical bandgap energy of wurtzite InN",
Applied Physics Letters **81**, 1246 (2002),
DOI: `10.1063/1.1499753`.

[32] J. Wu, and W. Walukiewicz,
"Band gaps of InN and group III nitride alloys",
Superlattices and Microstructures **34**, 63 (2003),
DOI: `10.1016/j.spmi.2004.03.069`.

[33] W. Walukiewicz, S. Li, J. Wu, K. Yu, J. W. Ager, E. Haller, H. Lu, and W. J. Schaff,
"Optical properties and electronic structure of InN and In-rich group III-nitride alloys",
Journal of Crystal Growth **269**, 119 (2004),
DOI: `10.1016/j.jcrysgro.2004.05.041`.

[34] H. P. Maruska, and J. Tietjen,
"The preparation and properties of vapor-deposited single-crystal-line GaN",
Applied Physics Letters **15**, 327 (1969),
DOI: `10.1063/1.1652845`.

[35] H. Amano, N. Sawaki, I. Akasaki, and Y. Toyoda,
"Metalorganic vapor phase epitaxial growth of a high quality GaN film using an AlN buffer layer",
Applied Physics Letters **48**, 353 (1986),
DOI: `10.1063/1.96549`.

[36] S. Nakamura,
"GaN growth using GaN buffer layer",
Japanese Journal of Applied Physics **30**, L1705 (1991),
DOI: `10.1143/JJAP.30.L1705`.

[37] W. Yim, E. Stofko, P. Zanzucchi, J. Pankove, M. Ettenberg, and S. Gilbert,
"Epitaxially grown AlN and its optical band gap",
Journal of Applied Physics **44**, 292 (1973),
DOI: `10.1063/1.1661876`.

[38] J. Wu, W. Walukiewicz, K. M. Yu, J. W. Ager, E. E. Haller, H. Lu, and W. J. Schaff,
"Small band gap bowing in InGaN alloys",
Applied Physics Letters **80**, 4741 (2002),
DOI: 10.1063/1.1489481.

[39] P. G. Moses, and C. G. Van de Walle,
"Band bowing and band alignment in InGaN alloys",
Applied Physics Letters **96**, 021908 (2010),
DOI: 10.1063/1.3291055.

[40] R. R. Pela, C. Caetano, M. Marques, L. G. Ferreira, J. Furthmüller, and L. K. Teles,
"Accurate band gaps of AlGaN, InGaN, and AlInN alloys calculations based on LDA-1/2 approach",
Applied Physics Letters **98**, 151907 (2011),
DOI: 10.1063/1.3576570.

[41] F. McIntosh, K. Boutros, J. Roberts, S. Bedair, E. Piner, and N. A. El-Masry,
"Growth and characterization of AlInGaN quaternary alloys",
Applied Physics Letters **68**, 40 (1996),
DOI: 10.1063/1.116749.

[42] M. Krames, J. Bhat, D. Collins, N. Gardner, W. Götz, C. Lowery, M. Ludowise, P. Martin, G. Mueller, R. Mueller-Mach, S. Rudaz, D. Steigerwald, S. Stockman, and J. Wierer,
"High-power III-nitride emitters for solid-state lighting",
physica status solidi (a) **192**, 237 (2002),
DOI: 10.1002/1521-396X(200208)192:2<237::AID-PSSA237>3.0.CO;2-I.

[43] T. Mukai,
"Recent progress in group-III nitride light-emitting diodes",
Selected Topics in Quantum Electronics, IEEE Journal of **8**, 264 (2002),
DOI: 10.1109/2944.999179.

[44] Y. Narukawa, J. Narita, T. Sakamoto, K. Deguchi, T. Yamada, and T. Mukai,
"Ultra-high efficiency white light emitting diodes",
Japanese Journal of Applied Physics **45**, L1084 (2006),
DOI: 10.1143/JJAP.45.L1084.

[45] M. R. Krames, O. B. Shchekin, R. Mueller-Mach, G. O. Mueller, L. Zhou, G. Harbers, and M. G. Craford,
"Status and future of high-power light-emitting diodes for solid-state lighting",
Journal of Display Technology **3**, 160 (2007),
DOI: 10.1109/JDT.2007.895339.

[46] M. Kneissl, T. Kolbe, C. Chua, V. Kueller, N. Lobo, J. Stellmach, A. Knauer, H. Rodriguez, S. Einfeldt, Z. Yang, N. Johnson, and M. Weyers,
"Advances in group III-nitride-based deep UV light-emitting diode technology",
Semiconductor Science and Technology **26**, 014036 (2010),
DOI: 10.1088/0268-1242/26/1/014036.

[47] S. Nakamura, M. Senoh, S.-i. Nagahama, N. Iwasa, T. Yamada, T. Matsushita, Y. Sugimoto, and H. Kiyoku,
"Room-temperature continuous-wave operation of InGaN multi-quantum-well-structure laser diodes with a long lifetime",
Applied Physics Letters **70**, 868 (1997),
DOI: 10.1063/1.118300.

[48] S.-i. Nagahama, T. Yanamoto, M. Sano, and T. Mukai,
"Wavelength dependence of InGaN laser diode characteristics",
Japanese Journal of Applied Physics **40**, 3075 (2001),
DOI: 10.1143/JJAP.40.3075.

[49] S. Nakamura,
"InGaN-based violet laser diodes",
Semiconductor Science and Technology **14**, R27 (1999),
DOI: 10.1088/0268-1242/14/6/201.

[50] D. Queren, A. Avramescu, G. Brüderl, A. Breidenassel, M. Schillgalies, S. Lutgen, and U. Strauß,
"500 nm electrically driven InGaN based laser diodes",
Applied Physics Letters **94**, 081119 (2009),
DOI: 10.1063/1.3089573.

[51] A. Avramescu, T. Lermer, J. Müller, S. Tautz, D. Queren, S. Lutgen, and U. Strauß,
"InGaN laser diodes with 50 mW output power emitting at 515 nm",
Applied Physics Letters **95**, 1103 (2009),
DOI: 10.1063/1.3206739.

[52] U. Strauß, A. Avramescu, T. Lermer, D. Queren, A. Gomez-Iglesias, C. Eichler, J. Müller, G. Brüderl, and S. Lutgen,
"Pros and cons of green InGaN laser on c-plane GaN",
physica status solidi (b) **248**, 652 (2011),
DOI: 10.1002/pssb.201046299.

[53] L. A. Reichertz, I. Gherasoiu, K. M. Yu, V. M. Kao, W. Walukiewicz, and J. W. Ager III,
"Demonstration of a III–nitride/silicon tandem solar cell",
Applied Physics Express **2**, 122202 (2009),
DOI: 10.1143/APEX.2.122202.

[54] J. Schalwig, G. Müller, M. Eickhoff, O. Ambacher, and M. Stutzmann,
"Group III-nitride-based gas sensors for combustion monitoring",
Materials Science and Engineering: B **93**, 207 (2002),
DOI: 10.1016/S0921-5107(02)00050-8.

[55] F. Machuca, Y. Sun, Z. Liu, K. Ioakeimidi, P. Pianetta, and R. Pease,
"Prospect for high brightness III–nitride electron emitter",
Journal of Vacuum Science & Technology B **18**, 3042 (2000),
DOI: 10.1116/1.1321270.

[56] O. Ambacher, J. Majewski, C. Miskys, A. Link, M. Hermann, M. Eickhoff, M. Stutzmann, F. Bernardini, V. Fiorentini, V. Tilak, B. Schaff, and L. F. Eastman,
"Pyroelectric properties of Al(In)GaN/GaN hetero- and quantum well structures",
Journal of Physics: Condensed Matter **14**, 3399 (2002),
DOI: 10.1088/0953-8984/14/13/302.

[57] F. Bernardini, V. Fiorentini, and D. Vanderbilt,
"Spontaneous polarization and piezoelectric constants of III-V nitrides",
Physical Review B **56**, R10024 (1997),
DOI: 10.1103/PhysRevB.56.R10024.

[58] F. Bernardini, and V. Fiorentini,
"Macroscopic polarization and band offsets at nitride heterojunctions",
Physical Review B **57**, R9427 (1998),
DOI: 10.1103/PhysRevB.57.R9427.

[59] S. Chichibu, and A. Abare,
"Effective band gap inhomogeneity and piezoelectric field in InGaN/GaN multiquantum well structures",
Applied Physics Letters **73**, 2006 (1998),
DOI: 10.1063/1.122350.

[60] J. Im, H. Kollmer, J. Off, and A. Sohmer,
"Reduction of oscillator strength due to piezoelectric fields in GaN/AlGaN quantum wells",
Physical Review B **57**, 9435 (1998),
DOI: 10.1103/PhysRevB.57.R9435.

[61] T. Deguchi, K. Sekiguchi, A. Nakamura, T. Sota, R. Matsuo, S. Chichibu, and S. Nakamura,
"Quantum-confined Stark effect in an AlGaN/GaN/AlGaN single quantum well structure",
Japanese Journal of Applied Physics **38**, L914 (1999),
DOI: 10.1143/JJAP.38.L914.

[62] T. Takeuchi, S. Sota, M. Katsuragawa, M. Komori, H. Takeuchi, H. Amano, and I. Akasaki,
"Quantum-Confined Stark Effect due to Piezoelectric Fields in GaInN Strained Quantum Wells",
Japanese Journal of Applied Physics **36**, L382 (1997),
DOI: 10.1143/JJAP.36.L382.

[63] L.-H. Peng, C.-W. Chuang, and L.-H. Lou,
"Piezoelectric effects in the optical properties of strained InGaN quantum wells",
Applied Physics Letters **74**, 795 (1999),
DOI: 10.1063/1.123370.

[64] J. Stark,
"Beobachtungen über den Effekt des elektrischen Feldes auf Spektrallinien. I. Quereffekt",
Annalen der Physik **348**, 965 (1914),
DOI: 10.1002/andp.19143480702.

[65] D. A. B. Miller, D. S. Chemla, T. C. Damen, A. C. Gossard, W. Wiegmann, T. H. Wood, and C. A. Burrus,
"Band-edge electroabsorption in quantum well structures: the quantum-confined Stark effect",
Physical Review Letters **53**, 2173 (1984),
DOI: 10.1103/PhysRevLett.53.2173.

[66] M. Leroux, N. Grandjean, M. Laügt, J. Massies, B. Gil, P. Lefebvre, and P. Bigenwald,
"Quantum confined Stark effect due to built-in internal polarization fields in (Al,Ga)N/GaN quantum wells",
Physical Review B **58**, R13371 (1998),
DOI: 10.1103/PhysRevB.58.R13371.

[67] O. Ambacher, R. Dimitrov, M. Stutzmann, B. Foutz, M. Murphy, J. Smart, J. Shealy, N. Weimann, K. Chu, M. Chumbes, B. Green, A. Sierakowski, W. Schaff, and L. Eastman,
"Role of spontaneous and piezoelectric polarization induced effects in group-III nitride based heterostructures and devices",
physica status solidi (b) **216**, 381 (1999),
DOI: 10.1002/(SICI)1521-3951(199911)216:1<381::AID-PSSB381>3.0.CO;2-O.

[68] J. Bai, T. Wang, and S. Sakai,
"Influence of the quantum-well thickness on the radiative recombination of InGaN/GaN quantum well structures",
Journal of Applied Physics **88**, 4729 (2000),
DOI: 10.1063/1.1311831.

[69] S. Chichibu, K. Wada, and S. Nakamura,
"Spatially resolved cathodoluminescence spectra of InGaN quantum wells",
Applied Physics Letters **71**, 2346 (1997),
DOI: 10.1063/1.120025.

[70] L. Bellaiche, T. Mattila, L.-W. Wang, S.-H. Wei, and A. Zunger,
"Resonant hole localization and anomalous optical bowing in InGaN alloys",
Applied Physics Letters **74**, 1842 (1999),
DOI: 10.1063/1.123687.

[71] A. Reznitsky, A. Klochikhin, S. Permogorov, L. Tenishev, W. Lundin, A. Usikov, M. Schmidt, and C. Klingshirn,
"Localization of excitons at small in clusters in diluted InGaN solid solutions",
physica status solidi (c), 280 (2003),
DOI: 10.1002/pssc.200390043.

[72] M. Auf der Maur, A. Pecchia, G. Penazzi, W. Rodrigues, and A. Di Carlo,
"Efficiency drop in green InGaN/GaN light emitting diodes: the role of random alloy fluctuations",
Physical Review Letters **116**, 027401 (2016),
DOI: 10.1103/PhysRevLett.116.027401.

[73] P. Ruterana, and S. Kret,
"Composition fluctuation in InGaN quantum wells made from molecular beam or metalorganic vapor phase epitaxial layers",
Journal of Applied Physics **91**, 8979 (2002),
DOI: 10.1063/1.1473666.

[74] N. Duxbury, and U. Bangert,
"Indium segregation in InGaN quantum-well structures",
Applied Physics Letters **76**, 1600 (2000),
DOI: 10.1063/1.126108.

[75] J. Jinschek, R. Erni, N. Gardner, a.Y. Kim, and C. Kisielowski,
"Local indium segregation and bang gap variations in high efficiency green light emitting InGaN/GaN diodes",
Solid State Communications **137**, 230 (2006),
DOI: 10.1016/j.ssc.2005.10.030.

[76] P. Specht, and C. Kisielowski,
"On the chemical homogeneity of InxGa1-xN alloys – Electron microscopy at the edge of technical limits",
Materials Science in Semiconductor Processing, (2016),
DOI: 10.1016/j.mssp.2016.07.011.

[77] H. K. Cho, J. Y. Lee, J. H. Song, P. W. Yu, G. M. Yang, and C. S. Kim,
"Influence of strain-induced indium clustering on characteristics of InGaN/GaN multiple quantum wells with high indium composition",
Journal of Applied Physics **91**, 1104 (2002),
DOI: 10.1063/1.1427143.

[78] Y.-H. Cho, S. K. Lee, H. S. Kwack, J. Y. Kim, K. S. Lim, H. M. Kim, T. W. Kang, S. N. Lee, M. S. Seon, O. H. Nam, and Y. J. Park,
"Carrier loss and luminescence degradation in green-light-emitting InGaN quantum wells with micron-scale indium clusters",
Applied Physics Letters **83**, 2578 (2003),
DOI: 10.1063/1.1613043.

[79] Y. Narukawa, Y. Kawakami, and S. Fujita,
"Recombination dynamics of localized excitons in In0.20Ga0.80N-In0.05Ga0.95N multiple quantum wells",
Physical Review B **55**, 1938 (1997),
DOI: 10.1103/PhysRevB.55.R1938.

[80] S. Nakamura,
"The roles of structural imperfections in InGaN-based blue light-emitting diodes and laser diodes",
Science **281**, 956 (1998),
DOI: 10.1126/science.281.5379.956.

[81] P. G. Eliseev, P. Perlin, J. Lee, and M. Osiński,
""Blue" temperature-induced shift and band-tail emission in InGaN-based light sources",
Applied Physics Letters **71**, 569 (1997),
DOI: 10.1063/1.119797.

[82] Y.-H. Cho, G. H. Gainer, a. J. Fischer, J. J. Song, S. Keller, U. K. Mishra, and S. P. DenBaars,
""S-shaped" temperature-dependent emission shift and carrier dynamics in InGaN/GaN multiple quantum wells",
Applied Physics Letters **73**, 1370 (1998),
DOI: 10.1063/1.122164.

[83] Y. Varshni,
"Temperature dependence of the energy gap in semiconductors",
Physica **34**, 149 (1967),
DOI: 10.1016/0031-8914(67)90062-6.

[84] S. F. Chichibu, A. Uedono, T. Onuma, B. A. Haskell, A. Chakraborty, T. Koyama, P. T. Fini, S. Keller, S. P. DenBaars, J. S. Speck, U. K. Mishra, S. Nakamura, S. Yamaguchi, S. Kamiyama, H. Amano, I. Akasaki, J. Han, and T. Sota,
"Origin of defect-insensitive emission probability in In-containing (Al, In, Ga) N alloy semiconductors",
Nature Materials **5**, 810 (2006),
DOI: 10.1038/nmat1726.

[85] T. Takeuchi, H. Amano, K. Hiramatsu, N. Sawaki, and I. Akasaki,
"Growth of single crystalline GaN film on Si substrate using 3C-SiC as an intermediate layer",
Journal of Crystal Growth **115**, 634 (1991),
DOI: 10.1016/0022-0248(91)90817-O.

[86] A. Watanabe, T. Takeuchi, K. Hirosawa, H. Amano, K. Hiramatsu, and I. Akasaki,
"The growth of single crystalline GaN on a Si substrate using AlN as an intermediate layer",
Journal of Crystal Growth **128**, 391 (1993),
DOI: 10.1016/0022-0248(93)90354-Y.

[87] A. Dadgar, J. Bläsing, A. Diez, A. Alam, M. Heuken, and A. Krost,
"Metalorganic chemical vapor phase epitaxy of crack-free GaN on Si (111) exceeding 1 μm in thickness",
Japanese Journal of Applied Physics **39**, L1183 (2000),
DOI: 10.1143/JJAP.39.L1183.

[88] A. Krost, and A. Dadgar,
"GaN-based devices on Si",
physica status solidi (a) **194**, 361 (2002),
DOI: 10.1002/1521-396X(200212)194:2<361::AID-PSSA361>3.0.CO;2-R.

[89] J. Li, J. Lin, and H. Jiang,
"Growth of III-nitride photonic structures on large area silicon substrates",
Applied Physics Letters **88**, 171909 (2006),
DOI: 10.1063/1.2199492.

[90] B. Galler, P. Drechsel, R. Monnard, P. Rode, P. Stauss, S. Froehlich, W. Bergbauer, M. Binder, M. Sabathil, B. Hahn, and J. Wagner,
"Influence of indium content and temperature on Auger-like recombination in InGaN quantum wells grown on (111) silicon substrates",
Applied Physics Letters **101**, 131111 (2012),
DOI: 10.1063/1.4754688.

[91] G. Chen, M. Craven, A. Kim, A. Munkholm, S. Watanabe, M. Camras, W. Götz, and F. Steranka,
"Performance of high-power III-nitride light emitting diodes",
physica status solidi (a) **205**, 1086 (2008),
DOI: 10.1002/pssa.200778747.

[92] A. Laubsch, M. Sabathil, W. Bergbauer, M. Strassburg, H. Lugauer, M. Peter, S. Lutgen, N. Linder, K. Streubel, J. Hader, J. V. Moloney, B. Pasenow, and S. W. Koch,
"On the origin of IQE-'droop' in InGaN LEDs",
physica status solidi (c) **6**, S913 (2009),
DOI: 10.1002/pssc.200880950.

[93] S.-H. Han, D.-Y. Lee, S.-J. Lee, C.-Y. Cho, M.-K. Kwon, S. Lee, D. Noh, D.-J. Kim, Y. C. Kim, and S.-J. Park,
"Effect of electron blocking layer on efficiency droop in InGaN/GaN multiple quantum well light-emitting diodes",
Applied Physics Letters **94**, 231123 (2009),
DOI: 10.1063/1.3153508.

[94] A. David, and M. J. Grundmann,
"Droop in InGaN light-emitting diodes: A differential carrier lifetime analysis",
Applied Physics Letters **96**, 103504 (2010),
DOI: 10.1002/pssb.201248286.

[95] S. Ganguly, J. Verma, G. Li, T. Zimmermann, H. Xing, and D. Jena,
"Presence and origin of interface charges at atomic-layer deposited Al2O3/III-nitride heterojunctions",
Applied Physics Letters **99**, 193504 (2011),
DOI: 10.1063/1.3658450.

[96] D. Schiavon, M. Binder, M. Peter, B. Galler, P. Drechsel, and F. Scholz,
"Wavelength-dependent determination of the recombination rate coefficients in single-quantum-well GaInN/GaN light emitting diodes",
physica status solidi (b) **250**, 283 (2013),
DOI: 10.1002/pssb.201248286.

[97] T. Miyoshi, S. Masui, T. Okada, T. Yanamoto, T. Kozaki, S.-i. Nagahama, and T. Mukai,
"510–515 nm InGaN-based green laser diodes on c-plane GaN substrate",
Applied Physics Express **2**, 062201 (2009),
DOI: 10.1143/APEX.2.062201.

[98] B. P. Yonkee, B. SaifAddin, J. T. Leonard, S. P. DenBaars, and S. Nakamura,
"Flip-chip blue LEDs grown on bulk GaN substrates utilizing photoelectrochemical etching for substrate removal",
Applied Physics Express **9**, 056502 (2016),
DOI: 10.7567/APEX.9.056502.

[99] B. Heying, R. Averbeck, L. F. Chen, E. Haus, H. Riechert, and J. S. Speck,
"Control of GaN surface morphologies using plasma-assisted molecular beam epitaxy",
Journal of Applied Physics **88**, 1855 (2000),
DOI: 10.1063/1.1305830.

[100] E. Calleja, M. A. Sánchez-García, F. J. Sánchez, F. Calle, F. B. Naranjo, E. Muñoz, U. Jahn, and K. Ploog,
"Luminescence properties and defects in GaN nanocolumns grown by molecular beam epitaxy",
Physical Review B **62**, 16826 (2000),
DOI: 10.1103/PhysRevB.62.16826.

[101] I. P. Smorchkova, L. Chen, T. Mates, L. Shen, S. Heikman, B. Moran, S. Keller, S. P. DenBaars, J. S. Speck, and U. K. Mishra,
"AlN/GaN and (Al,Ga)N/AlN/GaN two-dimensional electron gas structures grown by plasma-assisted molecular-beam epitaxy",
Journal of Applied Physics **90**, 5196 (2001),
DOI: 10.1063/1.1412273.

[102] N. Grandjean, B. Damilano, and J. Massies,
"Group-III nitride quantum heterostructures grown by molecular beam epitaxy",
Journal of Physics: Condensed Matter **13**, 6945 (2001),
DOI: 10.1088/0953-8984/13/32/305.

[103] J. Ristić, E. Calleja, M. Sanchez-Garcia, J. Ulloa, J. Sanchez-Paramo, J. Calleja, U. Jahn, A. Trampert, and K. Ploog,
"Characterization of GaN quantum discs embedded in Al x Ga 1- x N nanocolumns grown by molecular beam epitaxy",
Physical Review B **68**, 125305 (2003),
DOI: 10.1103/PhysRevB.68.125305.

[104] S. Kako, C. Santori, K. Hoshino, S. Götzinger, Y. Yamamoto, and Y. Arakawa,
"A gallium nitride single-photon source operating at 200 K",
Nature materials **5**, 887 (2006),
DOI: 10.1038/nmat1763.

[105] K. Kishino, H. Sekiguchi, and A. Kikuchi,
"Improved Ti-mask selective-area growth (SAG) by rf-plasma-assisted molecular beam epitaxy demonstrating extremely uniform GaN nanocolumn arrays",
Journal of Crystal Growth **311**, 2063 (2009),
DOI: 10.1016/j.jcrysgro.2008.11.056.

[106] D. Wang, A. Pierre, M. G. Kibria, K. Cui, X. Han, K. H. Bevan, H. Guo, S. Paradis, A.-R. Hakima, and Z. Mi,
"Wafer-level photocatalytic water splitting on GaN nanowire arrays grown by molecular beam epitaxy",
Nano letters **11**, 2353 (2011),
DOI: 10.1021/nl2006802.

[107] F. Schuster, M. Hetzl, S. Weiszer, J. A. Garrido, M. de la Mata, C. Magen, J. Arbiol, and M. Stutzmann,
"Position-controlled growth of GaN nanowires and nanotubes on diamond by molecular beam epitaxy",
Nano letters **15**, 1773 (2015),
DOI: 10.1021/nl504446r.

[108] J. N. Kuznia, M. A. Khan, D. T. Olson, R. Kaplan, and J. Freitas,
"Influence of buffer layers on the deposition of high quality single crystal GaN over sapphire substrates",
Journal of Applied Physics **73**, 4700 (1993),
DOI: 10.1063/1.354069.

[109] S. Keller, B. P. Keller, Y. Wu, B. Heying, D. Kapolnek, J. S. Speck, U. K. Mishra, and S. P. DenBaars,
"Influence of sapphire nitridation on properties of gallium nitride grown by metalorganic chemical vapor deposition",
Applied Physics Letters **68**, 1525 (1996),
DOI: 10.1063/1.115687.

[110] K. Uchida, A. Watanabe, F. Yano, M. Kouguchi, T. Tanaka, and S. Minagawa,
"Nitridation process of sapphire substrate surface and its effect on the growth of GaN",
Journal of Applied Physics **79**, 3487 (1996),
DOI: 10.1063/1.361398.

[111] N. Grandjean, J. Massies, and M. Leroux,
"Nitridation of sapphire. Effect on the optical properties of GaN epitaxial overlayers",
Applied Physics Letters **69**, 2071 (1996),
DOI: 10.1063/1.116883.

[112] S. Mohn, N. Stolyarchuk, T. Markurt, R. Kirste, M. P. Hoffmann, R. Collazo, A. Courville, R. Di Felice, Z. Sitar, P. Vennéguès, and M. Albrecht,
"Polarity Control in Group-III Nitrides beyond Pragmatism",
Physical Review Applied **5**, 054004 (2016),
DOI: 10.1103/PhysRevApplied.5.054004.

[113] M. Iwaya, T. Takeuchi, S. Yamaguchi, C. Wetzel, H. Amano, and I. Akasaki,
"Reduction of Etch Pit Density in Organometallic Vapor Phase Epitaxy-Grown GaN on Sapphire by Insertion of a Low-Temperature-Deposited Buffer Layer between High-Temperature-Grown GaN",
Japanese Journal of Applied Physics **37**, L316 (1998),
DOI: 10.1143/JJAP.37.L316.

[114] H. Amano, M. Iwaya, T. Kashima, M. Katsuragawa, I. Akasaki, J. Han, S. Hearne, J. A. Floro, E. Chason, and J. Figiel,
"Stress and Defect Control in GaN Using Low Temperature Interlayers",
Japanese Journal of Applied Physics **37**, L1540 (1998),
DOI: 10.1143/JJAP.37.L1540.

[115] K. Hiramatsu, S. Itoh, H. Amano, I. Akasaki, N. Kuwano, T. Shiraishi, and K. Oki,
"Growth mechanism of GaN grown on sapphire with AlN buffer layer by MOVPE",
Journal of Crystal Growth **115**, 628 (1991),
DOI: 10.1016/0022-0248(91)90816-N.

[116] A. Dadgar, M. Poschenrieder, J. Bläsing, K. Fehse, A. Diez, and A. Krost,
"Thick, crack-free blue light-emitting diodes on Si(111) using low-temperature AlN interlayers and in situSixNy masking",
Applied Physics Letters **80**, 3670 (2002),
DOI: 10.1063/1.1479455.

[117] J. Bläsing, A. Reiher, A. Dadgar, A. Diez, and A. Krost,
"The origin of stress reduction by low-temperature AlN interlayers",
Applied Physics Letters **81**, 2722 (2002),
DOI: 10.1063/1.1512331.

[118] S. Nakamura, T. Mukai, and M. Senoh,
"Si-and Ge-doped GaN films grown with GaN buffer layers",
Japanese Journal of Applied Physics **31**, 2883 (1992),
DOI: 10.1143/JJAP.31.2883.

[119] E. Schubert, I. Goepfert, W. Grieshaber, and J. Redwing,
"Optical properties of Si-doped GaN",
Applied Physics Letters **71**, 921 (1997),
DOI: 10.1063/1.119689.

[120] I.-H. Lee, I.-H. Choi, C.-R. Lee, E.-j. Shin, D. Kim, S. K. Noh, S.-J. Son, K. Y. Lim, and H. J. Lee,
"Stress relaxation in Si-doped GaN studied by Raman spectroscopy",
Journal of Applied Physics **83**, 5787 (1998),
DOI: 10.1063/1.367501.

[121] M. Yoshikawa, M. Kunzer, J. Wagner, H. Obloh, P. Schlotter, R. Schmidt, N. Herres, and U. Kaufmann,
"Band-gap renormalization and band filling in Si-doped GaN films studied by photoluminescence spectroscopy",
Journal of Applied Physics **86**, 4400 (1999),
DOI: 10.1063/1.371377.

[122] J. Xie, S. Mita, L. Hussey, A. Rice, J. Tweedie, J. LeBeau, R. Collazo, and Z. Sitar,
"On the strain in n-type GaN",
Applied Physics Letters **99**, 141916 (2011),
DOI: 10.1063/1.3647772.

[123] S. Fritze, A. Dadgar, H. Witte, M. Bügler, A. Rohrbeck, J. Bläsing, A. Hoffmann, and A. Krost,
"High Si and Ge n-type doping of GaN doping-Limits and impact on stress",
Applied Physics Letters **100**, 122104 (2012),
DOI: 10.1063/1.3695172.

[124] P. Hageman, W. Schaff, J. Janinski, and Z. Liliental-Weber,
"n-type doping of wurtzite GaN with germanium grown with plasma-assisted molecular beam epitaxy",
Journal of Crystal Growth **267**, 123 (2004),
DOI: 10.1016/j.jcrysgro.2004.03.024.

[125] A. Dadgar, J. Bläsing, A. Diez, and A. Krost,
"Crack-free, highly conducting GaN layers on Si substrates by Ge doping",
Applied Physics Express **4**, 011001 (2011),
DOI: 10.1143/APEX.4.011001.

[126] V. N. Lutskii,
"Quantum size effect–present state and perspectives of experimental investigations",
physica status solidi (a) **1**, 199 (1970),
DOI: 10.1002/pssa.19700010202.

[127] W. Guo, M. Zhang, A. Banerjee, and P. Bhattacharya,
"Catalyst-free InGaN/GaN nanowire light emitting diodes grown on (001) silicon by molecular beam epitaxy",
Nano Letters **10**, 3355 (2010),
DOI: 10.1021/nl101027x.

[128] W. Guo, A. Banerjee, P. Bhattacharya, and B. S. Ooi,
"InGaN/GaN disk-in-nanowire white light emitting diodes on (001) silicon",
Applied Physics Letters **98**, 193102 (2011),
DOI: 10.1063/1.3588201.

[129] C. Hahn, Z. Zhang, A. Fu, C. H. Wu, Y. J. Hwang, D. J. Gargas, and P. Yang,
"Epitaxial growth of InGaN nanowire arrays for light emitting diodes",
ACS Nano **5**, 3970 (2011),
DOI: 10.1021/nn200521r.

[130] S. Albert, A. Bengoechea-Encabo, X. Kong, M. Sanchez-Garcia, E. Calleja, and A. Trampert,
"Monolithic integration of InGaN segments emitting in the blue, green, and red spectral range in single ordered nanocolumns",
Applied Physics Letters **102**, 181103 (2013),
DOI: 10.1063/1.4804293.

[131] S. Li, X. Wang, S. Fündling, M. Erenburg, J. Ledig, J. Wei, H. H. Wehmann, A. Waag, W. Bergbauer, M. Mandl, M. Strassburg, A. Trampert, U. Jahn, H. Riechert, H. Jönen, and A. Hangleiter, "Nitrogen-polar core-shell GaN light-emitting diodes grown by selective area metalorganic vapor phase epitaxy", *Applied Physics Letters* **101**, 032103 (2012), DOI: 10.1063/1.4737395.

[132] M. Mandl, X. Wang, T. Schimpke, C. Kölper, M. Binder, J. Ledig, A. Waag, X. Kong, A. Trampert, F. Bertram, J. Christen, F. Barbagini, E. Calleja, and M. Strassburg, "Group III nitride core–shell nano-and microrods for optoelectronic applications", *physica status solidi (RRL)-Rapid Research Letters* **7**, 800 (2013), DOI: 10.1002/pssr.201307250.

[133] S. Albert, A. Bengoechea-Encabo, J. Ledig, T. Schimpke, M. A. Sanchez-Garcia, M. Strassburg, A. Waag, and E. Calleja, "Demonstration of (In, Ga) N/GaN core–shell micro light-emitting diodes grown by molecular beam epitaxy on ordered MOVPE GaN pillars", *Crystal Growth & Design* **15**, 3661 (2015), DOI: 10.1021/acs.cgd.5b00235.

[134] X. Wang, U. Jahn, M. Mandl, T. Schimpke, J. Hartmann, J. Ledig, M. Straßburg, H.-H. Wehmann, and A. Waag, "Growth and characterization of mixed polar GaN columns and core–shell LEDs", *physica status solidi (a)* **212**, 727 (2015), DOI: 10.1002/pssa.201400362.

[135] T. Schimpke, M. Mandl, I. Stoll, B. Pohl-Klein, D. Bichler, F. Zwaschka, J. Strube-Knyrim, B. Huckenbeck, B. Max, M. Müller, P. Veit, F. Bertram, J. Christen, J. Hartmann, A. Waag, H. Lugauer, and M. Strassburg, "Phosphor-converted white light from blue-emitting InGaN microrod LEDs", *physica status solidi (a)* **213**, 1577 (2016), DOI: 10.1002/pssa.201532904.

[136] B. Damilano, N. Grandjean, S. Dalmasso, and J. Massies, "Room-temperature blue-green emission from InGaN/GaN quantum dots made by strain-induced islanding growth", *Applied Physics Letters* **75**, 3751 (1999), DOI: 10.1063/1.125444.

[137] J. Wang, M. Nozaki, M. Lachab, Y. Ishikawa, R. Q. Fareed, T. Wang, M. Hao, and S. Sakai, "Metalorganic chemical vapor deposition selective growth and characterization of InGaN quantum dots", *Applied Physics Letters* **75**, 950 (1999), DOI: 10.1063/1.124564.

[138] O. Moriwaki, T. Someya, K. Tachibana, S. Ishida, and Y. Arakawa, "Narrow photoluminescence peaks from localized states in InGaN quantum dot structures", *Applied Physics Letters* **76**, 2361 (2000), DOI: 10.1063/1.126346.

[139] R. A. Oliver, G. A. D. Briggs, M. J. Kappers, C. J. Humphreys, S. Yasin, J. H. Rice, J. D. Smith, and R. A. Taylor,
"InGaN quantum dots grown by metalorganic vapor phase epitaxy employing a post-growth nitrogen anneal",
Applied Physics Letters **83**, 755 (2003),
DOI: 10.1063/1.1595716.

[140] T. Bartel, M. Dworzak, M. Strassburg, A. Hoffmann, A. Strittmatter, and D. Bimberg,
"Recombination dynamics of localized excitons in InGaN quantum dots",
Applied Physics Letters **85**, 1946 (2004),
DOI: 10.1002/pssa.200674834.

[141] D. Holec, P. Costa, M. Kappers, and C. Humphreys,
"Critical thickness calculations for InGaN/GaN",
Journal of Crystal Growth **303**, 314 (2007),
DOI: 10.1016/j.jcrysgro.2006.12.054.

[142] S. Y. Karpov,
"Suppression of phase separation in InGaN due to elastic strain",
MRS Internet Journal of Nitride Semiconductor Research **3**, 16 (1998),
DOI: 10.1557/S1092578300000880.

[143] Y.-K. Kuo, and Y.-A. Chang,
"Effects of electronic current overflow and inhomogeneous carrier distribution on InGaN quantum-well laser performance",
Quantum Electronics, IEEE Journal of **40**, 437 (2004),
DOI: 10.1109/JQE.2004.826437.

[144] A. David, M. J. Grundmann, J. F. Kaeding, N. F. Gardner, T. G. Mihopoulos, and M. R. Krames,
"Carrier distribution in InGaN GaN multiple quantum well light-emitting diodes",
Applied Physics Letters **92**, 053502 (2008),
DOI: 10.1063/1.2839305.

[145] J. P. Liu, J. H. Ryou, R. D. Dupuis, J. Han, G. D. Shen, and H. B. Wang,
"Barrier effect on hole transport and carrier distribution in InGaN /GaN multiple quantum well visible light-emitting diodes",
Applied Physics Letters **93**, 021102 (2008),
DOI: 10.1063/1.2957667.

[146] Y.-K. Kuo, J.-Y. Chang, M.-C. Tsai, and S.-H. Yen,
"Advantages of blue InGaN multiple-quantum well light-emitting diodes with InGaN barriers",
Applied Physics Letters **95**, 011116 (2009),
DOI: 10.1063/1.3176406.

[147] S. J. Chang, C. H. Kuo, Y. K. Su, L. W. Wu, J. K. Sheu, T. C. Wen, W. C. Lai, J. R. Chen, and J. M. Tsai,
"400-nm InGaN-GaN and InGaN-AlGaN multiquantum well light-emitting diodes",
IEEE Journal of Selected Topics in Quantum Electronics **8**, 744 (2002),
DOI: 10.1109/JSTQE.2002.801677.

[148] H. Zhao, G. Liu, R. A. Arif, and N. Tansu,
"Current injection efficiency induced efficiency-droop in InGaN quantum well light-emitting diodes",
Solid-State Electronics **54**, 1119 (2010),
DOI: 10.1016/j.sse.2010.05.019.

[149] S. Nakamura, N. Iwasa, M. Senoh, and T. Mukai,
"Hole compensation mechanism of p-type GaN films",
Japanese Journal of Applied Physics **31**, 1258 (1992),
DOI: 10.1143/JJAP.31.1258.

[150] W. Götz, N. Johnson, D. Bour, M. McCluskey, and E. Haller,
"Local vibrational modes of the Mg–H acceptor complex in GaN",
Applied Physics Letters **69**, 3725 (1996),
DOI: 10.1063/1.117202.

[151] L. Eckey, U. Von Gfug, J. Holst, A. Hoffmann, A. Kaschner, H. Siegle, C. Thomsen, B. Schineller, K. Heime, M. Heuken, O. Schön, and R. Beccard,
"Photoluminescence and Raman study of compensation effects in Mg-doped GaN epilayers",
Journal of Applied Physics **84**, 5828 (1998),
DOI: 10.1063/1.368853.

[152] C. G. Van de Walle, C. Stampfl, and J. Neugebauer,
"Theory of doping and defects in III–V nitrides",
Journal of Crystal Growth **189**, 505 (1998),
DOI: 10.1016/S0022-0248(98)00340-6.

[153] U. Kaufmann, P. Schlotter, H. Obloh, K. Köhler, and M. Maier,
"Hole conductivity and compensation in epitaxial GaN: Mg layers",
Physical Review B **62**, 10867 (2000),
DOI: 10.1103/PhysRevB.62.10867.

[154] P. Kozodoy, H. Xing, S. P. DenBaars, U. K. Mishra, A. Saxler, R. Perrin, S. Elhamri, and W. Mitchel,
"Heavy doping effects in Mg-doped GaN",
Journal of Applied Physics **87**, 1832 (2000),
DOI: 10.1063/1.372098.

[155] K. Köhler, T. Stephan, A. Perona, J. Wiegert, M. Maier, M. Kunzer, and J. Wagner,
"Control of the Mg doping profile in III-N light-emitting diodes and its effect on the electroluminescence efficiency",
Journal of Applied Physics **97**, 104914 (2005),
DOI: 10.1063/1.1901836.

[156] G. Callsen, M. Wagner, T. Kure, J. Reparaz, M. Bügler, J. Brunnmeier, C. Nenstiel, A. Hoffmann, M. Hoffmann, J. Tweedie, Z. Bryan, S. Aygun, R. Kirste, R. Collazo, and Z. Sitar,
"Optical signature of Mg-doped GaN: Transfer processes",
Physical Review B **86**, 075207 (2012),
DOI: 10.1103/PhysRevB.86.075207.

[157] R. Kirste, M. P. Hoffmann, J. Tweedie, Z. Bryan, G. Callsen, T. Kure, C. Nenstiel, M. R. Wagner, R. Collazo, A. Hoffmann, and Z. Sitar,
"Compensation effects in GaN: Mg probed by Raman spectroscopy and photoluminescence measurements",
Journal of Applied Physics **113**, 103504 (2013),
DOI: 10.1063/1.4794094.

[158] K. B. Nam, M. L. Nakarmi, J. Li, J. Y. Lin, and H. X. Jiang,
"Mg acceptor level in AlN probed by deep ultraviolet photoluminescence",
Applied Physics Letters **83**, 878 (2003),
DOI: 10.1063/1.1594833.

[159] J. Piprek,
"Comparative efficiency analysis of GaN-based light-emitting diodes and laser diodes",
Applied Physics Letters **109**, 021104 (2016),
DOI: 10.1063/1.4958619.

[160] S. Wei, and A. Zunger,
"Valence band splittings and band offsets of AlN, GaN, and InN",
Applied Physics Letters **69**, 2719 (1996),
DOI: 10.1063/1.117689.

[161] C. G. Van de Walle, and J. Neugebauer,
"Small valence-band offsets at GaN/InGaN heterojunctions",
Applied Physics Letters **70**, 2577 (1997),
DOI: 10.1063/1.118924.

[162] S. Choi, H. J. Kim, S.-S. Kim, J. Liu, J. Kim, J.-H. Ryou, R. D. Dupuis, A. M. Fischer, and F. A. Ponce,
"Improvement of peak quantum efficiency and efficiency droop in III-nitride visible light-emitting diodes with an InAlN electron-blocking layer",
Applied Physics Letters **96**, 221105 (2010),
DOI: 10.1063/1.3441373.

[163] C. Wang, C. Ke, C. Lee, S. Chang, W. Chang, J. Li, Z. Li, H. Yang, H. Kuo, T. Lu, and S. Wang,
"Hole injection and efficiency droop improvement in InGaN/GaN light-emitting diodes by band-engineered electron blocking layer",
Applied Physics Letters **97**, 261103 (2010),
DOI: 10.1063/1.3531753.

[164] J. Piprek,
"Efficiency droop in nitride-based light-emitting diodes",
physica status solidi (a) **207**, 2217 (2010),
DOI: 10.1002/pssa.201026149.

[165] W. van Roosbroeck, and W. Shockley,
"Photon-radiative recombination of electrons and holes in germanium",
Physical Review **94**, 1558 (1954),
DOI: 10.1103/PhysRev.94.1558.

[166] P. A. M. Dirac,
"The quantum theory of the emission and absorption of radiation",
Proceedings of the Royal Society of London A **114**, 243 (1927),
DOI: 10.1098/rspa.1927.0039.

[167] W. Shockley, and W. T. Read,
"Statistics of the recombinations of holes and electrons",
Physical Review **87**, 835 (1952),
DOI: 10.1103/PhysRev.87.835.

[168] R. N. Hall,
"Electron-hole recombination in germanium",
Physical Review **87**, 387 (1952),
DOI: 10.1103/PhysRev.87.387.

[169] R. N. Hall,
"Recombination processes in semiconductors",
Proceedings of the IEE - Part B: Electronic and Communication Engineering **106**, 923 (1959),
DOI: 10.1049/pi-b-2.1959.0171.

[170] A. R. Beattie, and P. T. Landsberg,
"Auger effect in semiconductors",
Proceedings of the Royal Society of London A **249**, 16 (1959),
DOI: 10.1098/rspa.1959.0003.

[171] P. Auger,
"The compound photoelectric effect",
Journal de Physique et Le Radium **6**, 205 (1925),
DOI: 10.1051/jphysrad:0192500606020500.

[172] K. A. Bulashevich, and S. Y. Karpov,
"Impact of surface recombination on efficiency of III-nitride light-emitting diodes",
physica status solidi (RRL)-Rapid Research Letters **10**, 480 (2016),
DOI: 10.1002/pssr.201600059.

[173] H.-Y. Ryu, H.-S. Kim, and J.-I. Shim,
"Rate equation analysis of efficiency droop in InGaN light-emitting diodes",
Applied Physics Letters **95**, 081114 (2009),
DOI: 10.1063/1.3216578.

[174] Q. Dai, Q. Shan, J. Wang, S. Chhajed, J. Cho, E. F. Schubert, M. H. Crawford, D. D. Koleske, M.-H. Kim, and Y. Park,
"Carrier recombination mechanisms and efficiency droop in GaInN/GaN light-emitting diodes",
Applied Physics Letters **97**, 133507 (2010),
DOI: 10.1063/1.3493654.

[175] S. Karpov,
"ABC-model for interpretation of internal quantum efficiency and its droop in III-nitride LEDs: a review",
Optical and Quantum Electronics **47**, 1293 (2015),
DOI: 10.1007/s11082-014-0042-9.

[176] I. Titkov, S. Karpov, A. Yadav, V. Zerova, M. Zulonas, B. Galler, M. Strassburg, I. Pietzonka, H.-J. Lugauer, and E. Rafailov,
"Temperature-dependent internal quantum efficiency of blue high-brightness light-emitting diodes",
Quantum Electronics, IEEE Journal of **50**, 911 (2014),
DOI: 10.1109/JQE.2014.2359958.

[177] Y. Narukawa, M. Ichikawa, D. Sanga, M. Sano, and T. Mukai,
"White light emitting diodes with super-high luminous efficacy",
Journal of Physics D: Applied Physics **43**, 354002 (2010),
DOI: 10.1088/0022-3727/43/35/354002.

[178] M. J. Cich, R. I. Aldaz, A. Chakraborty, A. David, M. J. Grundmann, A. Tyagi, M. Zhang, F. M. Steranka, and M. R. Krames,
"Bulk GaN based violet light-emitting diodes with high efficiency at very high current density",
Applied Physics Letters **101**, 223509 (2012),
DOI: 10.1063/1.4769228.

[179] S. Saito, R. Hashimoto, J. Hwang, and S. Nunoue,
"InGaN Light-Emitting Diodes on c -Face Sapphire Substrates in Green Gap Spectral Range",
Applied Physics Express **6**, 111004 (2013),
DOI: 10.7567/APEX.6.111004.

[180] K. A. Bulashevich, A. V. Kulik, and S. Y. Karpov,
"Optimal ways of colour mixing for high-quality white-light LED sources",
physica status solidi (a) **212**, 914 (2015),
DOI: 10.1002/pssa.201431576.

[181] F. Della Sala, A. Di Carlo, P. Lugli, F. Bernardini, V. Fiorentini, R. Scholz, and J.-M. Jancu,
"Free-carrier screening of polarization fields in wurtzite GaN/InGaN laser structures",
Applied Physics Letters **74**, 2002 (1999),
DOI: 10.1063/1.123727.

[182] T. Wang, J. Bai, S. Sakai, and J. K. Ho,
"Investigation of the emission mechanism in InGaN/GaN-based light-emitting diodes",
Applied Physics Letters **78**, 2617 (2001),
DOI: 10.1063/1.1368374.

[183] J. Hader, J. Moloney, and S. Koch,
"Temperature-dependence of the internal efficiency droop in GaN-based diodes",
Applied Physics Letters **99**, 181127 (2011),
DOI: 10.1063/1.3658031.

[184] K. Bulashevich, and S. Y. Karpov,
"Is Auger recombination responsible for the efficiency rollover in III-nitride light-emitting diodes?",
physica status solidi (c) **5**, 2066 (2008),
DOI: 10.1002/pssc.200778414.

[185] J. Iveland, L. Martinelli, J. Peretti, J. S. Speck, and C. Weisbuch,
"Direct measurement of Auger electrons emitted from a semiconductor light-emitting diode under electrical injection: Identification of the dominant mechanism for efficiency droop",
Physical Review Letters **110**, 177406 (2013),
DOI: 10.1103/PhysRevLett.110.177406.

[186] M. Binder, A. Nirschl, R. Zeisel, T. Hager, H.-J. Lugauer, M. Sabathil, D. Bougeard, J. Wagner, and B. Galler,
"Identification of nnp and npp Auger recombination as significant contributor to the efficiency droop in (GaIn) N quantum wells by visualization of hot carriers in photoluminescence",
Applied Physics Letters **103**, 071108 (2013),
DOI: 10.1063/1.4818761.

[187] K. T. Delaney, P. Rinke, and C. G. Van de Walle,
"Auger recombination rates in nitrides from first principles",
Applied Physics Letters **94**, 191109 (2009),
DOI: 10.1063/1.3133359.

[188] E. Kioupakis, P. Rinke, K. T. Delaney, and C. G. Van de Walle,
"Indirect Auger recombination as a cause of efficiency droop in nitride light-emitting diodes",
Applied Physics Letters **98**, 161107 (2011),
DOI: 10.1063/1.3570656.

[189] B. Galler, H.-J. Lugauer, M. Binder, R. Hollweck, Y. Folwill, A. Nirschl, A. Gomez-Iglesias, B. Hahn, J. Wagner, and M. Sabathil,
"Experimental determination of the dominant type of Auger recombination in InGaN quantum wells",
Applied Physics Express **6**, 112101 (2013),
DOI: 10.7567/APEX.6.112101.

[190] A. Nirschl, M. Binder, M. Schmid, I. Pietzonka, H.-J. Lugauer, R. Zeisel, M. Sabathil, D. Bougeard, and B. Galler,
"Towards quantification of the crucial impact of Auger recombination for the efficiency droop in (AlInGa) N quantum well structures",
Optics Express **24**, 2971 (2016),
DOI: 10.1364/OE.24.002971.

[191] K. W. Williams, N. R. Monahan, D. D. Koleske, M. H. Crawford, and X.-Y. Zhu,
"Ultrafast and band-selective Auger recombination in InGaN quantum wells",
Applied Physics Letters **108**, 141105 (2016),
DOI: 10.1063/1.4945669.

[192] G. G. Stokes,
"On the change of refrangibility of Light",
Philosophical Transactions of the Royal Society of London **142**, 463 (1852),
DOI: 10.1098/rstl.1852.0022.

[193] E. Burstein,
"Anomalous optical absorption limit in InSb",
Physical Review **93**, 632 (1954),
DOI: 10.1103/PhysRev.93.632.

[194] H. C. Casey, J. Muth, S. Krishnankutty, and J. M. Zavada,
"Dominance of tunneling current and band filling in InGaN/AlGaN double heterostructure blue light emitting diodes",
Applied Physics Letters **68**, 2867 (1996),
DOI: 10.1063/1.116351.

[195] B. E. Sernelius, K.-F. Berggren, Z.-C. Jin, I. Hamberg, and C. G. Granqvist, "Band-gap tailoring of ZnO by means of heavy Al doping", *Physical Review B* **37**, 10244 (1988), DOI: 10.1103/PhysRevB.37.10244.

[196] M. A. Reshchikov, and H. Morkoç, "Luminescence properties of defects in GaN", *Journal of Applied Physics* **97**, 061301 (2005), DOI: 10.1063/1.1868059.

[197] P. Lefebvre, A. Morel, M. Gallart, T. Taliercio, J. Allegre, B. Gil, H. Mathieu, B. Damilano, N. Grandjean, and J. Massies, "High internal electric field in a graded-width InGaN/GaN quantum well: Accurate determination by time-resolved photoluminescence spectroscopy", *Applied Physics Letters* **78**, 1252 (2001), DOI: 10.1063/1.1351517.

[198] D. V. O'Connor, W. R. Ware, and J. C. Andre, "Deconvolution of fluorescence decay curves. A critical comparison of techniques", *Journal of Physical Chemistry* **83**, 1333 (1979), DOI: 10.1021/j100473a019.

[199] T. Schulz, T. Remmele, T. Markurt, M. Korytov, and M. Albrecht, "Analysis of statistical compositional alloy fluctuations in InGaN from aberration corrected transmission electron microscopy image series", *Journal of Applied Physics* **112**, 033106 (2012), DOI: 10.1063/1.4742015.

[200] M. J. Davies, T. J. Badcock, P. Dawson, M. J. Kappers, R. a. Oliver, and C. J. Humphreys, "High excitation carrier density recombination dynamics of InGaN/GaN quantum well structures: Possible relevance to efficiency droop", *Applied Physics Letters* **102**, 022106 (2013), DOI: 10.1063/1.4781398.

[201] G. Sun, G. Xu, J. Yujie, H. Thao, G. Liu, J. Zhang, and N. Tansu, "Investigation of fast and slow decays in InGaN/GaN quantum wells", *Applied Physics Letters* **99**, 081104 (2011), DOI: 10.1063/1.3627166.

[202] A. Hangleiter, F. Hitzel, C. Netzel, D. Fuhrmann, U. Rossow, G. Ade, and P. Hinze, "Suppression of nonradiative recombination by V-shaped pits in GaInN/GaN quantum wells produces a large increase in the light emission efficiency", *Physical Review Letters* **95**, 127402 (2005), DOI: 10.1103/PhysRevLett.95.127402.

[203] T. L. Song, "Strain relaxation due to V-pit formation in InGaN GaN epilayers grown on sapphire", *Journal of Applied Physics* **98**, 084906 (2005), DOI: 10.1063/1.2108148.

[204] J. S. Reparaz, G. Callsen, M. R. Wagner, F. Güell, J. R. Morante, C. M. Sotomayor Torres, and A. Hoffmann,
"Spatial mapping of exciton lifetimes in single ZnO nanowires",
APL Materials **1**, 012103 (2013),
DOI: 10.1063/1.4808441.

[205] Y.-D. Lin, S. Yamamoto, C.-Y. Huang, C.-L. Hsiung, F. Wu, K. Fujito, H. Ohta, J. S. Speck, S. P. DenBaars, and S. Nakamura,
"High quality InGaN/AlGaN multiple quantum wells for semipolar InGaN green laser diodes",
Applied Physics Express **3**, 82001 (2010),
DOI: 10.1143/APEX.3.082001.

[206] S.-M. Ko, H.-S. Kwack, C. Park, Y.-S. Yoo, S.-Y. Kwon, H. Jin Kim, E. Yoon, L. Si Dang, and Y.-H. Cho,
"Strong carrier localization and diminished quantum-confined Stark effect in ultra-thin high-indium-content InGaN quantum wells with violet light emission",
Applied Physics Letters **103**, 222104 (2013),
DOI: 10.1063/1.4833917.

[207] G. Giudice, D. Kuksenkov, and H. Temkin,
"Measurement of differential carrier lifetime in vertical-cavity surface-emitting lasers",
Photonics Technology Letters, IEEE **10**, 920 (1998),
DOI: 10.1109/68.681270.

[208] M. Shatalov, A. Chitnis, A. Koudymov, J. Zhang, V. Adivarahan, G. Simin, and M. A. Khan,
"Differential carrier lifetime in AlGaN based multiple quantum well deep UV light emitting diodes at 325 nm",
Japanese Journal of Applied Physics **41**, L1146 (2002),
DOI: 10.1143/JJAP.41.L1146.

[209] I. Reklaitis, R. Kudžma, S. Miasojedovas, P. Vitta, A. Žukauskas, R. Tomašiūnas, I. Pietzonka, and M. Strassburg,
"Photoluminescence decay dynamics in blue and green InGaN LED structures revealed by the frequency-domain technique",
Journal of Electronic Materials **45**, 3290 (2016),
DOI: 10.1007/s11664-016-4557-7.

[210] K. Kim, W. R. L. Lambrecht, B. Segall, and M. van Schilfgaarde,
"Effective masses and valence-band splittings in GaN and AlN",
Physical Review B **56**, 7363 (1997),
DOI: 10.1103/PhysRevB.56.7363.

[211] W. G. Scheibenzuber, U. T. Schwarz, L. Sulmoni, J. Dorsaz, J.-F. Carlin, and N. Grandjean,
"Recombination coefficients of GaN-based laser diodes",
Journal of Applied Physics **109**, 093106 (2011),
DOI: 10.1063/1.3585872.

[212] A. David, and M. J. Grundmann,
"Influence of polarization fields on carrier lifetime and recombination rates in InGaN-based light-emitting diodes",
Appl. Phys. Lett. **97**, 033501 (2010),
DOI: 10.1063/1.3462916.

[213] S. Keller, B. P. Keller, D. Kapolnek, A. C. Abare, H. Masui, L. A. Coldren, U. K. Mishra, and S. P. Den Baars,
"Growth and characterization of bulk InGaN films and quantum wells",
Applied Physics Letters **68**, 3147 (1996),
DOI: 10.1063/1.115806.

[214] S. Hammersley, M. J. Kappers, F. C.-P. Massabuau, S.-L. Sahonta, P. Dawson, R. A. Oliver, and C. J. Humphreys,
"Effects of quantum well growth temperature on the recombination efficiency of InGaN/GaN multiple quantum wells that emit in the green and blue spectral regions",
Applied Physics Letters **107**, 132106 (2015),
DOI: 10.1063/1.4932200.

[215] A. David, C. A. Hurni, N. G. Young, and M. D. Craven,
"Electrical properties of III-Nitride LEDs: Recombination-based injection model and theoretical limits to electrical efficiency and electroluminescent cooling",
Applied Physics Letters **109**, 083501 (2016),
DOI: 10.1063/1.4961491.

[216] J. Xie, X. Ni, Q. Fan, R. Shimada, Ü. Özgür, and H. Morkoç,
"On the efficiency droop in InGaN multiple quantum well blue light emitting diodes and its reduction with p-doped quantum well barriers",
Applied Physics Letters **93**, 121107 (2008),
DOI: 10.1063/1.2988324.

[217] P. Wurfel,
"The chemical potential of radiation",
Journal of Physics C: Solid State Physics **15**, 3967 (1982),
DOI: 10.1088/0022-3719/15/18/012.

[218] Y. Arakawa, H. Sakaki, M. Nishioka, J. Yoshino, and T. Kamiya,
"Recombination lifetime of carriers in GaAs-GaAlAs quantum wells near room temperature",
Applied Physics Letters **46**, 519 (1985),
DOI: 10.1063/1.95578.

[219] T. Matsusue, and H. Sakaki,
"Radiative recombination coefficient of free carriers in GaAs-AlGaAs quantum wells and its dependence on temperature",
Applied Physics Letters **50**, 1429 (1987),
DOI: 10.1063/1.97844.

[220] L. V. Asryan,
"Spontaneous radiative recombination and nonradiative Auger recombination in quantum-confined heterostructures",
Quantum Electronics **35**, 1117 (2005),
DOI: 10.1070/QE2005v035n12ABEH013093.

[221] E. Kioupakis, Q. Yan, D. Steiauf, and C. G. Van de Walle,
"Temperature and carrier-density dependence of Auger and radiative recombination in nitride optoelectronic devices",
New Journal of Physics **15**, 125006 (2013),
DOI: 10.1088/1367-2630/15/12/125006.

[222] D. M. Graham, A. Soltani-Vala, P. Dawson, M. J. Godfrey, T. M. Smeeton, J. S. Barnard, M. J. Kappers, C. J. Humphreys, and E. J. Thrush,
"Optical and microstructural studies of InGaN/GaN single-quantum-well structures",
J. Appl. Phys. **97**, 103508 (2005),
DOI: 10.1063/1.1897070.

[223] S. Schulz, M. A. Caro, C. Coughlan, and E. P. O'Reilly,
"Atomistic analysis of the impact of alloy and well-width fluctuations on the electronic and optical properties of InGaN/GaN quantum wells",
Phys. Rev. B **91**, 035439 (2015),
DOI: 10.1103/PhysRevB.91.035439.

[224] Y. Jiang, Y. Li, Y. Li, Z. Deng, T. Lu, Z. Ma, P. Zuo, L. Dai, L. Wang, H. Jia, W. Wang, J. Zhou, W. Liu, and H. Chen,
"Realization of high-luminous-efficiency InGaN light-emitting diodes in the green gap range",
Scientific Reports **5**, 10883 (2015),
DOI: 10.1038/srep10883.

[225] A. Lobanova, A. Kolesnikova, A. Romanov, S. Y. Karpov, M. Rudinsky, and E. Yakovlev,
"Mechanism of stress relaxation in (0001) InGaN/GaN via formation of V-shaped dislocation half-loops",
Applied Physics Letters **103**, 152106 (2013),
DOI: 10.1063/1.4824835.

[226] K. Bulashevich, O. Khokhlev, I. Y. Evstratov, and S. Y. Karpov,
"Simulation of light-emitting diodes for new physics understanding and device design",
in *SPIE OPTO*, **8278**, pp. 827819–827819
International Society for Optics and Photonics (2012),
DOI: 10.1117/12.912305.

[227] G. Lasher, and F. Stern,
"Spontaneous and stimulated recombination radiation in semiconductors",
Physical Review **133**, A553 (1964),
DOI: 10.1103/PhysRev.133.A553.

[228] G. W. 't Hooft, and C. van Opdorp,
"Temperature dependence of interface recombination and radiative recombination in (Al, Ga)As heterostructures",
Applied Physics Letters **42**, 813 (1983),
DOI: 10.1063/1.94105.

[229] A. Levanyuk, and V. Osipov,
"Edge luminescence of direct-gap semiconductors",
Physics-Uspekhi **24**, 187 (1981),
DOI: 10.1070/PU1981v024n03ABEH004770.

[230] E. O. Kane,
"Band structure of indium antimonide",
Journal of Physics and Chemistry of Solids **1**, 249 (1957),
DOI: 10.1016/0022-3697(57)90013-6.

[231] M. Jacobson, D. Nelson, O. Konstantinov, and A. Matveentsev,
"The tail of localized states in the band gap of the quantum well in the In0. 2Ga0. 8N/GaN system and its effect on the laser-excited photoluminescence spectrum",
Semiconductors **39**, 1410 (2005),
DOI: 10.1134/1.2140315.

[232] E. Rashba, and G. Gurgenishvili,
"Edge absorption theory in semiconductors",
Soviet Physics-Solid State **4**, 759 (1962).

[233] J. Feldmann, G. Peter, E. O. Göbel, P. Dawson, K. Moore, C. Foxon, and R. J. Elliott,
"Linewidth dependence of radiative exciton lifetimes in quantum wells",
Physical Review Letters **59**, 2337 (1987),
DOI: 10.1103/PhysRevLett.59.2337.

[234] A. V. Kavokin,
"Exciton oscillator strength in quantum wells: From localized to free resonant states",
Physical Review B **50**, 8000 (1994),
DOI: 10.1103/PhysRevB.50.8000.

[235] I.-H. Kim, H.-S. Park, Y.-J. Park, and T. Kim,
"Formation of V-shaped pits in InGaN/GaN multiquantum wells and bulk InGaN films",
Applied Physics Letters **73**, 1634 (1998),
DOI: 10.1063/1.122229.

[236] D. Queren, M. Schillgalies, A. Avramescu, G. Brüderl, A. Laubsch, S. Lutgen, and U. Strauß,
"Quality and thermal stability of thin InGaN films",
Journal of Crystal Growth **311**, 2933 (2009),
DOI: 10.1016/j.jcrysgro.2009.01.066.

[237] T. Langer, A. Kruse, F. A. Ketzer, A. Schwiegel, L. Hoffmann, H. Jönen, H. Bremers, U. Rossow, and A. Hangleiter,
"Origin of the "green gap": Increasing nonradiative recombination in indium-rich GaInN/GaN quantum well structures",
physica status solidi (c) **8**, 2170 (2011),
DOI: 10.1002/pssc.201001051.

[238] F. C.-P. Massabuau, M. J. Davies, F. Oehler, S. K. Pamenter, E. J. Thrush, M. J. Kappers, A. Kovács, T. Williams, M. A. Hopkins, C. J. Humphreys, P. Dawson, R. E. Dunin-Borkowski, J. Etheridge, D. W. E. Allsopp, and R. A. Oliver,
"The impact of trench defects in InGaN/GaN light emitting diodes and implications for the "green gap" problem",
Applied Physics Letters **105**, 112110 (2014),
DOI: 10.1063/1.4896279.

[239] A. Chakraborty, B. A. Haskell, S. Keller, J. S. Speck, S. P. Denbaars, S. Nakamura, and U. K. Mishra,
"Demonstration of nonpolar m-plane InGaN/GaN light-emitting diodes on free-standing m-plane GaN substrates",
Japanese Journal of Applied Physics **44**, L173 (2005),
DOI: 10.1143/JJAP.44.L173.

[240] M. C. Schmidt, K.-C. Kim, H. Sato, N. Fellows, H. Masui, S. Nakamura, S. P. DenBaars, and J. S. Speck,
"High power and high external efficiency m-plane InGaN light emitting diodes",
Japanese Journal of Applied Physics **46**, L126 (2007),
DOI: 10.1143/JJAP.46.L126.

[241] H. Sato, R. B. Chung, H. Hirasawa, N. Fellows, H. Masui, F. Wu, M. Saito, K. Fujito, J. S. Speck, S. P. DenBaars, and S. Nakamura,
"Optical properties of yellow light-emitting diodes grown on semipolar (112xAF2) bulk GaN substrates",
Applied Physics Letters **92**, 1110 (2008),
DOI: 10.1063/1.2938062.

[242] J. Speck, and S. Chichibu,
"Nonpolar and semipolar group III nitride-based materials",
MRS Bulletin **34**, 304 (2009),
DOI: 10.1557/mrs2009.91.

[243] H. Masui, S. Nakamura, S. P. DenBaars, and U. K. Mishra,
"Nonpolar and semipolar III-nitride light-emitting diodes: achievements and challenges",
Electron Devices, IEEE Transactions on **57**, 88 (2010),
DOI: 10.1109/TED.2009.2033773.

[244] R. M. Farrell, E. C. Young, F. Wu, S. P. DenBaars, and J. S. Speck,
"Materials and growth issues for high-performance nonpolar and semipolar light-emitting devices",
Semiconductor Science and Technology **27**, 24001 (2012),
DOI: 10.1088/0268-1242/27/2/024001.

[245] D. F. Feezell, J. S. Speck, S. P. DenBaars, and S. Nakamura,
"Semipolar InGaN/GaN light-emitting diodes for high-efficiency solid-state lighting",
Display Technology, Journal of **9**, 190 (2013),
DOI: 10.1109/JDT.2012.2227682.

[246] S. H. Oh, B. P. Yonkee, M. Cantore, R. M. Farrell, J. S. Speck, S. Nakamura, and S. P. DenBaars,
"Semipolar III-nitride light-emitting diodes with negligible efficiency droop up to 1 W",
Applied Physics Express **9**, 102102 (2016),
DOI: 10.7567/APEX.9.102102.

[247] A. Tyagi, F. Wu, E. C. Young, A. Chakraborty, H. Ohta, R. Bhat, K. Fujito, S. P. DenBaars, S. Nakamura, and J. S. Speck,
"Partial strain relaxation via misfit dislocation generation at heterointerfaces in (Al,In)GaN epitaxial layers grown on semipolar (112¯2) GaN free standing substrates",
Applied Physics Letters **95**, 251905 (2009),
DOI: 10.1063/1.3275717.

[248] E. C. Young, C. S. Gallinat, A. E. Romanov, A. Tyagi, F. Wu, and J. S. Speck,
"Critical thickness for onset of plastic relaxation in (1122) and (2021) semipolar AlGaN heterostructures",
Applied Physics Express **3**, 111002 (2010),
DOI: 10.1143/APEX.3.111002.

[249] I. L. Koslow, M. T. Hardy, P. S. Hsu, F. Wu, A. E. Romanov, E. C. Young, S. Nakamura, S. P. DenBaars, and J. S. Speck,
"Onset of plastic relaxation in semipolar In x Ga 1- x N/GaN heterostructures",
Journal of Crystal Growth **388**, 48 (2014),
DOI: 10.1016/j.jcrysgro.2013.10.027.

[250] H.-G. Chen, T.-S. Ko, S.-C. Ling, T.-C. Lu, H.-C. Kuo, S.-C. Wang, Y.-H. Wu, and L. Chang,
"Dislocation reduction in GaN grown on stripe patterned r-plane sapphire substrates",
Applied Physics Letters **91**, 021914 (2007),
DOI: 10.1063/1.2754643.

[251] P. de Mierry, L. Kappei, F. Tendille, P. Vennéguès, M. Leroux, and J. Zuniga-Perez,
"Green emission from semipolar InGaN quantum wells grown on low-defect (112¯2) GaN templates fabricated on patterned r-sapphire",
physica status solidi (b) **253**, 105 (2016),
DOI: 10.1002/pssb.201552298.

[252] N. Kriouche, P. Vennéguès, M. Nemoz, G. Nataf, and P. D. Mierry,
"Stacking faults blocking process in (1 1 -2 2) semipolar GaN growth on sapphire using asymmetric lateral epitaxy",
Journal of Crystal Growth **312**, 2625 (2010),
DOI: 10.1016/j.jcrysgro.2010.05.038.

[253] F. Tendille, P. D. Mierry, P. Vennéguès, S. Chenot, and M. Teisseire,
"Defect reduction method in (11-22) semipolar GaN grown on patterned sapphire substrate by MOCVD: Toward heteroepitaxial semipolar GaN free of basal stacking faults",
Journal of Crystal Growth **404**, 177 (2014),
DOI: 10.1016/j.jcrysgro.2014.07.020.

[254] F. Scholz, T. Meisch, and K. Elkhouly,
"Efficiency studies on semipolar GaInN–GaN quantum well structures",
physica status solidi (a), n/a (2016),
DOI: 10.1002/pssa.201600340.

[255] M. J. Paisley, Z. Sitar, J. B. Posthill, and R. F. Davis,
"Growth of cubic phase gallium nitride by modified molecular-beam epitaxy",
Journal of Vacuum Science & Technology A **7**, 701 (1989),
DOI: 10.1116/1.575869.

[256] H. Okumura, S. Misawa, and S. Yoshida,
"Epitaxial growth of cubic and hexagonal GaN on GaAs by gas-source molecular-beam epitaxy",
Applied Physics Letters **59**, 1058 (1991),
DOI: 10.1063/1.106344.

[257] S. Strite, J. Ruan, Z. Li, A. Salvador, H. Chen, D. J. Smith, W. J. Choyke, and H. Morkoç,
"An investigation of the properties of cubic GaN grown on GaAs by plasma-assisted molecular-beam epitaxy",
Journal of Vacuum Science & Technology B **9**, 1924 (1991),
DOI: 10.1116/1.585381.

[258] T. Schupp, K. Lischka, and D. As,
"{MBE} growth of atomically smooth non-polar cubic AlN",
Journal of Crystal Growth **312**, 1500 (2010),
DOI: 10.1016/j.jcrysgro.2010.01.040.

[259] V. Cimalla, J. Pezoldt, G. Ecke, R. Kosiba, O. Ambacher, L. Spieß, G. Teichert, H. Lu, and W. Schaff,
"Growth of cubic InN on r-plane sapphire",
Applied Physics Letters **83**, 3468 (2003),
DOI: 10.1063/1.1622985.

[260] H. Yang, L. Zheng, J. Li, X. Wang, D. Xu, Y. Wang, X. Hu, and P. Han,
"Cubic-phase GaN light-emitting diodes",
Applied Physics Letters **74**, 2498 (1999),
DOI: 10.1063/1.123019.

[261] M. Bürger, G. Callsen, T. Kure, A. Hoffmann, A. Pawlis, D. Reuter, and D. J. As,
"Lasing properties of non-polar GaN quantum dots in cubic aluminum nitride microdisk cavities",
Applied Physics Letters **103**, 021107 (2013),
DOI: 10.1063/1.4813408.

[262] S. Kako, M. Holmes, S. Sergent, M. Bürger, D. J. As, and Y. Arakawa,
"Single-photon emission from cubic GaN quantum dots",
Applied Physics Letters **104**, 011101 (2014),
DOI: 10.1063/1.4858966.

[263] I. N. Stranski, and L. Krastanow,
"Zur Theorie der orientierten Ausscheidung von Ionenkristallen aufeinander",
Monatshefte für Chemie und verwandte Teile anderer Wissenschaften **71**, 351 (1937),
DOI: 10.1007/BF01798103.

[264] V. A. Shchukin, N. N. Ledentsov, P. S. Kop'ev, and D. Bimberg,
"Spontaneous ordering of arrays of coherent strained islands",
Physical Review Letters **75**, 2968 (1995),
DOI: 10.1103/PhysRevLett.75.2968.

[265] N. N. Ledentsov, V. A. Shchukin, M. Grundmann, N. Kirstaedter, J. Böhrer, O. Schmidt, D. Bimberg, V. M. Ustinov, A. Y. Egorov, A. E. Zhukov, P. S. Kop'ev, S. V. Zaitsev, N. Y. Gordeev, Z. I. Alferov, A. I. Borovkov, A. O. Kosogov, S. S. Ruvimov, P. Werner, U. Gösele, and J. Heydenreich,
"Direct formation of vertically coupled quantum dots in Stranski-Krastanow growth",
Physical Review B **54**, 8743 (1996),
DOI: 10.1103/PhysRevB.54.8743.

[266] H. Saito, K. Nishi, I. Ogura, S. Sugou, and Y. Sugimoto,
"Room-temperature lasing operation of a quantum-dot vertical-cavity surface-emitting laser",
Applied Physics Letters **69**, 3140 (1996),
DOI: 10.1063/1.116808.

[267] B. Daudin, F. Widmann, G. Feuillet, Y. Samson, M. Arlery, and J. L. Rouvière,
"Stranski-Krastanov growth mode during the molecular beam epitaxy of highly strained GaN",
Physical Review B **56**, R7069 (1997),
DOI: 10.1103/PhysRevB.56.R7069.

[268] S. Kako, M. Miyamura, K. Tachibana, K. Hoshino, and Y. Arakawa, "Size-dependent radiative decay time of excitons in GaN/AlN self-assembled quantum dots", *Applied Physics Letters* **83**, 984 (2003), DOI: 10.1063/1.1596382.

[269] G. Hönig, S. Rodt, G. Callsen, I. A. Ostapenko, T. Kure, A. Schliwa, C. Kindel, D. Bimberg, A. Hoffmann, S. Kako, and Y. Arakawa, "Identification of electric dipole moments of excitonic complexes in nitride-based quantum dots", *Physical Review B* **88**, 045309 (2013), DOI: 10.1103/PhysRevB.88.045309.

[270] M. Miyamura, K. Tachibana, and Y. Arakawa, "High-density and size-controlled GaN self-assembled quantum dots grown by metalorganic chemical vapor deposition", *Applied Physics Letters* **80**, 3937 (2002), DOI: 10.1063/1.1482416.

[271] K. Hoshino, S. Kako, and Y. Arakawa, "Formation and optical properties of stacked GaN self-assembled quantum dots grown by metalorganic chemical vapor deposition", *Applied Physics Letters* **85**, 1262 (2004), DOI: 10.1063/1.1784524.

[272] C. Kindel, G. Callsen, S. Kako, T. Kawano, H. Oishi, G. Hönig, A. Schliwa, A. Hoffmann, and Y. Arakawa, "Spectral diffusion in nitride quantum dots: Emission energy dependent linewidths broadening via giant built-in dipole moments", *physica status solidi (RRL)–Rapid Research Letters* **8**, 408 (2014), DOI: 10.1002/pssr.201409096.

[273] S. C. Davies, D. J. Mowbray, F. Ranalli, P. J. Parbrook, Q. Wang, T. Wang, B. S. Yea, B. J. Sherliker, M. P. Halsall, R. J. Kashtiban, and U. Bangert, "Optical and microstructural studies of InGaN/GaN quantum dot ensembles", *Applied Physics Letters* **95**, 111903 (2009), DOI: 10.1063/1.3226645.

[274] T. Xu, A. Y. Nikiforov, R. France, C. Thomidis, A. Williams, and T. D. Moustakas, "Blue–green–red LEDs based on InGaN quantum dots grown by plasma-assisted molecular beam epitaxy", *physica status solidi (a)* **204**, 2098 (2007), DOI: 10.1002/pssa.200674834.

[275] M. Zhang, P. Bhattacharya, and W. Guo, "InGaN/GaN self-organized quantum dot green light emitting diodes with reduced efficiency droop", *Applied Physics Letters* **97**, 011103 (2010), DOI: 10.1063/1.3460921.

[276] C. Kölper, M. Sabathil, F. Römer, M. Mandl, M. Strassburg, and B. Witzigmann, "Core–shell InGaN nanorod light emitting diodes: Electronic and optical device properties", *physica status solidi (a)* **209**, 2304 (2012), DOI: 10.1002/pssa.201228178.

Acknowledgements

I would like to thank everyone who supported this work, helped me on the way, or otherwise contributed. In particular:

- Prof. Dr. Axel Hoffmann for giving me the opportunity to work on this interesting topic, bringing me together with a broad consortium of partners in the NEWLED project, many opportunities to present my research on international conferences, continous feedback on scientific progress and freedom to persue the lines of research presented in this thesis.
- Prof. Dr. Janina Maultzsch for co-supervision of this work and the nice working atmosphere in the joint Hoffmann/Maultzsch/Thomsen working group.
- Prof. Dr. Andreas Waag for agreeing to review this thesis and taking part in my defense.
- Prof. Dr. Lehmann for chairing my defense.
- Dr. Sergey Karpov for extraordinarily efficient cooperation.
- Anna Nirschl and Dr. Ines Pietzonka for sample growth and fruitful discussions.
- Dr. Bastian Galler, Dr. Hans-Jürgen Lugauer and Dr. Martin Straßburg for cooperation.
- Ignas Reklaitis for interesting discussions regarding our similar measurement approaches, and the best bar in Vilnius.
- The members of the NEWLED consortium for collaboration and widening my scientific horizon, as well as pleasant evenings spent somewhere in Europe.
- Daniela Beiße, Marco Haupt and Andreas Ludewig for swift and competent drilling, flexing, soldering, building, drilling again because we forgot something..

- Thomas Kure for long-time office sharing, dealing with me even on monday mornings, excessive cringling and micado help.
- Dr. Gordon Callsen for office sharing, "optimizing" wordings in publications and fruitful discussions regarding the origin of the CHC luminescence.
- Christian Nenstiel for second opinions.
- Dr. Dirk Heinrich, CCO (Chief Caffeine Officer)
- Asmus Vierck for sharing the urge to program things in Python which may or may not be useful.
- All former and current members of the working groups Hoffmann, Maultzsch, and Thomsen for shared lunch and/or coffee breaks.

I also acknowledge the financial support of the European Union FP7-ICT Project NEWLED, No. FP7-318388, the German Science Foundation with the Collobarative Research Center (CRC 787) and the CRC 787's School of Nanophotonics.

I thank Angelina Helen Ciaglia for love, understanding and support.